

# Analysis of Terahertz-Regime Electromagnetic Waves in Photonic Crystals Generating Fano Resonances

Andreas Grøndal Schjøtt, Laurits Vejen,  
Veronica Elze Hjorth

Physics  
Fys5.325a, 2023-06

Master's Project



Copyright © Aalborg University 2023

Typeset using  $\LaTeX$ . Illustrations made with Vectr©Imagine 2023, and plots made on MATLAB®.





Department of Materials and Production  
Aalborg University  
<http://www.aau.dk>

# AALBORG UNIVERSITY

## STUDENT REPORT

**Title:**

Analysis of Terahertz-Regime Electromagnetic Waves in Photonic Crystals Generating Fano Resonances

**Project Period:**

Spring Semester 2023

**Project Group:**

5.325a

**Participants:**

Andreas Grøndal Schjøtt  
Laurits Vejen  
Veronica Elze Hjorth

**Supervisor:**

Thomas M. Søndergaard

**Page Numbers:** 135**Date of Completion:**

June 1, 2023

**Abstract:**

This project seeks out to find, analyze and characterize Fano resonances found in a photonic crystal made off silicon rods on a silicon plate in the terahertz regime. To realize this, three different formulations of the three-dimensional Fourier modal method are constructed in order to calculate the transmittance spectrum of the structure. The three models differ in how the permittivity is calculated and are a simple model, calculating the permittivity coefficients directly, a model utilizing Lifeng Li's factorization rules, and lastly, a model treating the permittivity as a tensor. All three models converged to the same and the Lifeng Li formulation was found to converge the fastest. Furthermore, a two-dimensional Fourier modal method is constructed to be compared against and lastly, a model is constructed to locate the Fano resonances. Multiple tests were done to understand the behavior of the resonances, which includes changing the angle of the incidence light and polarization, describing the rods either as square or cylindrical, changing the height, the side length and the periodicity of the rods and the height of the plate.

*The content of this report is freely available, but publication (with reference) may only be pursued due to agreement with the authors.*

# Resumé

Dette projekt omhandler Fano resonanser fundet i terahertz regimet i fotoniske krystaller. Der er blevet modelleret nogle forskellige strukturer: En endimensionel periodisk struktur lavet af silicium og luft, en todimensionel periodisk struktur af silicium stænger og en todimensionel periodisk struktur af lufthuller i en siliciumplade. Ydermere kan den todimensionelle periodiske struktur både sættes i kvadratisk gitter og i et heksagonalt gitter og stængerne kan udregnes både med firkantet eller rundt tværsnitsareal.

Transmittansen af lyset igennem den fotoniske krystal er udregnet ved brug af en tredimensionel Fourier modal metode. Tre forskellige formuleringer af metoden er udarbejdet og sammenlignet, hvor forskellen på formuleringerne findes i måden permitiviteten er inkorporeret. I den første formulering regnes Fourier koefficienterne direkte, mens metode to indebærer at bruge Lifeng Li's faktoreringsregler, og derved regne den inverse af permittiviteten. Til sidst bruges en formulering, hvor permitiviteten er beskrevet som en tensor i reelt rum. Alle tre formuleringer blev testet for konvergens, hvor det blev set, at det hele konvergerede til det samme. Derudover er den simple og Li's metode yderligere testet og sammenlignet med en udregning for en endimensionel periodisk struktur, udregnet ved brug af Fourier modal metoden i 2D. Dette resultat var også positivt og begge metoder gav ens transmittanser. Efter alle konvergenstests fortsatte processen med at karakterisere Fano resonanser fundet i strukturen.

Næste resultat omhandlede at lokalisere Fano resonanser, ved at udregne de ledede bølgetilstande i strukturen, da disse er hvad den indkommende bølge kan koble til. Dette resultat var også tilfredsstillende og for den endimensionelle periodiske struktur, var det muligt at lokalisere samtlige resonanser, hvorimod for den todimensionelle struktur var der resonanser som ikke havde en tilsvarende bølgetilstand. Dette blev forklaret ved at disse resonanser kom fra en superposition af S- og P-polariseret lys.

Der blev herefter undersøgt, hvordan det ændrede transmittansen at ændre på formen af stængerne fra firkanter til runde tværsnit. Resultatet her, viser at transmittansen, er tæt på identiske, hvis tværsnitsareal holdes konstant.

Herefter var vinklen på det indkomne lys ændret, hvilket viste at resonanser splittede i to, som gik til højere og lavere bølgelængde for en større vinkel. I virkeligheden kunne dette fjerne resonanser fra strukturen, hvis lyset ikke er et parallelt strålebundt, da de forskudte resonanser udligner hinanden.

At ændre på højden af stængerne, havde en effekt på position og form af resonanser, hvor en lavere stang resulterer i en højere frekvens resonans position, samtidig med at resonansen bliver smallere. Q-faktoren for strukturen er udregnet, og den mindre stang gav en højere Q-faktor, hvilket tyder på, det er sværere for bølgen at koble ind og ud af bølgetilstandene. Ændrer man i stedet på tværsnitsarealet af stængerne, ser man at helt små

stænger og helt store stænger, giver en højere Q-faktor og altså en sværere kobling, imens et større areal stadig rykker resonansen til lavere frekvens, hvilket kan skyldes den højere effektive permittivitet for materialet. Den samme vej rykker resonansen sig også, hvis man gør tykkelsen på den homogene siliciumplade større, hvilket skyldes, at bølgelederen bliver større, og dette giver anledning til højere bølgelængde tilstande. Ændrer man nu i stedet på perioden af stængerne, ser man den modsatte effekt, altså at den større periode giver mindre effektiv permittivitet, men rykker resonansen til højere bølgelængder. Dette skyldes, at de forskellige diffraktionsordener er afhængige af perioden, hvilket betyder at en højere periode, resulterer i en lavere propagationskonstant.



# Contents

<b>Preface</b>	<b>1</b>
<b>1 Introduction</b>	<b>3</b>
<b>2 Photonic Crystal Structure</b>	<b>7</b>
2.1 Lattice . . . . .	7
2.2 Shape . . . . .	8
2.3 Layers . . . . .	10
2.4 The Structures . . . . .	11
<b>3 The Fourier Modal Method</b>	<b>13</b>
3.1 Floquet Theorem . . . . .	14
3.2 Fourier Expansion . . . . .	14
3.3 The Homogeneous Layer . . . . .	15
3.4 The Periodic Layer . . . . .	19
3.5 The Permittivity Matrix . . . . .	22
3.6 Li's Rules for Fourier Factorization . . . . .	25
3.6.1 The Eigenvalue Problem . . . . .	30
3.6.2 Permittivity Integrals . . . . .	31
3.7 Fourier Modal Method by Tensor Averaging . . . . .	31
3.8 Two-Dimensional Photonic Crystal . . . . .	34
3.8.1 Two-Dimensional Fourier Modal Method . . . . .	34
<b>4 Propagation of Light</b>	<b>37</b>
4.1 Reflection and Transmission . . . . .	37
4.2 Guided Modes in a Planar Wave Guide . . . . .	40
4.2.1 Single Interface Fresnel Transmission and Reflection . . . . .	40
4.2.2 Many Layered Waveguide . . . . .	42

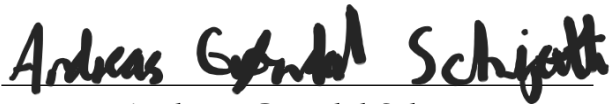
<b>5 Results</b>	<b>45</b>
5.1 The Two-Dimensional Photonic Crystal . . . . .	45
5.1.1 Convergence Test of the 2D FMM . . . . .	45
5.1.2 Comparison of 2D/3D FMM . . . . .	50
5.2 Comparing Different 3D FMMs . . . . .	52
5.3 Coupling to Guided Modes . . . . .	60
5.4 Square or Cylindrical Rods . . . . .	63
5.5 Transmittance for Angled Incidence Field . . . . .	66
5.6 Effect of the Structural Variables . . . . .	69
5.6.1 Resonator Quality vs. Structure Height . . . . .	69
5.6.2 Changing $a$ . . . . .	71
5.6.3 Changing $h_2$ . . . . .	74
5.6.4 Changing $\Lambda$ . . . . .	75
5.7 Discussion . . . . .	76
<b>6 Conclusion</b>	<b>81</b>
<b>Bibliography</b>	<b>83</b>
<b>A Full Transmission: Different Structures</b>	<b>87</b>
<b>B Plots for Varying Angles</b>	<b>91</b>
<b>C Coupled Modes for Different <math>\Lambda</math></b>	<b>93</b>
<b>D Other Lattices/Rods</b>	<b>95</b>
<b>E Scripts</b>	<b>99</b>
E.1 3D FMM . . . . .	99
E.1.1 Simple Formulation . . . . .	99
E.1.2 Li's Formulation . . . . .	107
E.1.3 Tensor Formulation . . . . .	115
E.2 2D FMM . . . . .	123
E.2.1 S-Polarization . . . . .	123
E.2.2 P-Polarization . . . . .	126
E.3 Guided Modes . . . . .	129
E.3.1 S-Polarization . . . . .	129
E.3.2 P-Polarization . . . . .	132

# Preface

**Reading guide:** This project consists of six main chapters. The first chapter is an introduction describing the relevant parts of the fields of photonic crystals and Fano resonances. The second chapter will present all properties of the different structures, for which the transmittances are calculated. The next two chapters describe the theory used in the calculations, Chapter 3 being about the Fourier modal method, while Chapter 4 is about the light properties when interacting with the crystal. In Chapter 5, different results are presented and discussed and lastly, they will all be concluded upon in Chapter 6.

References are denoted by a supscript as <sup>[n]</sup> or [n] when directly referred to in the text, where  $n$  is the number in the bibliography. A thank you to our supervisor *Thomas Søndergaard* for helping us throughout this project.

Aalborg University, June 1, 2023



---

Andreas Grøndal Schjøtt  
aschja18@student.aau.dk



---

Laurits Vejen  
lvejen18@student.aau.dk



---

Veronica Elze Hjorth  
vhjort18@student.aau.dk



# Chapter 1

## Introduction

### The Fano Resonance

A Fano resonance, named after Italian American physicist Ugo Fano, is in the broadest definition a type of resonant scattering that is described by an asymmetric line shape. The first observations of this phenomenon are described already in 1902 by R. W. Wood<sup>[1]</sup> in experiments consisting of sending light of varying wavelengths through a diffraction grating. The odd line shapes observed were then theoretically described in 1907 by Lord Rayleigh.<sup>[2]</sup> However, only the position of the resonances was described and not the shape as the anomalies were described by a singularity. This problem was then sought to be fixed by Ugo Fano describing the asymmetric shapes being associated with excitations of surface waves along the grating.<sup>[3]</sup>

Sharp peaks in the absorption spectra were first described by Fano for noble gases and as it turns out all Fano resonances arise when continuous and discrete states interfere.<sup>[4, 5]</sup> Fano observed the photoionization of an atom, which can occur in different ways. First of all it of course can occur when the photon has enough energy to ionize the inner-shell electron ( $A + \hbar\nu \rightarrow A^+ + e$ ). Another way to ionize the atom is to excite the electron into a quasi-discrete state after which the electron is able to spontaneously eject an electron ( $A + \hbar\nu \rightarrow A^* \rightarrow A^+ + e$ ) which is known as autoionization. A possible way to autoionize is when two electrons get excited by the same photon, where the excitation energy for both electrons is of the same order of magnitude. Now when one electron decays into a lower energy state again, the other electron ionizes. These two different paths for ionization are coupled, which leads to the process being described by a superposition of these processes. This was what Fano utilized to obtain a formula for the resonance profile of the scattering cross section of the system as

$$\sigma = \frac{(\epsilon + q)^2}{e^2 + 1}, \quad (1.1)$$

where  $\epsilon = \frac{2(E-E_F)}{\Gamma}$  is the reduced energy,  $E_F$  is the resonant energy and  $\Gamma$  is the width of the autoionized state.  $q$  is the asymmetry parameter originally described as the ratio between the transition probability of the mixed state and the continuum state. Writing out the parentheses results in three terms, each belonging to a different state:

$$\sigma = \frac{q^2 - 1}{\epsilon^2 + 1} + \frac{2q\epsilon}{\epsilon^2 + 1} + 1. \quad (1.2)$$

The first term describes the discrete state, the second term is the mixing and the last term describes the continuum.

Looking at the profile in equation (1.1) there would exist a specific minimum and maximum at  $\epsilon = -q \rightarrow \sigma_{min} = 0$  and  $\epsilon = \frac{1}{q} \rightarrow \sigma_{max} = 1 + q^2$  respectively. However, the introduced asymmetry parameter can change these values according to the transition probabilities. The limit  $|q| \rightarrow \infty$  the transition is almost entirely determined by the discrete state and has a very weak link to the continuous state. If  $q = 1$  both transitions are of equal importance. Lastly,  $q = 0$  describes a symmetrical dip or an antiresonance and here the lineshape is entirely dependent on the continuum transition. In Figure 1.1 the three cases are presented. The feature of the Fano resonance exists at  $q = 1$  where the two transitions are able to destructively interfere.<sup>[3]</sup>

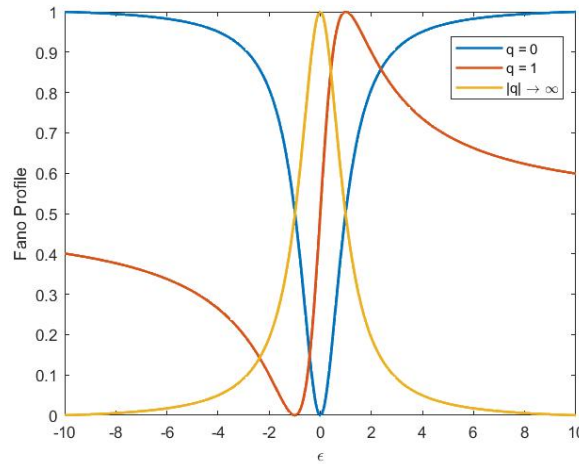


**Figure 1.1:** Normalized Fano profiles for different values of the asymmetry parameter  $q$ . For  $q = 0$  the continuum transition determines the line shape. At  $q = 1$  the two transitions have the same effect on the line shape and for  $q \rightarrow \infty$  the line shape is almost entirely dependent on the discrete state transition.

## Photonic Crystals

Micro- and nanostructures with a dimensional periodic change of dielectric function are called photonic crystals (PhCs). This structure can be useful for many things such as waveg-

uities, photonic circuitry, microlasers and microcavities.<sup>[6]</sup> Fano resonances can be found in many of these nanoscale structures such as when the light scattered off a photonic crystal slab couples with guided modes in the two-dimensional periodic structure.<sup>[3]</sup> The guided modes can affect the transmission and reflection of the external light leading to sharp features in the transmission spectra related to Fano resonances making a photonic crystal mirror that can reflect at a much higher rate for specific wavelengths than what would be seen by a uniform dielectric slab.

For normal incident light on the slab, there are two ways for the light to travel through the slab. It can go through without coupling to any guided mode of the slab or it can follow a pathway assisted by the mode, where the photon will couple to the mode before being let go into free space once again. These two paths can interfere destructively leaving the light not being able to pass through. This effect leaves for the transmission and reflection amplitudes to be calculated as

$$t = t_d + f \frac{\gamma}{i(\omega - \omega_0) + \gamma'}, \quad (1.3)$$

$$r = r_d \pm f \frac{\gamma}{i(\omega - \omega_0) + \gamma'}, \quad (1.4)$$

where  $t_d$  and  $r_d$  are the transmission and reflection coefficients for the direct path,  $\omega_0$  the resonance frequency and  $\gamma$  the width of the resonance. Lastly,  $f$  is the normalized complex amplitude of the resonant mode where the sign corresponds to even or odd modes. For energy conservation, it is required that  $f = -(t_d \pm r_d)$  and for Fano lineshapes to appear it is required that  $0 < t_d < 1$ <sup>[7]</sup>.

Now, to find the properties in (1.3) the problem can be modeled in various ways, however in this project a three-dimensional Fourier modal method (FMM) will be utilized.

## State of the art

The Fano resonance mechanism appears in a multitude of different fields of study. These include scattering of waves through complex geometries, light and plasmonics, by complex, time-dependent, or nonlinear interactions, excitation of nanocavities and quantum dots in photonic structures and scattering of light in photonic devices.<sup>[3]</sup> Fano resonances require when working with electromagnetic waves, discrete modes coupling with a continuum. Galli et. al have analyzed a system where the discrete modes were provided by nanocavities in a PhC slab<sup>[8]</sup>. The Fano resonances in question were the interaction between the confined resonator modes and the incident light. In an experiment they showed that the lineshape of the resonance, and the Q-factor depended on the spot-size of the incident beam.

Harbers et. al explored another type of Fano interaction in PhC slabs.<sup>[9]</sup> The PhC slab was manufactured with embedded organic dye molecules, which could be excited by a laser and

the emission from the molecules could then either emit directly to free space or emit into the PhC first. In these experiments, the structure had a differentiable Q-factor, across the surface thus the shape parameter was investigated as a function of the Q-factor. Further tuning of the lineshape was performed by changing the temperature of the sample since the permittivity of the PhC depended on temperature.

Other than defects in PhCs, Fano resonances can also arise from coupling between incident light and guided modes in the PhC. This has been investigated in nanomembranes on either plastic or glass substrates, by Zhou et. al<sup>[10]</sup>, Qiang et. al<sup>[11]</sup> and Yang et. al<sup>[12]</sup>. Zhou et. al measured transmission spectra for different angles of incidence and polarizations and compared them to FDTD and FMM simulations. Qiang et. al measured and simulated transmission spectra for different angles and polarizations as well. While Yang et. al measured and simulated, with FDTD, transmission spectra for normal incidence.

Free-standing PhC slabs transmission spectra were also analyzed for different structure sizes by Fan et. al<sup>[13, 14]</sup> with a theoretical model and FDTD simulations. Koshino<sup>[15]</sup> similarly analyzed 1D PhC slabs for different rod sizes and angles of incidence.<sup>531</sup>

Just as in Zhou et. al<sup>[10]</sup>, the structures in this report will be calculated utilizing the Fourier modal method. This is both a popular and versatile method that has been changed and reformulated throughout the years with a widely used reformulation which came in 1996 when Lifeng Li improved the convergence time for P-polarized electromagnetic waves<sup>[16]</sup>.

Since then, the Fourier modal method has been used for calculating the optical properties of a multitude of components of photonics, such as bent waveguides by utilizing cylindrical coordinates<sup>[17]</sup>, Moiré lattices<sup>[18]</sup> as well as multiple metal structures exhibiting extremely large fields due to surface plasmons<sup>[18, 19, 20, 21]</sup>. It can also be used as in this project, calculating a dielectric grating incident by a light source from above<sup>[22, 23]</sup>

This project seeks to investigate three different formulations of the three-dimensional Fourier modal method by calculations of the transmittance of photonic crystals for frequencies in the terahertz regime. First by a simple approach where Fourier coefficients of the permittivity are calculated by direct integration. Secondly the approach developed by Lifeng Li<sup>[16, 24]</sup>. Thirdly, an approach that removes the jump discontinuities from the problem by utilizing tensor averaging in real space, like the technique used by Johnson and Joannopoulos<sup>[25]</sup>. Furthermore, how the geometric properties of the crystal affects the transmittance through the crystal is examined as well as a model trying to locate Fano resonances of the structure is constructed.

# Chapter 2

## Photonic Crystal Structure

The microstructures being modeled in this project will have different parameters influencing the desired results, i.e. the absorption and transmission spectra of the electromagnetic waves that are sent through these structures. The photonic crystal consists of a periodic structure, and two examples will be used: a plate with finite thickness and rods placed periodically and a plate, also with finite thickness, and periodically displaced holes.

These structures will be described in this chapter and their characteristics and permittivities as a function of position will be presented. Lastly, tables listing the structures with their characteristics and parameters will be provided.

### 2.1 Lattice

The way the rods/holes are displaced will define the unit cell to be used when modeling the material. Two types of lattices will be approached in this project: the primitive rectangular and the hexagonal lattices. Examples of these periodic patterns are illustrated in Figure 2.1, where the unit cells are represented with a white-contoured rectangle.

The rectangular lattice from Figure 2.1a has periods  $\Lambda_x$  and  $\Lambda_y$  and in a case where  $\Lambda_x = \Lambda_y$ , the structure is a square (Sq.) lattice.

In the hexagonal (Hex.) lattice, the proportion between the periods will be constant, i.e.  $\Lambda_x = \sqrt{3}\Lambda_y$ . Knowing that the angle between the two right corners from the center of the cell is of 60 degrees, the length of the period is given by

$$\Lambda_x = \Lambda_y 2 \sin \frac{\pi}{3}. \quad (2.1)$$

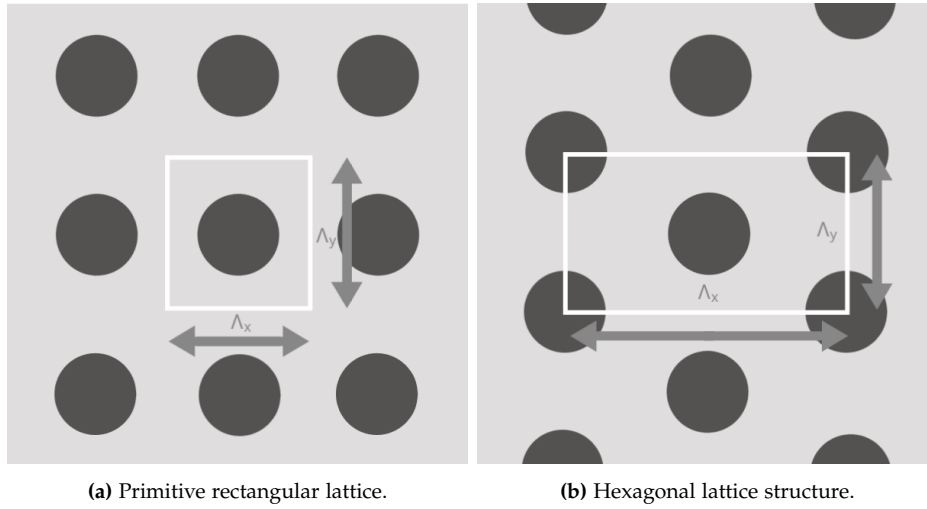


**Figure 2.1:** Structure of the periodic layer, showcasing the rectangular and hexagonal lattice. The white rectangles mark the border of the respective unit cells.

These periods will help describe the permittivity of the structure, where  $m$  and  $n$  are integers:

$$\varepsilon(x, y) = \varepsilon(x + m\Lambda_x, y + n\Lambda_y). \quad (2.2)$$

## 2.2 Shape

Considering periodic structures with varying permittivities, another essential attribute will be the shape, more specifically, the shape of the cross section of the structure in the  $x, y$ -plane. Within a unit cell, the permittivity will vary and can thus be described depending on the shape. The permittivity  $\varepsilon_2$  refers to the material inside, i.e. the rods or holes, while  $\varepsilon_1$  is the material outside, as illustrated in Figure 2.2.

Figures 2.3, 2.4 and 2.5 show a three-dimensional illustration of the photonic crystals. In a rectangular lattice with rectangular-shaped rods/holes, the square rods will have sides  $a$  and  $b$ , respectively in the  $x$  and  $y$  directions, for instance, the rectangular-shaped rods presented in Figure 2.3. In a lattice with circular rods/holes, the circles will have a radius  $a$ , an example of circular rods in a rectangular lattice is depicted in Figure 2.4.

In these cases, the permittivity is usually written with step functions  $\Theta(\vec{r})$ . For instance,



**Figure 2.2:** Unit cell of a material with permittivity  $\varepsilon_1$  in the surroundings and  $\varepsilon_2$  inside the structure.

rectangular-shaped rods/holes yield

$$\varepsilon(x, y) = (\varepsilon_2 - \varepsilon_1) \Theta_x \left( |x| - \frac{a}{2} \right) \Theta_y \left( |y| - \frac{b}{2} \right) + \varepsilon_1. \quad (2.3)$$

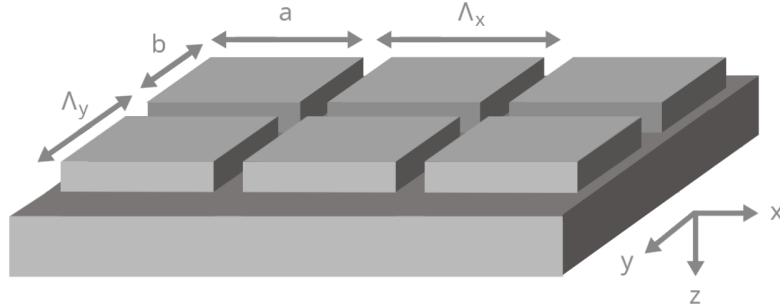


**Figure 2.3:** Rectangular lattice with rectangular-shaped rods on a homogeneous plate.

As for circular-shaped structures with  $\mathbf{r} = x\hat{\mathbf{x}} + y\hat{\mathbf{y}}$ , the permittivity is given by

$$\varepsilon(\mathbf{r}) = (\varepsilon_2 - \varepsilon_1) \Theta(|\mathbf{r}| - a) + \varepsilon_1. \quad (2.4)$$

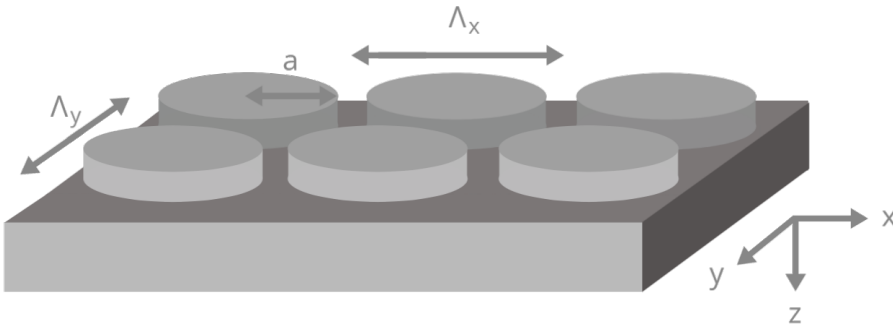


**Figure 2.4:** Rectangular lattice with circular-shaped rods on a homogeneous plate.

Furthermore, the third case being approached will be one-dimensional periodic bars, as illustrated in Figure 2.5. The permittivity will only depend on the  $x$ -direction:

$$\varepsilon(x) = (\varepsilon_2 - \varepsilon_1) \Theta \left( |x| - \frac{a}{2} \right) + \varepsilon_1. \quad (2.5)$$

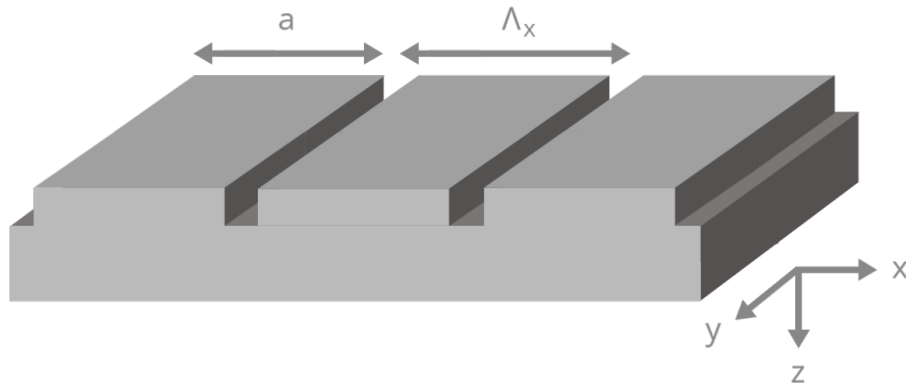


**Figure 2.5:** One-dimensional periodic structure on a homogeneous plate.

## 2.3 Layers

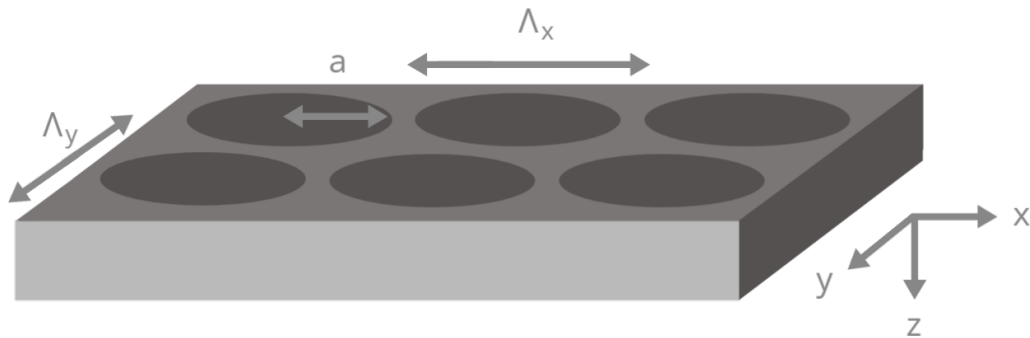


**Figure 2.6:** Circular-shaped holes with radius  $a$  periodically displaced on a plate in a primitive rectangular lattice with periods  $\Lambda_x$  and  $\Lambda_y$ .

The two types of photonic crystals modeled in this report are referred to as rods and holes. They consist of the following:

- An infinite slab of a homogeneous material with a layer of periodically arranged rods or bars of the same material of permittivity  $\varepsilon_2$  surrounded by another material with parameter  $\varepsilon_1$  (see Figures 2.3, 2.4 and 2.5).
- An infinite slab of some material with permittivity  $\varepsilon_1$  with periodically arranged holes with the same permittivity as the surroundings, i.e.  $\varepsilon_2$  (see Figure 2.6).

In the first case, the model will consist of four layers, the upper layer with homogeneous surrounding material (air), the periodic layer, the homogeneous plate (silicon) and the bottom layer with the surrounding material (air). The second case will only have three layers, the upper one with the surrounding medium (air), the periodic layer, and the bottom one just as the upper layer.

The thickness of the periodic layer is given by  $h_1$ , and  $h_2$  will refer to the homogeneous silicon layer, when it is present (see Figure 2.7).

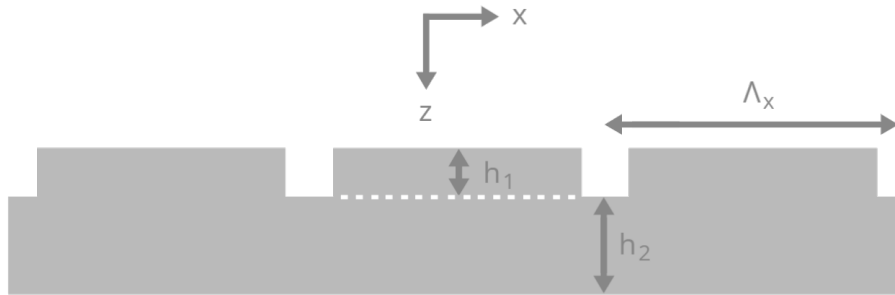


**Figure 2.7:** Cross section of the microstructure with periodic and homogeneous layers. The periodic layer consisting of air and silicon has thickness  $h_1$  and the homogeneous Silicon layer has thickness  $h_2$ .

## 2.4 The Structures

The different structures modeled will be referred to by their different names, which are presented in the following tables: Table 2.1 names all the structures with bars and square-shaped rods/holes, while Table 2.2 names the circular-shaped ones.

Structure	Lattice	R/H	$\Lambda_x$ [ $\mu\text{m}$ ]	$\Lambda_y$ [ $\mu\text{m}$ ]	$a$ [ $\mu\text{m}$ ]	$b$ [ $\mu\text{m}$ ]	$h_1$ [ $\mu\text{m}$ ]	$h_2$ [ $\mu\text{m}$ ]
SRS1	Sq.	Rods	99.7	99.7	32.5	32.5	12.9	92.1
SRS2	Sq.	Rods	99.7	99.7	42.5	42.5	12.9	92.1
SHS1	Sq.	Holes	99.7	99.7	32.5	32.5	105	N/A
SHS2	Sq.	Holes	99.7	99.7	42.5	42.5	105	N/A
B1	N/A	N/A	99.7	N/A	32.5	N/A	12.9	92.1
B2	N/A	N/A	99.7	N/A	42.5	N/A	12.9	92.1

**Table 2.1:** Characteristics of different bars as well as square-shaped rods/holes structures. SRS and SHS are square rods/holes and B is two versions of the 1D periodic structure.

The names of the structures are intuitively related to their characteristics, such that, in the three-letter names, the first letter represents the lattice structures: square - S, and hexagonal - H. The second letter stands for rods - R, and holes - H. The last letter represents the shape: square - S, and circular - C. As for the one-letter names, the B stands for bar, meaning the structure is periodic only in one dimension, as seen in Figure 2.5.

Structure	Lattice	R/H	$\Lambda_x$ [ $\mu\text{m}$ ]	$\Lambda_y$ [ $\mu\text{m}$ ]	$a$ [ $\mu\text{m}$ ]	$h_1$ [ $\mu\text{m}$ ]	$h_2$ [ $\mu\text{m}$ ]
SRC1	Sq.	Rods	99.7	99.7	18.34	12.9	92.1
SRC2	Sq.	Rods	99.7	99.7	16.25	12.9	92.1
SHC1	Sq.	Holes	99.7	99.7	18.34	105	N/A
HRC1	Hex.	Rods	99.7	99.7	18.34	12.9	92.1
HHC1	Hex.	Holes	99.7	99.7	18.34	105	N/A

**Table 2.2:** Characteristics of different circular-shaped rods/holes with radius  $a$ .

Knowing the structures of interest will allow one to understand their interaction with electromagnetic waves by setting up models and utilizing the parameters described above. Furthermore, it also allows one to analyze how these parameters influence the behavior.

# Chapter 3

## The Fourier Modal Method

This chapter aims to present and construct a model to find propagating modes, which allow one to calculate the transmission of electromagnetic waves through a material with some periodic structure with permittivity using the Fourier modal method. First, the Floquet Theorem and Fourier expansion will be introduced, since they cover the theory behind the method. After that, the method will start being constructed focusing on the three-dimensional structure and include both S- and P-polarized electromagnetic waves.

The homogeneous and periodic layers will be approached separately since the field in the periodic layer will be described making use of an eigenvalue problem. Furthermore, the averaging of the permittivity of the periodic structure will be presented using the simple method as well as Lifeng Li's rules<sup>[16, 24]</sup>. Finally, the tensor averaging is addressed. All these methods will be applied to the structures described in Chapter 2.

The materials are assumed to be non-magnetic, leading to a relative permeability  $\mu$  equal to unity. The well-known differential Maxwell's equations below will be the governing equations throughout the theory

$$\nabla \times \mathbf{E} = -\partial_t \mathbf{B} = i\omega\mu_0 \mathbf{H} \quad (3.1)$$

$$\nabla \times \mathbf{H} = \partial_t \mathbf{D} + \mathbf{J} = -i\omega\varepsilon_0\varepsilon \mathbf{E} \quad (3.2)$$

$$\nabla \cdot \mathbf{D} = \rho = 0 \quad (3.3)$$

$$\nabla \cdot \mathbf{B} = 0, \quad (3.4)$$

where  $\mathbf{B} = \mu_0 \mathbf{H}$  and  $\mathbf{D} = \varepsilon_0 \varepsilon \mathbf{E}$ .  $\mathbf{J}$  is the electric current density and  $\rho$  is the electric charge density, which equal zero for materials without charges and currents.<sup>[6]</sup> The second equality in equations (3.1) and (3.2) comes from the time dependence of the electric and magnetic fields, which is  $e^{-i\omega t}$ , for some angular frequency  $\omega$ .

### 3.1 Floquet Theorem

The first step will be to present the Floquet Theorem. The Floquet Theorem gives a solution to a system with some translational symmetry provided by a periodic potential for instance in semiconductors or, in the case approached in this project, a structure with periodic permittivity. The three-dimensional version of this theorem is the Bloch Theorem and the solutions to the system are called Bloch waves.<sup>[6]</sup> The generalized form of the Floquet Theorem will be described below.

For a system of linear differential equations

$$\frac{d\mathbf{x}(t)}{dt} = A(t)\mathbf{x}(t), \quad (3.5)$$

where  $\mathbf{x}(t)$  is an  $n$  dimensional vector and  $A(t)$  is an  $n \times n$  dimensional coefficient matrix, with the period  $T$  i.e.

$$A(t + T) = A(t), \quad (3.6)$$

the solutions to this system have the form,

$$\mathbf{x}(t) = \sum_i^n c_i e^{k_i t} \mathbf{p}_i(t), \quad (3.7)$$

where  $c_i$  and  $k_i$  are constants and  $\mathbf{p}_i(t)$  is an  $n$  dimensional vector with the same period  $T$  as  $A(t)$ . The wave equation for electromagnetic fields is

$$\left( \nabla^2 + k_0^2 \varepsilon(\mathbf{r}) \right) \mathbf{F}(\mathbf{r}) = 0 \quad (3.8)$$

with periodic permittivity  $\varepsilon(\mathbf{r})$  that fulfills the Floquet theorem requirement (3.5), since a higher order partial differential equation (PDE) can be transformed into a system of first-order PDEs<sup>[26]</sup>. Consequently, the fields can be written on the form,

$$\mathbf{F}(\mathbf{r}) = F(\mathbf{r}) e^{i\beta z} \hat{\alpha} = e^{i\mathbf{k}_\perp \cdot \mathbf{r}} f(\mathbf{r}) e^{i\beta z} \hat{\alpha}, \quad (3.9)$$

where  $f(\mathbf{r})$  is a function with the same periodicity as the structure,  $\hat{\alpha}$  is the polarization,  $\beta$  is the propagation constant and  $\mathbf{k} = (k_x \hat{x} + k_y \hat{y})$ .<sup>[6, 27]</sup>

### 3.2 Fourier Expansion

The solution to the wave equation for electromagnetic fields is given by (3.9), where  $f(\mathbf{r})$  is a periodic function and this leads to a way of representing it, which can then be applied

when constructing the model for the photonic crystals since the system satisfies the Floquet Theorem.

Any periodic function can be expressed as a Fourier sum of harmonic functions, such as plane waves, with the same period as the expanded function<sup>[28]</sup>. Thus,

$$f(\mathbf{r}) = \sum_{m=-\infty}^{\infty} \sum_{n=-\infty}^{\infty} \tilde{f}_{mn} e^{i\mathbf{G}_{mn} \cdot \mathbf{r}}, \quad (3.10)$$

where  $\mathbf{G}_{mn} = (mG_x \hat{x} + nG_y \hat{y})$ ,  $G_\sigma = 2\pi/\Lambda_\sigma$ ,  $\Lambda_\sigma$  is the period of the structure, in the  $\sigma$  direction and  $\tilde{f}_{mn}$  are the Fourier coefficients. Finally, the expansion of the fields become,

$$F(\mathbf{r}) = \sum_{m=-\infty}^{\infty} \sum_{n=-\infty}^{\infty} \tilde{f}_{mn} e^{i\mathbf{k}_\perp \cdot \mathbf{r}} e^{i\mathbf{G}_{mn} \cdot \mathbf{r}}. \quad (3.11)$$

The permittivity is expanded in a Fourier series as well:

$$\varepsilon(x, y) = \sum_{m=-\infty}^{\infty} \sum_{n=-\infty}^{\infty} \tilde{\varepsilon}_{mn} e^{imG_x x} e^{inG_y y}. \quad (3.12)$$

The expansion of the electromagnetic field and the permittivity will be used to develop the desired model for the photonic crystals.

### 3.3 The Homogeneous Layer

Now, the Floquet Theorem and Fourier Expansion will be applied and the model will start being constructed. As stated in the previous section, it involves the expansion of the electromagnetic field and permittivity. The model will consist of homogeneous layers and a periodic layer. Each type will need to be approached differently, and as a starting point, the homogeneous layer is the one to be described.

The Fourier modal method in three dimensions will be developed taking into account both S- and P-polarization. Consider an infinite structure with periods  $\Lambda_x$  and  $\Lambda_y$  in the  $x, y$ -plane and a finite length in the  $z$ -direction. Here, the problem is described with the electric field as a starting point, from which the magnetic field can be derived. The wavevector components of the  $m, n$  mode are given by:

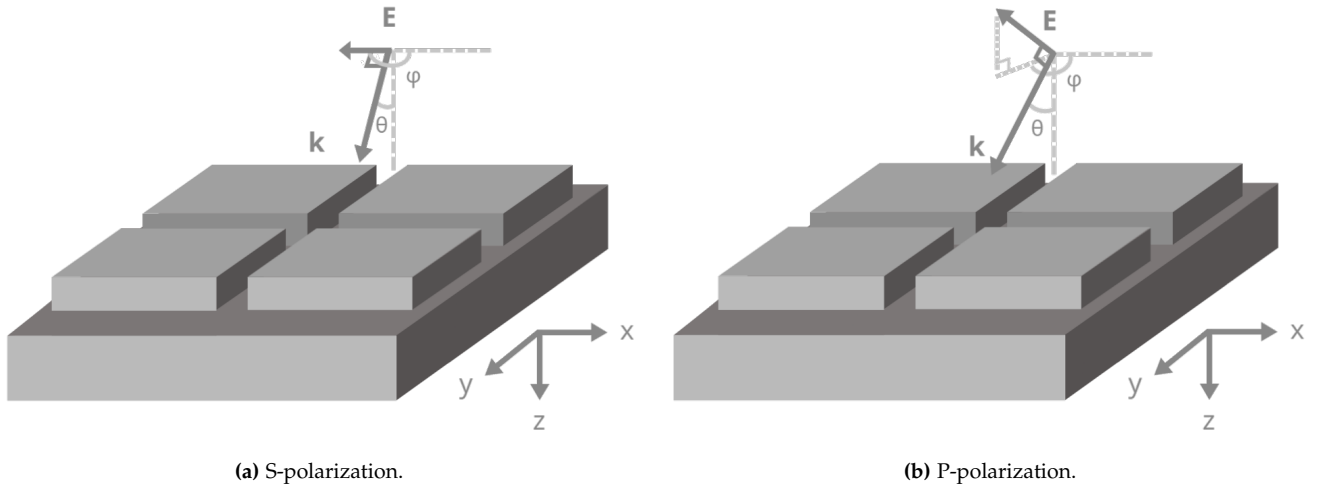


**Figure 3.1:** Illustration of photonic crystals with incident electric fields in both S- and P-polarizations.

$$k_{x,m,n} = k_{x0} + mG_x, \quad k_{x0} = k_0 \sin \theta \cos \varphi, \quad (3.13)$$

$$k_{y,m,n} = k_{y0} + nG_y, \quad k_{y0} = k_0 \sin \theta \sin \varphi, \quad (3.14)$$

where  $k_0 = \frac{2\pi}{\lambda_0}$ , for an incident wave with vacuum wavelength  $\lambda_0$  satisfying the relation

$$k_0^2 \varepsilon = k_{x,m,n}^2 + k_{y,m,n}^2 + k_{z,m,n}^2 \quad (3.15)$$

for a homogeneous material with relative permittivity  $\varepsilon$ . This allows the  $z$  component of the wavevector  $\mathbf{k}_{m,n} = k_{x,m,n}\hat{\mathbf{x}} + k_{y,m,n}\hat{\mathbf{y}} + k_{z,m,n}\hat{\mathbf{z}}$  to be written as

$$k_{z,m,n} = \sqrt{k_0^2 \varepsilon - k_{x,m,n}^2 - k_{y,m,n}^2}. \quad (3.16)$$

Examples of electric fields incident on a photonic crystal are illustrated in Figure 3.1 for each polarization. The components of the electric field can be written in the following general form:

$$E_x^{(j)}(x, y, z) = \sum_q \sum_{m=-M}^M \sum_{n=-N}^N E_{x,m,n}^{(j,q)} e^{i\mathbf{k}_{m,n} \cdot \mathbf{r}}, \quad (3.17)$$

$$E_y^{(j)}(x, y, z) = \sum_q \sum_{m=-M}^M \sum_{n=-N}^N E_{y,m,n}^{(j,q)} e^{i\mathbf{k}_{m,n} \cdot \mathbf{r}} \quad (3.18)$$

$$E_z^{(j)}(x, y, z) = \sum_q \sum_{m=-M}^M \sum_{n=-N}^N E_{z,m,n}^{(j,q)} e^{i\mathbf{k}_{m,n} \cdot \mathbf{r}} \quad (3.19)$$

for  $\mathbf{r} = x\hat{\mathbf{x}} + y\hat{\mathbf{y}} + z\hat{\mathbf{z}}$ , layer  $j$  and  $q$ , which indexes the modes and sums from  $q = 1$  to  $(2M + 1)(2N + 1)$ . The structure is divided into layers, as described in Section 2.3, such that one layer will be periodic and the others consist of some homogeneous material. The number of modes is  $2M + 1$  in the  $x$ -direction and  $2N + 1$  in  $y$ -direction. The reciprocal lattice vector components are  $G_{x,y} = \frac{2\pi}{\Lambda_{x,y}}$ .

The coefficients  $E_{x,m,n}^{(i)}$  and  $E_{y,m,n}^{(i)}$  are found for each layer, and in the periodic case, an eigenvalue problem is set up. For homogeneous layers, equation (3.3) is used and can be rewritten as  $\nabla \cdot \mathbf{E} = 0$ .

The electric field in the S-polarization will have components in the  $x$  and  $y$  directions, while the  $z$  component simply equals 0. Taking the divergence of each term in the sum yields

$$\begin{aligned} & \partial_x(E_{x,m,n}e^{i\mathbf{k}_{m,n}\cdot\mathbf{r}}) + \partial_y(E_{y,m,n}e^{i\mathbf{k}_{m,n}\cdot\mathbf{r}}) \\ &= ik_{x,m,n}E_{x,m,n}e^{i\mathbf{k}_{m,n}\cdot\mathbf{r}} + ik_{y,m,n}E_{y,m,n}e^{i\mathbf{k}_{m,n}\cdot\mathbf{r}} = 0. \end{aligned} \quad (3.20)$$

The electric field Fourier coefficients need to be chosen such that eq. (3.20) is satisfied. The coefficients for the  $x$  component can be chosen to be  $-Ak_{y,m,n}$  and thus the  $y$  component needs to be  $Ak_{x,m,n}$ , where  $A$  is a normalizing constant:

$$\mathbf{E}_{m,n}^S(x, y, z) = A(-\hat{\mathbf{x}}k_{y,m,n} + \hat{\mathbf{y}}k_{x,m,n})e^{i(mG_x x + nG_y y)}e^{i(k_{x0}x + k_{y0}y)}e^{ik_{z,m,n}z}. \quad (3.21)$$

The field in the P-polarization can be found by taking the cross-product of the wave vector and the S-polarization.

$$\mathbf{E}_{m,n}^P(x, y, z) = \mathbf{k}_{m,n} \times \mathbf{E}_{m,n}^S \quad (3.22)$$

$$= A(-k_{x,m,n}k_{z,m,n}\hat{\mathbf{x}} - k_{y,m,n}k_{z,m,n}\hat{\mathbf{y}} + (k_{x,m,n}k_{x,m,n} + k_{y,m,n}k_{y,m,n})\hat{\mathbf{z}})e^{i\mathbf{k}_{m,n}\cdot\mathbf{r}}. \quad (3.23)$$

The transformation of the electric field in homogeneous layers to the Fourier space can thus be presented

$$\bar{\bar{\mathbf{E}}} = \begin{bmatrix} \bar{\bar{E}}_x \\ \bar{\bar{E}}_y \end{bmatrix} = \begin{bmatrix} -\bar{\bar{K}}_y & -\bar{\bar{K}}_x \\ \bar{\bar{K}}_x & -\bar{\bar{K}}_y \end{bmatrix}. \quad (3.24)$$

The first column refers to the S-polarization and the second column to the P-polarization,

and the matrices  $\overline{\overline{\mathbf{K}}}_x$  and  $\overline{\overline{\mathbf{K}}}_y$  are built as

$$\overline{\overline{\mathbf{K}}}_x = \begin{bmatrix} \overline{\overline{\mathbf{K}}}_{x,-M} & \overline{\mathbf{0}} & \cdots & \overline{\mathbf{0}} \\ \overline{\mathbf{0}} & \overline{\overline{\mathbf{K}}}_{x,-M+1} & \cdots & \overline{\mathbf{0}} \\ \vdots & \vdots & \ddots & \vdots \\ \overline{\mathbf{0}} & \overline{\mathbf{0}} & \cdots & \overline{\overline{\mathbf{K}}}_{x,M} \end{bmatrix}, \quad (3.25)$$

$$\overline{\overline{\mathbf{K}}}_y = \begin{bmatrix} \overline{\overline{\mathbf{K}}}_{y,-M} & \overline{\mathbf{0}} & \cdots & \overline{\mathbf{0}} \\ \overline{\mathbf{0}} & \overline{\overline{\mathbf{K}}}_{y,-M+1} & \cdots & \overline{\mathbf{0}} \\ \vdots & \vdots & \ddots & \vdots \\ \overline{\mathbf{0}} & \overline{\mathbf{0}} & \cdots & \overline{\overline{\mathbf{K}}}_{y,M} \end{bmatrix}, \quad (3.26)$$

where

$$\overline{\overline{\mathbf{K}}}_{x,m} = \begin{bmatrix} k_{x,m,-N} & 0 & \cdots & 0 \\ 0 & k_{x,m,-N+1} & \cdots & 0 \\ \vdots & \vdots & \ddots & \vdots \\ 0 & 0 & \cdots & k_{x,m,N} \end{bmatrix}, \quad (3.27)$$

$$\overline{\overline{\mathbf{K}}}_{y,m} = \begin{bmatrix} k_{y,m,-N} & 0 & \cdots & 0 \\ 0 & k_{y,m,-N+1} & \cdots & 0 \\ \vdots & \vdots & \ddots & \vdots \\ 0 & 0 & \cdots & k_{y,m,N} \end{bmatrix}. \quad (3.28)$$

From the electric field it is possible to find the magnetic field from equations (3.1) and (3.2):

$$i\omega\mu_0 H_x = \partial_y E_z - \partial_z E_y, \quad (3.29)$$

$$i\omega\mu_0 H_y = \partial_z E_x - \partial_x E_z, \quad (3.30)$$

$$i\omega\mu_0 H_z = \partial_x E_y - \partial_y E_x. \quad (3.31)$$

$$-i\omega\varepsilon_0\varepsilon E_x = \partial_y H_z - \partial_z H_y, \quad (3.32)$$

$$-i\omega\varepsilon_0\varepsilon E_y = \partial_z H_x - \partial_x H_z, \quad (3.33)$$

$$-i\omega\varepsilon_0\varepsilon E_z = \partial_x H_y - \partial_y H_x, \quad (3.34)$$

Isolating  $\partial_z H_x$  and  $\partial_z H_y$  from equations (3.32) and (3.33), and writing  $H_z$  in terms of  $E_x$  and  $E_y$ , as in eq. (3.31), yields

$$\partial_z H_x = \frac{1}{i\omega\mu_0} \partial_x (\partial_x E_y - \partial_y E_x) - i\omega\varepsilon_0\varepsilon E_y, \quad (3.35)$$

$$\partial_z H_y = \frac{1}{i\omega\mu_0} \partial_y (\partial_x E_y - \partial_y E_x) + i\omega\varepsilon_0\varepsilon E_x. \quad (3.36)$$

From equations (3.17) and (3.18), it can be shown that taking the partial derivative of a component of the electric field will also result in a periodic function  $f(x, y, z)$  that can as well be expressed as a Fourier expansion with coefficients  $f_{m,n}$ . For example for  $E_x$ :

$$f(x, y, z) = \partial_x E_x(x, y) = \sum_{n,m} i(mG_x + k_x) E_{x,m,n} e^{i(mG_x x + nG_y y)} e^{i(k_{x0}x + k_{y0}y)} e^{ik_{z,m,n}z} \quad (3.37)$$

$$= \sum_{m,n} f_{m,n} e^{i(nG_x x + mG_y y)} e^{i(k_{x0}x + k_{y0}y)} e^{ik_{z,m,n}z}. \quad (3.38)$$

This means that the matrix with the Fourier coefficients is given by

$$\bar{\bar{f}} = i\bar{\bar{K}}_x \bar{\bar{E}}_x. \quad (3.39)$$

Thus, applying this to equations (3.35) and (3.36), an expression for the magnetic field can be written

$$\bar{\bar{H}} = \begin{bmatrix} \bar{\bar{H}}_x \\ \bar{\bar{H}}_y \end{bmatrix} = \frac{1}{\omega\mu_0} \begin{bmatrix} -\bar{\bar{K}}_x \bar{\bar{K}}_y & \bar{\bar{K}}_x \bar{\bar{K}}_x - \omega^2 \mu_0 \epsilon_0 \bar{\bar{\epsilon}} \\ -\bar{\bar{K}}_y \bar{\bar{K}}_y + \omega^2 \mu_0 \epsilon_0 \bar{\bar{\epsilon}} & \bar{\bar{K}}_y \bar{\bar{K}}_x \end{bmatrix} \begin{bmatrix} \bar{\bar{E}}_x \\ \bar{\bar{E}}_y \end{bmatrix} \bar{\bar{K}}_z^{-1}. \quad (3.40)$$

Since this relation is derived from Maxwell's equations it also applies to the electromagnetic fields in dielectric periodic layer.

### 3.4 The Periodic Layer

The periodic layer is however not as simple, since equation (3.16) does not apply. The periodic structure consists of materials with different permittivity, and thus the eigenmodes  $\beta = k_{z,m,n}$  that propagate through the structure are to be found by setting up an eigenvalue problem.

Given that the permittivity in this layer is periodic along the  $x, y$ -plane, it can be written as in equation (2.2):

$$\varepsilon(x, y) = \varepsilon(x + m\Lambda_x, y + n\Lambda_y),$$

for integers of  $m$  and  $n$ . This allows one to express it as a Fourier expansion:

$$\varepsilon(\mathbf{r}) = \varepsilon(x, y) = \sum_{m,n} \varepsilon_{m,n} e^{imG_x x} e^{inG_y y}, \quad (3.41)$$

where the coefficients can be found with the following integral

$$\varepsilon_{m,n} = \frac{1}{\Lambda_x \Lambda_y} \int_{-\frac{\Lambda_y}{2}}^{\frac{\Lambda_y}{2}} \int_{-\frac{\Lambda_x}{2}}^{\frac{\Lambda_x}{2}} \varepsilon(x, y) e^{-imG_x x} e^{-inG_y y} dx dy, \quad (3.42)$$

and the permittivity matrix consisting of these coefficients is

$$\bar{\bar{\epsilon}} = \begin{bmatrix} \bar{\bar{\epsilon}}_0 & \bar{\bar{\epsilon}}_{-1} & \cdots & \bar{\bar{\epsilon}}_{-2M} \\ \bar{\bar{\epsilon}}_1 & \bar{\bar{\epsilon}}_0 & \cdots & \bar{\bar{\epsilon}}_{-2M+1} \\ \vdots & \vdots & \ddots & \vdots \\ \bar{\bar{\epsilon}}_{2M} & \bar{\bar{\epsilon}}_{2M-1} & \cdots & \bar{\bar{\epsilon}}_0 \end{bmatrix} \quad (3.43)$$

for matrices  $\bar{\bar{\epsilon}}_m$  in the form

$$\bar{\bar{\epsilon}}_m = \begin{bmatrix} \epsilon_{m,0} & \epsilon_{m,-1} & \cdots & \epsilon_{m,-2N} \\ \epsilon_{m,1} & \epsilon_{m,0} & \cdots & \epsilon_{m,-2N+1} \\ \vdots & \vdots & \ddots & \vdots \\ \epsilon_{m,2N} & \epsilon_{m,2N-1} & \cdots & \epsilon_{m,0} \end{bmatrix}. \quad (3.44)$$

The problem will be derived from Maxwell's equations. From eqs. (3.1) and (3.2), it can be written that

$$i\omega\mu_0 H_x = \partial_y E_z - i\beta E_y, \quad (3.45)$$

$$i\omega\mu_0 H_y = i\beta E_x - \partial_x E_z, \quad (3.46)$$

$$i\omega\mu_0 H_z = \partial_x E_y - \partial_y E_x, \quad (3.47)$$

$$-i\omega\epsilon_0\epsilon E_x = \partial_y H_z - i\beta H_y, \quad (3.48)$$

$$-i\omega\epsilon_0\epsilon E_y = i\beta H_x - \partial_x H_z, \quad (3.49)$$

$$-i\omega\epsilon_0\epsilon E_z = \partial_x H_y - \partial_y H_x, \quad (3.50)$$

where  $\beta$  is the propagation constant in the  $z$ -direction. From eqs. (3.3) and (3.4), the relations below are found:

$$\nabla \cdot \mathbf{H} = 0 \implies i\beta H_z + \partial_x H_x + \partial_y H_y = 0 \implies H_z = \frac{i}{\beta}(\partial_x H_x + \partial_y H_y), \quad (3.51)$$

$$\nabla \cdot \epsilon \mathbf{E} = 0 \implies i\beta\epsilon E_z + \partial_x \epsilon E_x + \partial_y \epsilon E_y = 0 \implies E_z = \frac{i}{\beta\epsilon}(\partial_x \epsilon E_x + \partial_y \epsilon E_y). \quad (3.52)$$

Inserting equation (3.47) into (3.48) and (3.49) gives

$$E_x = \frac{i}{\omega\epsilon_0\epsilon} \left( \partial_y \left( -\frac{i}{\omega\mu_0}(\partial_x E_y - \partial_y E_x) \right) - i\beta H_y \right), \quad (3.53)$$

$$E_y = \frac{i}{\omega\mu_0} \left( i\beta H_x - \partial_x \left( -\frac{i}{\omega\mu_0}(\partial_x E_y - \partial_y E_x) \right) \right). \quad (3.54)$$

In order to have an eigenvalue problem, the magnetic field terms left in the equations will be substituted by (3.45) and (3.46):

$$\omega^2 \mu_0 \varepsilon_0 \varepsilon E_x = i (\partial_y (-i(\partial_x E_y - \partial_y E_x)) - i\beta (-i(i\beta E_x - \partial_x E_z))), \quad (3.55)$$

$$\omega^2 \mu_0 \varepsilon_0 \varepsilon E_y = i (i\beta (-i(\partial_y E_z - i\beta E_y)) - \partial_x (-i(\partial_x E_y - \partial_y E_x))). \quad (3.56)$$

Furthermore,  $E_z$  from equation (3.52) can be inserted:

$$k_0^2 \varepsilon E_x = \partial_y (\partial_x E_y - \partial_y E_x) + \beta \left( \beta E_x + i \partial_x \frac{i}{\beta \varepsilon} (\partial_x \varepsilon E_x + \partial_y \varepsilon E_y) \right), \quad (3.57)$$

$$k_0^2 \varepsilon E_y = -\beta \left( -i(\partial_y \frac{i}{\beta \varepsilon} (\partial_x \varepsilon E_x + \partial_y \varepsilon E_y) - i\beta E_y) \right) - \partial_x (\partial_x E_y - \partial_y E_x). \quad (3.58)$$

Note that  $k_0^2 = \omega^2 \mu_0 \varepsilon_0$ . Rearranging the equations results in:

$$\beta^2 E_x = k_0^2 \varepsilon E_x - \partial_y \partial_x E_y + \partial_y \partial_y E_x + \partial_x \frac{1}{\varepsilon} \partial_x \varepsilon E_x + \partial_x \frac{1}{\varepsilon} \partial_y \varepsilon E_y, \quad (3.59)$$

$$\beta^2 E_y = k_0^2 \varepsilon E_y + \partial_y \frac{1}{\varepsilon} \partial_x \varepsilon E_x + \partial_y \frac{1}{\varepsilon} \partial_y \varepsilon E_x + \partial_x \partial_x E_y - \partial_x \partial_y E_x. \quad (3.60)$$

Making use of the rule explained in the previous section regarding the partial derivatives of the Fourier expanded terms (equations (3.37)-(3.39)), the relations will now be written as a system of matrix equations applying the matrices  $\overline{\overline{\mathbf{K}}}_x$ ,  $\overline{\overline{\mathbf{K}}}_y$  and  $\overline{\overline{\varepsilon}}$ . Each eigenvalue will have its corresponding eigenvector  $\mathbf{E} = \begin{bmatrix} \mathbf{E}_x \\ \mathbf{E}_y \end{bmatrix}$  such that

$$\mathbf{E}_x = \begin{bmatrix} E_{x,-M,-N} \\ \vdots \\ E_{x,-M,N} \\ E_{x,-M+1,-N} \\ \vdots \\ E_{x,-M+1,N} \\ \vdots \\ E_{x,M,-N} \\ \vdots \\ E_{x,M,N} \end{bmatrix}, \quad (3.61)$$

and similarly for  $\mathbf{E}_y$ . At last, the matrix eigenvalue problem will be:

$$\beta^2 \begin{bmatrix} \mathbf{E}_x \\ \mathbf{E}_y \end{bmatrix} = \left( k_0^2 \begin{bmatrix} \overline{\overline{\varepsilon}} & \overline{\mathbf{0}} \\ \overline{\mathbf{0}} & \overline{\overline{\varepsilon}} \end{bmatrix} - \left[ \begin{array}{l} \left( \overline{\overline{\mathbf{K}}}_y \overline{\overline{\mathbf{K}}}_y + \overline{\overline{\mathbf{K}}}_x \overline{\overline{\varepsilon}}^{-1} \overline{\overline{\mathbf{K}}}_x \overline{\overline{\varepsilon}} \right) \left( \overline{\overline{\mathbf{K}}}_x \overline{\overline{\varepsilon}}^{-1} \overline{\overline{\mathbf{K}}}_y \overline{\overline{\varepsilon}} - \overline{\overline{\mathbf{K}}}_y \overline{\overline{\mathbf{K}}}_x \right) \\ \left( \overline{\overline{\mathbf{K}}}_y \overline{\overline{\varepsilon}}^{-1} \overline{\overline{\mathbf{K}}}_x \overline{\overline{\varepsilon}} - \overline{\overline{\mathbf{K}}}_x \overline{\overline{\mathbf{K}}}_y \right) \left( \overline{\overline{\mathbf{K}}}_y \overline{\overline{\varepsilon}}^{-1} \overline{\overline{\mathbf{K}}}_y \overline{\overline{\varepsilon}} + \overline{\overline{\mathbf{K}}}_x \overline{\overline{\mathbf{K}}}_x \right) \end{array} \right] \right) \begin{bmatrix} \mathbf{E}_x \\ \mathbf{E}_y \end{bmatrix}. \quad (3.62)$$

Once again, the magnetic field in the periodic layer can be found from the electric field by using equation (3.40), and the vectors  $\mathbf{H}_x$  and  $\mathbf{H}_y$  are constructed in the same way as the electric field in eq. (3.61).

### 3.5 The Permittivity Matrix

Now, the structures described in Chapter 2 come into play. The permittivity matrix will vary depending on the periodic structure of the photonic crystal. This means that in order to build equation (3.43), the characteristics are needed: the coefficients will depend on the size, shape and lattice structure.

As stated before, the coefficients can be found by solving for the integral in equation (3.42)

$$\varepsilon_{m,n} = \frac{1}{\Lambda_x \Lambda_y} \int_{-\frac{\Lambda_y}{2}}^{\frac{\Lambda_y}{2}} \int_{-\frac{\Lambda_x}{2}}^{\frac{\Lambda_x}{2}} \varepsilon(x, y) e^{-imG_x x} e^{-inG_y y} dx dy,$$

and since  $\varepsilon(x, y)$  is known, it can be inserted into the equation. The coefficients for the structures of interest will be calculated below.

#### Rectangular-shaped rods/holes in rectangular lattices

The structure described in Section 2.2 has its permittivity given by equation (2.3):

$$\varepsilon(x, y) = (\varepsilon_2 - \varepsilon_1) \Theta_x \left( |x| - \frac{a}{2} \right) \Theta_y \left( |y| - \frac{b}{2} \right) + \varepsilon_1,$$

and inserting it in the integral in order to find the Fourier coefficients will give different expressions depending on values of  $m$  and  $n$ . For example, for  $m, n = 0$ , the coefficients will correspond to the geometric mean of the structure:

$$\varepsilon_{0,0} = \frac{1}{\Lambda_x \Lambda_y} \int_{-\frac{\Lambda_y}{2}}^{\frac{\Lambda_y}{2}} \int_{-\frac{\Lambda_x}{2}}^{\frac{\Lambda_x}{2}} \varepsilon(x, y) dx dy \quad (3.63)$$

$$= \frac{ab}{\Lambda_x \Lambda_y} (\varepsilon_2 - \varepsilon_1) + \frac{\Lambda_x \Lambda_y}{\Lambda_x \Lambda_y} \varepsilon_1. \quad (3.64)$$

However, for all equations where  $m \vee n \neq 0$ , the term of the integral

$$\frac{1}{\Lambda_x \Lambda_y} \int_y \int_x \varepsilon_1 e^{-imG_x x} e^{-inG_y y} dx dy$$

will equal zero, since:

$$\frac{1}{\Lambda_x \Lambda_y} \int_{-\frac{\Lambda_y}{2}}^{\frac{\Lambda_y}{2}} \int_{-\frac{\Lambda_x}{2}}^{\frac{\Lambda_x}{2}} \varepsilon_1 e^{-imG_x x} e^{-inG_y y} dx dy = \frac{\varepsilon_1}{\Lambda_x \Lambda_y} \left[ \frac{e^{-imG_x x}}{-imG_x} \right]_{-\frac{\Lambda_x}{2}}^{\frac{\Lambda_x}{2}} \left[ \frac{e^{-inG_y y}}{-inG_y} \right]_{-\frac{\Lambda_y}{2}}^{\frac{\Lambda_y}{2}} \quad (3.65)$$

$$= \frac{\varepsilon_1}{\Lambda_x \Lambda_y} \frac{2i \sin(m \frac{2\pi}{\Lambda_x} \frac{\Lambda_x}{2})}{imG_x} \frac{2i \sin(n \frac{2\pi}{\Lambda_y} \frac{\Lambda_y}{2})}{inG_y}, \quad (3.66)$$

where  $\sin m\pi = 0$  and  $\sin n\pi = 0$  for integers of  $m$  and  $n$ . For  $m \neq 0, n = 0$ , the step function will only give 1 when the integral goes from  $-\frac{a}{2}$  to  $\frac{a}{2}$ :

$$\varepsilon_{m,0} = (\varepsilon_2 - \varepsilon_1) \frac{b}{\Lambda_x \Lambda_y} \int_{-\frac{a}{2}}^{\frac{a}{2}} e^{-imG_x x} dx \quad (3.67)$$

$$= (\varepsilon_2 - \varepsilon_1) \frac{b}{\Lambda_x \Lambda_y} \frac{2i \sin(mG_x \frac{a}{2})}{imG_x}, \quad (3.68)$$

and similarly for  $m = 0, n \neq 0$ :

$$\varepsilon_{0,n} = (\varepsilon_2 - \varepsilon_1) \frac{a}{\Lambda_x \Lambda_y} \int_{-\frac{b}{2}}^{\frac{b}{2}} e^{-inG_y y} dy \quad (3.69)$$

$$= (\varepsilon_2 - \varepsilon_1) \frac{a}{\Lambda_x \Lambda_y} \frac{2i \sin(nG_y \frac{b}{2})}{inG_y}. \quad (3.70)$$

The last case involves  $m, n \neq 0$ , which results in:

$$\varepsilon_{m,n} = (\varepsilon_2 - \varepsilon_1) \frac{1}{\Lambda_x \Lambda_y} \int_{-\frac{a}{2}}^{\frac{a}{2}} e^{-imG_x x} dx \int_{-\frac{b}{2}}^{\frac{b}{2}} e^{-inG_y y} dy \quad (3.71)$$

$$= (\varepsilon_2 - \varepsilon_1) \frac{1}{\Lambda_x \Lambda_y} \frac{2i \sin(mG_x \frac{a}{2})}{imG_x} \frac{2i \sin(nG_y \frac{b}{2})}{inG_y}. \quad (3.72)$$

### Circular-shaped rods/holes in rectangular lattices

The symmetry in the circular rods/holes will allow one to solve the integral using polar coordinates. The permittivity is given by eq. (2.4), which in polar coordinates writes:

$$\varepsilon(r) = (\varepsilon_2 - \varepsilon_1) \Theta_r(r - a) + \varepsilon_1, \quad (3.73)$$

where the term  $\varepsilon_1$ , when integrated for  $m \vee n \neq 0$ , will give zero for the same reason as equation (3.65). However, for  $m, n = 0$ , the coefficients will be equal to the geometric mean of the structure:

$$\varepsilon_{0,0} = \frac{\pi a^2}{\Lambda_x \Lambda_y} (\varepsilon_2 - \varepsilon_1) + \frac{\Lambda_x \Lambda_y}{\Lambda_x \Lambda_y} \varepsilon_1. \quad (3.74)$$

As for the other coefficients, the reciprocal lattice vector  $\mathbf{G}_{m,n} = \hat{\mathbf{x}}mG_x + \hat{\mathbf{y}}nG_y$ , with a length given by  $G_{m,n} = \sqrt{m^2G_x^2 + n^2G_y^2}$ , the coordinate system will be chosen such that  $\mathbf{G}_{m,n} = G_{m,n}\hat{\mathbf{y}}$ . The integral can thus be rewritten:

$$\varepsilon_{m,n} = \frac{1}{\Lambda_x\Lambda_y} \int_{\varphi=0}^{2\pi} \int_{r=0}^a (\varepsilon_2 - \varepsilon_1) e^{-i\mathbf{G}_{m,n}\cdot\mathbf{r}} r dr d\varphi \quad (3.75)$$

$$= \frac{1}{\Lambda_x\Lambda_y} \int_{\varphi=0}^{2\pi} \int_{r=0}^a (\varepsilon_2 - \varepsilon_1) e^{-iG_{m,n}r \sin \varphi} r dr d\varphi \quad (3.76)$$

$$= \frac{1}{\Lambda_x\Lambda_y} (\varepsilon_2 - \varepsilon_1) \int_{r=0}^a 2\pi J_0(G_{m,n}r) r dr \quad (3.77)$$

$$= \frac{1}{\Lambda_x\Lambda_y} (\varepsilon_2 - \varepsilon_1) \frac{2\pi a}{G_{m,n}} J_1(G_{m,n}a). \quad (3.78)$$

The identities used when solving this integral are<sup>[29, 30]</sup>

$$\int_0^{2\pi} e^{-ix \sin \varphi} d\varphi = 2\pi J_0(x), \quad (3.79)$$

$$\int_0^a x J_0(x) dx = a J_1(a), \quad (3.80)$$

where  $J_\alpha$  are Bessel functions of the first kind.

### Circular-shaped rods/holes in hexagonal lattices

The hexagonal lattice described in Section 2.1 will have permittivity coefficients similar to the ones for the square lattice circular rods/holes. The main difference lies in the unit cell consisting of two rods/holes with some shift. This means that each rod/hole will contribute to the coefficients. For  $m, n = 0$ , the geometric mean gives

$$\varepsilon_{0,0} = \frac{2\pi a^2}{\Lambda_x\Lambda_y} (\varepsilon_2 - \varepsilon_1) + \frac{\Lambda_x\Lambda_y}{\Lambda_x\Lambda_y} \varepsilon_1. \quad (3.81)$$

And the other elements are given by the following sum of integrals for each rod/hole  $j$ :

$$\varepsilon_{m,n} = \sum_j \int \int_{x_j^2 + y_j^2 \leq a^2} (\varepsilon_2 - \varepsilon_1) e^{-imG_x x} e^{-inG_y y} dx dy \quad (3.82)$$

$$= (\varepsilon_2 - \varepsilon_1) \sum_j \int \int_{x_j^2 + y_j^2 \leq a^2} e^{-i(mG_x x_{c_j} + nG_y y_{c_j})} e^{-imG_x(x-x_{c_j})} e^{-inG_y(y-y_{c_j})} dx dy \quad (3.83)$$

Here, the variables  $x_j = x - x_{c_j}$  and  $y_j = y - y_{c_j}$  are introduced, such that  $(x_{c_j}, y_{c_j})$  refers to the center of the cylinder  $j$ . The integral was multiplied by 1 as  $e^{i(mG_x x_{c_j} + nG_y y_{c_j})} e^{-i(mG_x x_{c_j} + nG_y y_{c_j})}$ , and it can now be rewritten in polar coordinates for  $\mathbf{r} = x_j \hat{\mathbf{x}} + y_j \hat{\mathbf{y}}$  and  $r = \sqrt{x_j^2 + y_j^2}$ :

$$\varepsilon_{m,n} = (\varepsilon_2 - \varepsilon_1) \sum_j e^{-i(mG_x x_{c_j} + nG_y y_{c_j})} \int_{\varphi=0}^{2\pi} \int_{r=0}^a e^{-i\mathbf{G}_{m,n} \cdot \mathbf{r}} r dr d\varphi, \quad (3.84)$$

which makes it possible to calculate the integral as done in equations (3.75)-(3.78):

$$\varepsilon_{m,n} = (\varepsilon_2 - \varepsilon_1) \frac{1}{\Lambda_x \Lambda_y} \left( \sum_j e^{-i(mG_x x_{c_j} + nG_y y_{c_j})} \right) \frac{2\pi a}{G_{m,n}} J_1(G_{m,n} a) \quad (3.85)$$

$$= (\varepsilon_2 - \varepsilon_1) \frac{1}{\Lambda_x \Lambda_y} \left( 1 + e^{-i(mG_x \frac{\Lambda_x}{2} + nG_y \frac{\Lambda_y}{2})} \right) \frac{2\pi a}{G_{m,n}} J_1(G_{m,n} a). \quad (3.86)$$

The first rod/hole was chosen to be in the center  $(x_{c_1}, y_{c_1}) = (0, 0)$  and the other was chosen to be one arbitrary nearest neighbor centered at  $(x_{c_2}, y_{c_2}) = (\frac{\Lambda_x}{2}, \frac{\Lambda_y}{2})$ .

### 3.6 Li's Rules for Fourier Factorization

The content of this section aims to improve the computational time with the use of factorization rules that should result in the FMM converging faster. This section is a detailed derivation of the method described by Lifeng Li in the article [24]. A more specific structure with an orthogonal coordinate system will be described. The structure is divided into three layers where the top and bottom layers are homogeneous and the middle layer is the grating which will be the main focus of this section (see Figure 3.2).

First off, the notation will be defined for the Fourier coefficients for the two-dimensional periodic permittivity  $\varepsilon(x, y)$ , which are given by

$$\varepsilon_{m,n} = \frac{1}{\Lambda_x \Lambda_y} \int_0^{\Lambda_y} \int_0^{\Lambda_x} \varepsilon(x, y) e^{-i(mG_x x + nG_y y)} dx dy. \quad (3.87)$$

Now, it is defined that

$$[[\varepsilon]]_{mn, jl} = \varepsilon_{m-j, n-l}. \quad (3.88)$$

The Fourier coefficients in relation to either the  $x$  or  $y$  direction respectively are written as

$$[\varepsilon]_{mn} = \frac{1}{\Lambda_x} \int_0^{\Lambda_x} \varepsilon(x, y) e^{-i(m-n)G_x x} dx, \quad (3.89)$$

$$[\varepsilon]_{mn} = \frac{1}{\Lambda_y} \int_0^{\Lambda_y} \varepsilon(x, y) e^{-i(m-n)G_y y} dy. \quad (3.90)$$

Now the last notation to be defined is the combination of the two directions

$$[[\varepsilon]]_{mn,jl} = [\{[1/\varepsilon]^{-1}\}_{mj}]_{nl} = \frac{1}{\Lambda_y} \int_0^{\Lambda_y} \{[1/\varepsilon]^{-1}\}_{mj}(y) e^{-i(n-l)G_y y} dy \quad (3.91)$$

$$[[\varepsilon]]_{mn,jl} = [\{[1/\varepsilon]^{-1}\}_{nl}]_{mj} = \frac{1}{\Lambda_x} \int_0^{\Lambda_x} \{[1/\varepsilon]^{-1}\}_{nl}(x) e^{-i(m-j)G_x x} dx. \quad (3.92)$$

In all of this  $n, m, j, l$  runs from  $-M$  to  $M$  as was the case in Section 3.4.

In the homogeneous regions of the structure, the problem is straightforward and will briefly be defined. The incident plane wave vector can be expressed as

$$\mathbf{k} = k_{x0}\hat{x} + k_{y0}\hat{y} - k_{z0}^{(+1)}\hat{z} \quad (3.93)$$

where (+1) denotes that  $k_{z0}$  belongs to region +1 (above the grating layer in relation to the  $z$  direction). The coefficients are

$$\begin{aligned} k_{x0} &= k^{(+1)} \sin(\theta) \cos(\varphi), \\ k_{y0} &= k^{(+1)} \sin(\theta) \sin(\varphi), \\ k_{z0}^{(+1)} &= k^{(+1)} \cos(\theta), \end{aligned}$$

where  $k^{(+1)} = \frac{2\pi\sqrt{\varepsilon^{(+1)}\mu}}{\lambda_0}$ ,  $\theta$  and  $\varphi$  are the angles between the  $z$ - and  $x$ -axis, respectively, and the incident wave.

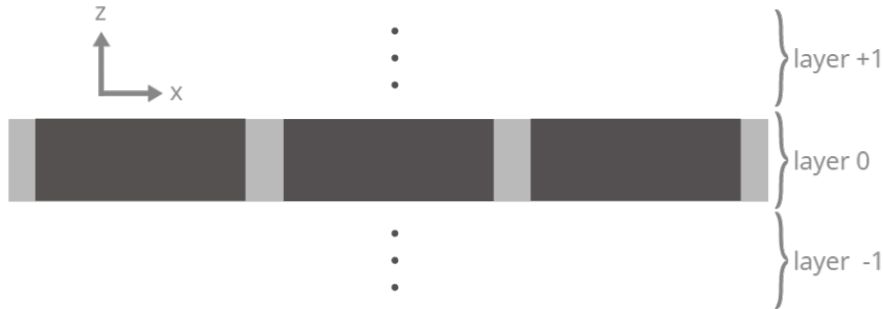


**Figure 3.2:** Illustration of the structure consisting of a periodic layer of air and silicon surrounded by homogeneous layers of air.

The components of the electric field can be expressed in regions  $\pm 1$  by Rayleigh expansion

as

$$E^{(+1)}(\mathbf{r}) = Ie^{i(k_{x0}x+k_{y0}y-k_{z0}^{(+1)}z)} + \sum_{m,n} R_{mn}e^{i(k'_x x+k'_y y+k_z'^{(+1)}z)}, \quad (3.94)$$

$$E^{(-1)}(\mathbf{r}) = \sum_{m,n} T_{mn}e^{i(k'_x x+k'_y y-k_z'^{(-1)}z)}, \quad (3.95)$$

where  $I, R_{mn}$  and  $T_{mn}$  are the incident, reflected and transmitted field amplitudes.

$$k'_x = k_{x0} + mG_x, \quad k'_y = k_{y0} + nG_y \quad (3.96)$$

and  $k_z'^{(a)}$  where  $a = \pm 1$  according to which region is described, can be found by

$$k^{(a)} = \sqrt{k_x'^2 + k_y'^2 + k_z'^{(a)2}}. \quad (3.97)$$

Before the electromagnetic field is to be described in the layer, the three factorization rules of Lifeng Li will be presented for a Fourier series that is the product of two periodic functions  $f$  and  $g$ . The rules are as follows<sup>[16]</sup>:

1. A product of two piecewise-smooth, bounded, periodic functions that have no concurrent jump can be Fourier factorized by Laurent's rule which writes:

$$h_n^{(M)} = \sum_{m=-M}^M f_{n-m} g_m \quad (3.98)$$

2. A product of two piecewise-smooth, bounded, periodic functions that have only pairwise complementary jump discontinuities cannot be Fourier factorized by Laurent's rule but can in most cases be Fourier factorized by the inverse rule which writes:

$$h_n^{(M)} = \sum_{m=-M}^M \left[ \left[ \frac{1}{f} \right] \right]_{n,m}^{(M)-1} g_m \quad (3.99)$$

3. A product of two piecewise-smooth, bounded, periodic functions that have concurrent but not complimentary jump discontinuities cannot be Fourier factorized by either Laurent's nor the inverse rule

By these rules, an eigenvalue problem for the grating layer can be built. First of all six components of the electromagnetic field can be expanded in the Floquet-Fourier series

$$\psi(x, y, z) = \sum_{m,n} \psi_{mn}(z)e^{i(k'_x x+k'_y y)}, \quad (3.100)$$

where  $\psi$  could be any of  $E_x, E_y, E_z, H_x, H_y$  or  $H_z$ . The Fourier coefficients are found through Maxwell's equations as seen in equations (3.29) to (3.34) with the slight rewriting of  $\omega = ck_0$ ,  $c$  being the speed of light in vacuum, becoming

$$\partial_y E_z - \partial_z E_y = ick_0 \mu H_x, \quad (3.101)$$

$$\partial_z E_x - \partial_x E_z = ick_0 \mu H_y, \quad (3.102)$$

$$\partial_x E_y - \partial_y E_x = ick_0 \mu H_z, \quad (3.103)$$

$$\partial_y H_z - \partial_z H_y = -ick_0 \varepsilon E_x, \quad (3.104)$$

$$\partial_z H_x - \partial_x H_z = -ick_0 \varepsilon E_y, \quad (3.105)$$

$$\partial_x H_y - \partial_y H_x = -ick_0 \varepsilon E_z. \quad (3.106)$$

Equations (3.101) to (3.103) as well as (3.106) have no product of discontinuities and can readily be factorized by Laurent's rule. Rewriting equation (3.106) as

$$E_z = \frac{i}{ck_0} \frac{1}{\varepsilon} (\partial_x H_y - \partial_y H_x), \quad (3.107)$$

and inserting in equation (3.101) yields

$$\frac{i}{ck_0} \partial_y \left( \frac{1}{\varepsilon} (\partial_x H_y - \partial_y H_x) \right) - \partial_z E_y = ick_0 \mu H_x \quad (3.108)$$

or

$$\frac{ck_0}{i} \partial_z E_y = -c^2 k_0^2 \mu H_x + \partial_y \left( \frac{1}{\varepsilon} (\partial_x H_y + \partial_y H_x) \right). \quad (3.109)$$

Now by Laurent's rule with the permittivity given as

$$\varepsilon(x, y) = \sum_{m,n} [\varepsilon]_{mn,jl} e^{i(m-j)G_x x + i(n-l)G_y y} \quad (3.110)$$

where, by equation (3.96), the exponent is rewritten to be

$$\begin{aligned} i(m-j)G_x x + i(n-l)G_y y &= imG_x x + inG_y y - ijG_x x - ilG_y y \\ &= i(k'_x x - k_{x0} x + k'_y y - k_{y0} y) - i(k''_x x - k_{x0} x + k''_y y - k_{y0} y) \\ &= i(k'_x x + k'_y y) - i(k''_x x + k''_y y) \end{aligned} \quad (3.111)$$

where  $k''_x = k_{x0} + jG_x$  and  $k''_y = k_{y0} + lG_y$ . Equation (3.109) becomes,

$$\begin{aligned} \frac{ck_0}{i} \partial_z \sum_{m,n} E_{ymn} e^{i(k'_x x + k'_y y)} &= -c^2 k_0^2 \mu \sum_{m,n} H_{xmn} e^{i(k'_x x + k'_y y)} \\ \partial_y \left( \sum_{j,l} \sum_{m,n} [\varepsilon]_{mn,jl}^{-1} e^{i(k'_x x + k'_y y) - i(k''_x x + k''_y y)} \right) &\left( \partial_x H_{yjl} e^{i(k''_x x + k''_y y)} - \partial_y H_{xjl} e^{i(k'_x x + k'_y y)} \right) \end{aligned} \quad (3.112)$$

$$\Rightarrow \frac{ck_0}{i} \partial_z E_{Eymn} = -c^2 k_0^2 \mu H_{xmn} - k'_y \sum_{j,l} [\varepsilon]_{mn,jl}^{-1} (k''_x H_{yjl} - k''_y H_{xjl}). \quad (3.113)$$

In the same manner by once again inserting equation(3.106) into (3.102) a second equation can be found to be

$$\frac{ck_0}{i} \partial_z E_{xmn} = c^2 k_0^2 \mu H_{ymn} - k'_x \sum_{j,l} [\varepsilon]_{mn,jl}^{-1} (k''_x H_{yjl} - k''_y H_{xjl}). \quad (3.114)$$

The equations (3.104) and (3.105) get slightly more complicated.  $\varepsilon E_x$  in relation to the  $x$ -direction and  $\varepsilon E_y$  to the  $y$ -direction is continuous, however  $\varepsilon$ ,  $E_x$  and  $E_y$  is not. Lifeng Li's inverse rule applies, meaning that the permittivity will be represented by coefficients  $\left[\frac{1}{\varepsilon}\right]^{-1}$ . Starting out with equation (3.103) and rewriting it as

$$H_z = \frac{1}{ik_0 \mu} (\partial_x E_y - \partial_y E_x), \quad (3.115)$$

and inserting it into equation (3.104) yields

$$\frac{1}{ick_0} \left( \frac{\partial_y}{ick_0 \mu} (\partial_x E_y - \partial_y E_x) - \partial_z H_y \right) = -\varepsilon E_x \quad (3.116)$$

Now, first expanding in a Fourier series related to the  $x$ -direction it becomes

$$\begin{aligned} & \frac{1}{ick_0} \left( \frac{\partial_y}{ick_0 \mu} \left( \partial_x \sum_m E_{ym} e^{ik'_x x} - \partial_y \sum_m E_{xm} e^{ik'_x x} \right) - \partial_z \sum_m H_{ym} e^{ik'_x x} \right) \\ &= - \sum_m \sum_j \left[ \frac{1}{\varepsilon} \right]_{mj}^{-1} e^{i(k'_x x - k''_x x)} E_{xj} e^{ik'_x x} \end{aligned} \quad (3.117)$$

$$\Rightarrow \left( \frac{-\partial_y}{c^2 k_0^2 \mu} (ik'_x E_{ym} - \partial_y E_{xm}) - \frac{1}{ick_0} \partial_z H_{ym} \right) = - \sum_j \left[ \frac{1}{\varepsilon} \right]_{mj}^{-1} E_{xj}. \quad (3.118)$$

$E_x$  is continuous in the  $y$ -direction which means that when expanding in this direction, Laurent's rule should be used once again.

$$\begin{aligned} & \frac{ck_0 \mu}{i} \partial_z \sum_n H_{ymn} e^{ik'_y y} \\ &= c^2 k_0^2 \mu \sum_j \sum_{n,l} [\varepsilon]_{mn,jl} e^{i(k'_y y - k''_y y)} E_{xjl} e^{ik'_y y} - \partial_y \left( ik'_x \sum_n E_{ymn} e^{ik'_y y} - \partial_y \sum_n E_{xmn} e^{ik'_y y} \right) \end{aligned} \quad (3.119)$$

$$\Rightarrow \frac{ck_0\mu}{i}\partial_z H_{ymn} = k'_y \left( k'_x E_{ymn} - k'_y E_{xmn} \right) + c^2 k_0^2 \mu \sum_{j,l} [\varepsilon]_{mn,jl} E_{xjl} \quad (3.120)$$

Lastly, in the same manner, equations (3.105) and (3.103) yield

$$\frac{ck_0}{i}\partial_z H_{xmn} = k'_x (k'_x E_{ymn} - k'_y E_{xmn}) - c^2 k_0^2 \mu \sum_{j,l} [\varepsilon]_{mn,jl} E_{yjl}. \quad (3.121)$$

### 3.6.1 The Eigenvalue Problem

The equations found can now be written in matrix form in the following way. From equation(3.113) and (3.114) the matrix form becomes

$$\frac{ck_0}{i}\partial_z \begin{bmatrix} \mathbf{E}_x \\ \mathbf{E}_y \end{bmatrix} = \begin{bmatrix} \overline{\overline{\mathbf{K}_x \bar{\varepsilon}^{-1} \mathbf{K}_y}} & \mu c^2 k_0^2 \mathbb{1} - \overline{\overline{\mathbf{K}_x \bar{\varepsilon}^{-1} \mathbf{K}_x}} \\ \overline{\overline{\mathbf{K}_y \bar{\varepsilon}^{-1} \mathbf{K}_y}} - \mu c^2 k_0^2 \mathbb{1} & -\overline{\overline{\mathbf{K}_y \bar{\varepsilon}^{-1} \mathbf{K}_x}} \end{bmatrix} \begin{bmatrix} \mathbf{H}_x \\ \mathbf{H}_y \end{bmatrix} = \overline{\overline{\mathbf{F}}} \begin{bmatrix} \mathbf{H}_x \\ \mathbf{H}_y \end{bmatrix}, \quad (3.122)$$

where  $\mathbb{1}$  is the identity matrix, and from (3.120) and (3.121),

$$\frac{ck_0\mu}{i}\partial_z \begin{bmatrix} \mathbf{H}_x \\ \mathbf{H}_y \end{bmatrix} = \begin{bmatrix} -\overline{\overline{\mathbf{K}_x \mathbf{K}_y}} & \overline{\overline{\mathbf{K}_x}}^2 - \mu c^2 k_0^2 [\varepsilon] \\ \mu c^2 k_0^2 [\varepsilon] - \overline{\overline{\mathbf{K}_y}}^2 & \overline{\overline{\mathbf{K}_x \mathbf{K}_y}} \end{bmatrix} \begin{bmatrix} \mathbf{E}_x \\ \mathbf{E}_y \end{bmatrix} = \overline{\overline{\mathbf{G}}} \begin{bmatrix} \mathbf{E}_x \\ \mathbf{E}_y \end{bmatrix}. \quad (3.123)$$

Now assuming a solution to these equations proportional to  $e^{ik_z z}$ , then from these two equations an eigenvalue problem appears as

$$ck_0 k_z \begin{bmatrix} \mathbf{E}_x \\ \mathbf{E}_y \end{bmatrix} = \overline{\overline{\mathbf{F}}} \frac{1}{ck_0 \mu k_z} \overline{\overline{\mathbf{G}}} \begin{bmatrix} \mathbf{E}_x \\ \mathbf{E}_y \end{bmatrix}, \quad (3.124)$$

$$\overline{\overline{\mathbf{F}\mathbf{G}}} \begin{bmatrix} \mathbf{E}_x \\ \mathbf{E}_y \end{bmatrix} = c^2 k_0^2 k_z^2 \mu \begin{bmatrix} \mathbf{E}_x \\ \mathbf{E}_y \end{bmatrix}. \quad (3.125)$$

### 3.6.2 Permittivity Integrals

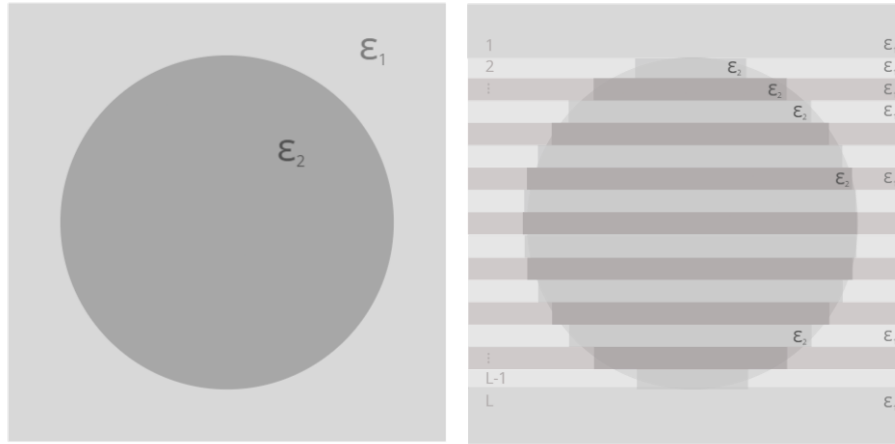


**Figure 3.3:** Example of a unit cell with a circular shaped rod/hole with permittivity  $\epsilon_2$  and a surrounding medium of permittivity  $\epsilon_1$ . To the left, the unit cell is represented in its actual shape and to the right, a division of the cell into  $L$  layers is depicted. In each layer that includes part of the cylinder, the permittivity is approximated to be a rectangle instead of having round corners. Layers 1 and  $L$  will only consist of the surrounding medium.

The permittivity functions for the different structures, used in equations (3.89) and (3.90) can be found in Section 2.2. For the square rod structure, these integrals each depend on a single piecewise constant function. And the resulting equations (3.89) and (3.90) are piecewise constant functions of the remaining coordinate. Each piecewise constant function consists of three parts, one for  $|x, y| < a$  and two for  $|x, y| \geq a$ . For the cylindrical rod structure, the calculations are similar. However, in this case the structure is approximated by dividing the cell cross section into  $L$  different layers each of which is a piecewise constant function, like in the square rod case, but with width  $a_l(x)$  dependant on the layer of the cylinder cross section (see Figure 3.3). Equations (3.89) and (3.90) are now piecewise constant functions with  $L$  layers.

## 3.7 Fourier Modal Method by Tensor Averaging

An alternative procedure to compute the Fourier coefficients of  $\bar{\bar{\epsilon}}$  directly, as previous approaches in this section, is to transform the field from Fourier space into real space, compute  $\overleftarrow{\epsilon} \cdot \vec{E}$ , and transform the product back to Fourier space and proceed with FMM. The real space computational domain is discretized into  $N \times N \times N$  cells, and the transformations can

be done efficiently with the fast Fourier transform and the inverse fast Fourier transform algorithms. The product is straight forward for cells located in regions of constant permittivity. In cells with a jump in permittivity however, tensor averaging is performed in order to determine  $\overleftarrow{\varepsilon} \cdot \vec{E}$ . This averaging is done by separating the permittivity tensor into the part parallel and perpendicular with the polarization of the field, and average each part appropriately<sup>[25]</sup>. This procedure together with the FMM will be referred to as the tensor formulation. A more detailed description of the tensor averaging and tensor eigenvalue equations are given on the following section.

In tensor notation the permittivity will be divided into a parallel and a orthogonal term relating to the direction of the field and is written as

$$\varepsilon_{\parallel} = \frac{1}{A} \int_A \varepsilon(x, y) dx dy, \quad (3.126)$$

$$\varepsilon_{\perp}^{-1} = \frac{1}{A} \int_A \frac{1}{\varepsilon(x, y)} dx dy. \quad (3.127)$$

The entire permittivity tensor is then written as  $\overleftarrow{\varepsilon} = \hat{n}\hat{n}\varepsilon_{\perp} + (\overleftarrow{\mathbf{I}} - \hat{n}\hat{n})\varepsilon_{\parallel}$  where  $\mathbf{I} = \hat{x}\hat{x} + \hat{y}\hat{y} + \hat{z}\hat{z}$  and  $\hat{n} = \hat{n}_x + \hat{n}_y + \hat{n}_z$ .<sup>[25]</sup> The terms will then work as follows

$$\hat{n}\hat{n}\varepsilon_{\perp} = (\hat{n}_x + \hat{n}_y + \hat{n}_z)(\hat{n}_x + \hat{n}_y + \hat{n}_z)\varepsilon_{\perp} \quad (3.128)$$

$$= \hat{n}_x\hat{n}_x\varepsilon_{\perp xx} + \hat{n}_x\hat{n}_y\varepsilon_{\perp xy} + \hat{n}_y\hat{n}_x\varepsilon_{\perp yx} + \hat{n}_y\hat{n}_y\varepsilon_{\perp yy} + \hat{n}_z\hat{n}_z\varepsilon_{\perp zz}, \quad (3.129)$$

where  $\varepsilon_{\perp xz} = \varepsilon_{\perp yz} = \varepsilon_{\perp zx} = \varepsilon_{\perp zy} = 0$ . From equation (3.2)

$$(-i\omega\varepsilon_0 \overleftarrow{\varepsilon} \cdot \mathbf{E})_x = -i\omega\varepsilon_0(\varepsilon_{xx}E_x + \varepsilon_{xy}E_y) = \partial_y H_z - \partial_z H_y = \partial_y H_z - i\beta H_y \quad (3.130)$$

and from equation (3.1)

$$i\omega\mu_0 H_x = \partial_y E_x - \partial_z E_y = \partial_y E_x - i\beta E_y, \quad (3.131)$$

$$i\omega\mu_0 H_y = \partial_z E_x - \partial_x E_z = i\beta E_x - \partial_x E_z, \quad (3.132)$$

$$i\omega\mu_0 H_z = \partial_x E_y + \partial_y E_x, \quad (3.133)$$

Inserting equations (3.132) and (3.133) into equation (3.130) it becomes

$$-i\omega\varepsilon_0(\varepsilon_{xx}E_x + \varepsilon_{xy}E_y) = \partial_y \frac{-i}{\omega\mu_0} (\partial_x E_y - \partial_y E_x) - i\beta \frac{-i}{\omega\mu_0} (i\beta E_x - \partial_x E_z). \quad (3.134)$$

$E_z$  can be rewritten as

$$\nabla \cdot (\overleftarrow{\varepsilon} \cdot \mathbf{E}) = 0 = \partial_x(\varepsilon_{xx}E_x + \varepsilon_{xy}E_y) + \partial_y(\varepsilon_{yy}E_y + \varepsilon_{yx}E_x) + \partial_z\varepsilon_{zz}E_z \quad (3.135)$$

and as  $\partial_z(\varepsilon_{zz}E_z) = \varepsilon_{zz}i\beta E_z$

$$\Rightarrow E_z = \frac{i}{\beta}\varepsilon_{zz}^{-1} \left\{ \partial_x(\varepsilon_{xx}E_x + \varepsilon_{xy}E_y) + \partial_y(\varepsilon_{yy}E_y + \varepsilon_{yx}E_x) \right\} \quad (3.136)$$

so equation (3.134) becomes

$$\begin{aligned} -i\omega\varepsilon_0(\varepsilon_{xx}E_x + \varepsilon_{xy}E_y) = \\ \partial_y \frac{-i}{\omega\mu_0} (\partial_x E_y - \partial_y E_x) - i\beta \frac{-i}{\omega\mu_0} \left( i\beta E_x - \partial_x \frac{i}{\beta}\varepsilon_{zz}^{-1} \left\{ \partial_x(\varepsilon_{xx}E_x + \varepsilon_{xy}E_y) + \partial_y(\varepsilon_{yy}E_y + \varepsilon_{yx}E_x) \right\} \right). \end{aligned} \quad (3.137)$$

Rewriting this on matrix form,

$$\begin{aligned} -i\omega\varepsilon_0(\bar{\varepsilon}_{xx}\mathbf{E}_x + \bar{\varepsilon}_{xy}\mathbf{E}_y) = i\bar{\mathbf{K}}_y \frac{-i}{\omega\mu_0} (i\bar{\mathbf{K}}_x\mathbf{E}_y - i\bar{\mathbf{K}}_y\mathbf{E}_x) \\ - i\beta \frac{-i}{\omega\mu_0} \left( i\beta\mathbf{E}_x - i\bar{\mathbf{K}}_x i\beta^{-1}\bar{\varepsilon}_{zz}^{-1} \left\{ i\bar{\mathbf{K}}_x(\bar{\varepsilon}_{xx}\bar{\mathbf{E}}_x + \bar{\varepsilon}_{xy}\mathbf{E}_y) + i\bar{\mathbf{K}}_y(\bar{\varepsilon}_{yy}\mathbf{E}_y + \bar{\varepsilon}_{yx}\mathbf{E}_x) \right\} \right). \end{aligned} \quad (3.138)$$

Multiplying with  $-i\omega\mu_0$  and using that  $\frac{\omega}{k_0} = c = \frac{1}{\sqrt{\mu_0\varepsilon_0}}$  the equation becomes

$$\begin{aligned} k_0^2(\bar{\varepsilon}_{xx}\bar{\mathbf{E}}_x + \bar{\varepsilon}_{xy}\mathbf{E}_y) = \bar{\mathbf{K}}_y(\bar{\mathbf{K}}_y\mathbf{E}_x - \bar{\mathbf{K}}_x\mathbf{E}_y) \\ + \beta \left( \beta\mathbf{E}_x + \bar{\mathbf{K}}_x\beta^{-1}\bar{\varepsilon}_{zz}^{-1} \left\{ \bar{\mathbf{K}}_x(\bar{\varepsilon}_{xx}\mathbf{E}_x + \bar{\varepsilon}_{xy}\mathbf{E}_y) + \bar{\mathbf{K}}_y(\bar{\varepsilon}_{yy}\mathbf{E}_y + \bar{\varepsilon}_{yx}\mathbf{E}_x) \right\} \right) \end{aligned} \quad (3.139)$$

$$\begin{aligned} = \bar{\mathbf{K}}_y^2\mathbf{E}_x - \bar{\mathbf{K}}_y\bar{\mathbf{K}}_x\mathbf{E}_y + \beta^2\mathbf{E}_x + \bar{\mathbf{K}}_x\bar{\varepsilon}_{zz}^{-1}\bar{\mathbf{K}}_x\bar{\varepsilon}_{xx}\mathbf{E}_x \\ + \bar{\mathbf{K}}_x\bar{\varepsilon}_{zz}^{-1}\bar{\mathbf{K}}_x\bar{\varepsilon}_{xy}\mathbf{E}_y + \bar{\mathbf{K}}_x\bar{\varepsilon}_{zz}^{-1}\bar{\mathbf{K}}_y\bar{\varepsilon}_{yy}\mathbf{E}_y + \bar{\mathbf{K}}_x\bar{\varepsilon}_{zz}^{-1}\bar{\mathbf{K}}_y\bar{\varepsilon}_{yx}\mathbf{E}_x \end{aligned} \quad (3.140)$$

leading to the first equation to be used in relation to  $\mathbf{E}_x$  and  $\mathbf{E}_y$  being,

$$\begin{aligned} \beta^2\mathbf{E}_x = (k_0^2\bar{\varepsilon}_{xx} - \bar{\mathbf{K}}_y^2 - \bar{\mathbf{K}}_x\bar{\varepsilon}_{zz}^{-1}\bar{\mathbf{K}}_x\bar{\varepsilon}_{xx} - \bar{\mathbf{K}}_x\bar{\varepsilon}_{zz}^{-1}\bar{\mathbf{K}}_y\bar{\varepsilon}_{xx})\mathbf{E}_x \\ + (k_0^2\bar{\varepsilon}_{xy} + \bar{\mathbf{K}}_y\bar{\mathbf{K}}_x - \bar{\mathbf{K}}_x\bar{\varepsilon}_{zz}^{-1}\bar{\mathbf{K}}_y\bar{\varepsilon}_{xy} - \bar{\mathbf{K}}_x\bar{\varepsilon}_{zz}^{-1}\bar{\mathbf{K}}_y\bar{\varepsilon}_{yy})\mathbf{E}_y. \end{aligned} \quad (3.141)$$

Using the same derivation another equation relating  $\mathbf{E}_x$ ,  $\mathbf{E}_y$  is found, by using (3.131), (3.133) and

$$(-i\omega\varepsilon_0 \overleftrightarrow{\varepsilon} \cdot \mathbf{E})_y = -i\omega\varepsilon_0(\varepsilon_{yy}E_y + \varepsilon_{yx}E_x) = \partial_z H_x - \partial_x H_z = i\beta H_x - \partial_x H_z, \quad (3.142)$$

becomes

$$\begin{aligned} \beta^2\mathbf{E}_y = (k_0^2\bar{\varepsilon}_{yx} - \bar{\mathbf{K}}_y\bar{\varepsilon}_{zz}^{-1}\bar{\mathbf{K}}_x\bar{\varepsilon}_{xx} - \bar{\mathbf{K}}_y\bar{\varepsilon}_{zz}^{-1}\bar{\mathbf{K}}_y\bar{\varepsilon}_{yx} + \bar{\mathbf{K}}_x\bar{\mathbf{K}}_y)\mathbf{E}_x \\ + (k_0^2\bar{\varepsilon}_{yy} - \bar{\mathbf{K}}_y\bar{\varepsilon}_{zz}^{-1}\bar{\mathbf{K}}_x\bar{\varepsilon}_{xy} - \bar{\mathbf{K}}_y\bar{\varepsilon}_{zz}^{-1}\bar{\mathbf{K}}_y\bar{\varepsilon}_{yy} - \bar{\mathbf{K}}_x^2)\mathbf{E}_y. \end{aligned} \quad (3.143)$$

What is left is to derive an equation that makes it possible to calculate the magnetic field when the electric field is known. From equations (3.1), (3.130) a relation is found to be

$$-i\omega\varepsilon_0(\varepsilon_{xx}E_x + \varepsilon_{xy}E_y) = \frac{\partial}{\partial y} \left( \frac{-i}{\omega\mu_0} \left( \frac{\partial E_y}{\partial x} - \frac{\partial E_x}{\partial y} \right) \right) - ik_z H_y \quad (3.144)$$

which makes it possible to write  $H_y$  as

$$H_y = \frac{-i}{k_z} \left( i\omega\varepsilon_0(\varepsilon_{xx}E_x + \varepsilon_{xy}E_y) + \frac{\partial}{\partial y} \left( \frac{-i}{\omega\mu_0} \left( \frac{\partial E_y}{\partial x} - \frac{\partial E_x}{\partial y} \right) \right) \right) \quad (3.145)$$

and once again in matrix form:

$$\bar{\bar{H}}_y = -i \left( i\omega\varepsilon_0(\bar{\bar{\varepsilon}}_{xx}\bar{\bar{E}}_x + \bar{\bar{\varepsilon}}_{xy}\bar{\bar{E}}_y) + i\bar{\bar{K}}_y \frac{-i}{\omega\mu_0} (i\bar{\bar{K}}_x\bar{\bar{E}}_y - i\bar{\bar{K}}_y\bar{\bar{E}}_x) \right) \bar{\bar{K}}_z^{-1} \quad (3.146)$$

$$= \left( (\omega\varepsilon_0\bar{\bar{\varepsilon}}_{xx} - \frac{1}{\omega\mu_0}\bar{\bar{K}}_y\bar{\bar{K}}_y)\bar{\bar{E}}_x + (\omega\varepsilon_0\bar{\bar{\varepsilon}}_{xy} + \frac{1}{\omega\mu_0}\bar{\bar{K}}_y\bar{\bar{K}}_x)\bar{\bar{E}}_y \right) \bar{\bar{K}}_z^{-1}. \quad (3.147)$$

Using the same derivation but using equation (3.142) it can be found that

$$ik_z H_x - \frac{\partial}{\partial x} \left( \frac{-i}{\omega\mu_0} \left( \frac{\partial E_y}{\partial x} - \frac{\partial E_x}{\partial y} \right) \right) = -i\omega\varepsilon_0(\varepsilon_{yx}E_x + \varepsilon_{yy}E_y). \quad (3.148)$$

In matrix form  $H_x$  becomes

$$\bar{\bar{H}}_x = \left( (-\omega\varepsilon_0\bar{\bar{\varepsilon}}_{yx} - \frac{1}{\omega\mu_0}\bar{\bar{K}}_x\bar{\bar{K}}_y)\bar{\bar{E}}_x + (-\omega\varepsilon_0\bar{\bar{\varepsilon}}_{yy} + \frac{1}{\omega\mu_0}\bar{\bar{K}}_x\bar{\bar{K}}_x)\bar{\bar{E}}_y \right) \bar{\bar{K}}_z^{-1}. \quad (3.149)$$

## 3.8 Two-Dimensional Photonic Crystal

The first calculations to be made are for a two-dimensional version of the 3D FMM that is otherwise to be examined. This is to be compared to the results of the 3D FMM when setting one of the side lengths of the silicon squares to be equal to the period  $\Lambda$  effectively turning the structure into a one-dimensional periodic structure of layers of air and silicon. Before the models will be compared, the validity and convergence of the 2D FMM will be examined.

### 3.8.1 Two-Dimensional Fourier Modal Method

The model in two dimensions is of course just a simpler version of the 3D FMM. The structure in question is seen in Figure 2.5. For S-polarization the electric field only has a z-component and will be expanded into  $2N + 1$  modes in the  $x$  and  $y$  direction that propagates up or down in the structure,

$$E^{(j)}(x, y) = \sum_{n=-N}^N \sum_{m=1}^{2N+1} E_{m,n}^{(j)}(x) e^{inGx} e^{ikx} \left( a_m^{(j)} e^{-i\beta_m^{(j)}y} + b_m^{(j)} e^{i\beta_m^{(j)}y} \right). \quad (3.150)$$

The entire electric field matrix will consist of columns containing the Fourier coefficients of the different modes. In the homogeneous layers the electric field matrix will just be the identity matrix. In the periodic layer the Fourier coefficient for the permittivity is found through

$$\varepsilon(x) = \sum_{n=-N}^N \varepsilon_n e^{inGx} \quad (3.151)$$

which can be found to give coefficients

$$\varepsilon_0 = \frac{a}{\Lambda} \varepsilon_2 + \left(1 - \frac{a}{\Lambda}\right) \varepsilon_1 \quad (3.152)$$

$$\varepsilon_n = \frac{\varepsilon_2 - \varepsilon_1}{\Lambda n G} 2 \sin \frac{nGa}{2}, \quad n \neq 0. \quad (3.153)$$

Now the electric field in the periodic layer can be found through the eigenvalue equation

$$\left( \frac{\partial^2}{\partial x^2} + k_0^2 \varepsilon(x) \right) E_m(x) = \beta_m^2 E_m(x), \quad (3.154)$$

such that

$$E_m(x) = \sum_{n=-N}^N E_{m,n} e^{i(nG+k)x}. \quad (3.155)$$

This becomes the eigenvalue problem

$$\left( -\overline{\overline{\mathbf{K}}} + k_0^2 \overline{\overline{\varepsilon}} \right) \mathbf{E}_m = \beta_m^2 \mathbf{E}_m, \quad (3.156)$$

where  $\overline{\overline{\mathbf{K}}}$  is a diagonal matrix containing elements  $nG + k$  for  $n = -N : N$ .

The magnetic field will be found from the equation

$$H_{m,n}^{(j)} = -\frac{\beta_m^{(j)}}{\omega \mu_0} E_{m,n}^{(j)} \quad (3.157)$$

and  $\beta_m^{(j)}$  can be found from the dispersion relation:<sup>[31]</sup>

$$k_j^2 + \beta^2 = \varepsilon_j k_0^2. \quad (3.158)$$

In the same manner it can be calculated for P-polarized light with the exception that the equation relating the magnetic and electric field is now

$$\mathbf{E}_m^{(j)} = \frac{\beta_m^{(j)}}{\omega \varepsilon_0} \overline{\overline{\boldsymbol{\eta}}} \mathbf{H}_m^{(j)}, \quad (3.159)$$

where  $\overline{\overline{\eta}}$  is a matrix containing the Fourier coefficients of  $\frac{1}{\varepsilon(x)}$ . The eigenvalue problem to solve in the periodic layer becomes

$$\overline{\overline{\eta}}^{-1} \left( -\overline{\overline{\mathbf{K}}} \overline{\overline{\varepsilon}}^{-1} \overline{\overline{\mathbf{K}}} + k_0^2 \mathbb{1} \right) \mathbf{H}_m = \beta_m^2 \mathbf{E}_m \quad (3.160)$$

The reflection and transmission coefficients will be calculated using the S matrix theory.<sup>[31]</sup>

For P-polarization Lifeng Li's rules will also be tested by calculating the spectrum without using the  $\eta$  matrix but simply  $\varepsilon^{-1}$ .

# Chapter 4

## Propagation of Light

In this chapter, the theory behind the propagation of electromagnetic waves, namely the reflection and transmission matrices used to understand the interaction of these waves with the photonic crystal is the first to be introduced. After, a model for calculating the guided modes in the structure is derived. These discrete modes are what the light can couple to inside the structure creating the Fano resonances. This will allow one to localize these resonances within a frequency spectrum.

### 4.1 Reflection and Transmission

The Fourier coefficients and the eigenvalues obtained with the Fourier modal method can now be used to find the reflectance and transmittance of light from the structure. Now, all the layers will be put together in order to find the reflection and transmission matrices for the whole structure. This means that the propagation through the layers as well as the boundary conditions between them need to be taken into consideration.

The incident wave can either be transmitted or reflected at each interface, and the propagation through a layer will result in a phase shift dependent on the length  $h_j$  of the layer  $j$ . The propagation matrix for a layer  $j$  is given by

$$\bar{\bar{P}}_j = \begin{bmatrix} \bar{\bar{p}}_j & \bar{\bar{0}} \\ \bar{\bar{0}} & \bar{\bar{p}}_j \end{bmatrix}, \quad (4.1)$$

where for a homogeneous layer

$$\bar{\bar{\mathbf{p}}}_j = \begin{bmatrix} e^{ik_{z,-M,-N}^{(j)}h_j} & 0 & 0 & \dots & 0 \\ 0 & e^{ik_{z,-M,-N+1}^{(j)}h_j} & 0 & \dots & 0 \\ \vdots & & \ddots & & \vdots \\ 0 & 0 & 0 & \dots & e^{ik_{z,M,N}^{(j)}h_j} \end{bmatrix}, \quad (4.2)$$

and for a periodic layer

$$\bar{\bar{\mathbf{p}}}_j = \begin{bmatrix} e^{ik_{z,1}^{(j)}h_j} & 0 & 0 & \dots & 0 \\ 0 & e^{ik_{z,2}^{(j)}h_j} & 0 & \dots & 0 \\ \vdots & & \ddots & & \vdots \\ 0 & 0 & 0 & \dots & e^{ik_{z,2(2N+1)2}^{(j)}h_j} \end{bmatrix}, \quad (4.3)$$

where  $k_{z,m,n}^{(j)}$  is given as in equation (3.16) for the homogeneous layers and in the periodic layer it is found with the eigenvalue problem in equation (3.62) by taking the square-root of  $\beta^2$ .

The components of the electric field in each layer can be written as follows

$$E_x^{(j)}(x, y) = \sum_q \sum_m \sum_n E_{x,m,n}^{(j,q)} e^{i(mG_x x + nG_y y)} e^{ik_{x0}x} e^{ik_{y0}y} \left( c_{x,q,m,n}^{(j)} e^{ik_{z,q}^{(j)}z} + d_{x,q,m,n}^{(j)} e^{-ik_{z,q}^{(j)}z} \right) \quad (4.4)$$

$$E_y^{(j)}(x, y) = \sum_q \sum_m \sum_n E_{y,m,n}^{(j,q)} e^{i(mG_x x + nG_y y)} e^{ik_{x0}x} e^{ik_{y0}y} \left( c_{y,q,m,n}^{(j)} e^{ik_{z,q}^{(j)}z} + d_{y,q,m,n}^{(j)} e^{-ik_{z,q}^{(j)}z} \right) \quad (4.5)$$

where  $c_{x,q,m,n}^{(j)}$  are the Fourier coefficients of the waves traveling in the positive  $z$  direction, while  $d_{x,q,m,n}^{(j)}$  are the Fourier coefficients of the waves traveling in the negative  $z$  direction. The coefficients can be organized in a vector such that

$$\mathbf{c}_j = \begin{bmatrix} \mathbf{c}_x^{(j)} \\ \mathbf{c}_y^{(j)} \end{bmatrix}, \quad \mathbf{d}_j = \begin{bmatrix} \mathbf{d}_x^{(j)} \\ \mathbf{d}_y^{(j)} \end{bmatrix}, \quad (4.6)$$

where

$$\mathbf{c}_x^{(j)} = \begin{bmatrix} c_{x,q,-M,-N}^{(j)} \\ \vdots \\ c_{x,q,-M,N}^{(j)} \\ \vdots \\ c_{x,q,M,-N}^{(j)} \\ \vdots \\ c_{x,q,M,N}^{(j)} \end{bmatrix}, \quad \mathbf{d}_x^{(j)} = \begin{bmatrix} d_{x,q,-M,-N}^{(j)} \\ \vdots \\ d_{x,q,-M,N}^{(j)} \\ \vdots \\ d_{x,q,M,-N}^{(j)} \\ \vdots \\ d_{x,q,M,N}^{(j)} \end{bmatrix}. \quad (4.7)$$

The relation between the coefficients of each layer will be given by transmission and reflection matrices, and matrix equations relating them can be written as<sup>[31]</sup>:

$$\begin{bmatrix} \mathbf{d}_j \\ \mathbf{c}_{j+1} \end{bmatrix} = \begin{bmatrix} \overline{\overline{\mathbf{R}}}_{jj+1} & \overline{\overline{\mathbf{T}}}_{j+1j} \\ \overline{\overline{\mathbf{T}}}_{jj+1} & \overline{\overline{\mathbf{T}}}_{j+1j} \end{bmatrix} \begin{bmatrix} \mathbf{c}_j \\ \mathbf{d}_{j+1} \end{bmatrix}. \quad (4.8)$$

As for the total structure, it yields

$$\begin{bmatrix} \mathbf{d}_0 \\ \mathbf{c}_3 \end{bmatrix} = \begin{bmatrix} \overline{\overline{\mathbf{R}}}_{03} & \overline{\overline{\mathbf{T}}}_{30} \\ \overline{\overline{\mathbf{T}}}_{03} & \overline{\overline{\mathbf{T}}}_{30} \end{bmatrix} \begin{bmatrix} \mathbf{c}_0 \\ \mathbf{d}_3 \end{bmatrix}. \quad (4.9)$$

In the last layer, the coefficients  $d_{x,m,n}$  and  $d_{y,m,n}$  will equal zero, since there are no waves traveling in the  $-z$ -direction. In order to find the reflection and transmission matrices, a set of boundary conditions relating the layers can be written:

$$\mathbf{E}_j(\mathbf{c}_j + \mathbf{d}_j) = \mathbf{E}_{j+1}(\mathbf{c}_{j+1} + \mathbf{d}_{j+1}) \quad (4.10)$$

$$\mathbf{H}_j(\mathbf{c}_j - \mathbf{d}_j) = \mathbf{H}_{j+1}(\mathbf{c}_{j+1} - \mathbf{d}_{j+1}). \quad (4.11)$$

As for the reflection and transmission matrices, the equations taken from equation (4.8) become:

$$\mathbf{d}_j = \overline{\overline{\mathbf{R}}}_{jj+1} \mathbf{c}_j + \overline{\overline{\mathbf{T}}}_{j+1j} \mathbf{d}_{j+1} \quad (4.12)$$

$$\mathbf{c}_{j+1} = \overline{\overline{\mathbf{T}}}_{jj+1} \mathbf{c}_j + \overline{\overline{\mathbf{T}}}_{j+1j} \mathbf{d}_{j+1}. \quad (4.13)$$

Now, with the system of equations consisting of (4.10), (4.11), (4.12) and (4.13) for all layers, the matrices  $\overline{\overline{\mathbf{R}}}_{jj+1}$ ,  $\overline{\overline{\mathbf{R}}}_{j+1j}$ ,  $\overline{\overline{\mathbf{T}}}_{jj+1}$  and  $\overline{\overline{\mathbf{T}}}_{j+1j}$  can be found:

$$\overline{\overline{\mathbf{R}}}_{jk} = \left( \overline{\overline{\mathbf{E}}}_k^{-1} \overline{\overline{\mathbf{E}}}_j + \overline{\overline{\mathbf{H}}}_k^{-1} \overline{\overline{\mathbf{H}}}_j \right)^{-1} \left( \overline{\overline{\mathbf{H}}}_k^{-1} \overline{\overline{\mathbf{H}}}_j - \overline{\overline{\mathbf{E}}}_k^{-1} \overline{\overline{\mathbf{E}}}_j \right), \quad (4.14)$$

$$\overline{\overline{\mathbf{T}}}_{jk} = \overline{\overline{\mathbf{E}}}_k^{-1} \overline{\overline{\mathbf{E}}}_j (\mathbf{1} + \overline{\overline{\mathbf{R}}}_{jk}). \quad (4.15)$$

As for the matrices relating layer  $j$  to  $j + 2$ , it will result in repeat propagation and reflections from the interfaces. The rule to be used in order to write the matrices is

$$\sum_{n=0}^{\infty} x^n = \frac{1}{1-x} \quad (4.16)$$

and will result in

$$\bar{\bar{T}}_{02} = \bar{\bar{T}}_{12} \left( \mathbb{1} - \bar{\bar{P}}_1 \bar{\bar{R}}_{10} \bar{\bar{P}}_1 \bar{\bar{R}}_{12} \right)^{-1} \bar{\bar{P}}_2 \bar{\bar{T}}_{01}, \quad (4.17)$$

$$\bar{\bar{T}}_{20} = \bar{\bar{T}}_{10} \left( \mathbb{1} - \bar{\bar{P}}_1 \bar{\bar{R}}_{12} \bar{\bar{P}}_1 \bar{\bar{R}}_{10} \right)^{-1} \bar{\bar{P}}_1 \bar{\bar{T}}_{21}, \quad (4.18)$$

$$\bar{\bar{R}}_{02} = \bar{\bar{R}}_{01} + \bar{\bar{T}}_{10} \left( \mathbb{1} - \bar{\bar{P}}_1 \bar{\bar{R}}_{12} \bar{\bar{P}}_1 \bar{\bar{R}}_{10} \right)^{-1} \bar{\bar{P}}_1 \bar{\bar{R}}_{12} \bar{\bar{P}}_1 \bar{\bar{T}}_{01}, \quad (4.19)$$

$$\bar{\bar{R}}_{20} = \bar{\bar{R}}_{21} + \bar{\bar{T}}_{12} \left( \mathbb{1} - \bar{\bar{P}}_1 \bar{\bar{R}}_{10} \bar{\bar{P}}_1 \bar{\bar{R}}_{12} \right)^{-1} \bar{\bar{P}}_1 \bar{\bar{R}}_{10} \bar{\bar{P}}_1 \bar{\bar{T}}_{21}. \quad (4.20)$$

For the transmission and reflection from a structure with four layers, the matrices are:

$$\bar{\bar{T}}_{03} = \bar{\bar{T}}_{23} \left( \mathbb{1} - \bar{\bar{P}}_2 \bar{\bar{R}}_{20} \bar{\bar{P}}_2 \bar{\bar{R}}_{23} \right)^{-1} \bar{\bar{P}}_2 \bar{\bar{T}}_{02} \quad (4.21)$$

$$\bar{\bar{R}}_{03} = \bar{\bar{R}}_{02} + \bar{\bar{T}}_{20} \left( \mathbb{1} - \bar{\bar{P}}_2 \bar{\bar{R}}_{23} \bar{\bar{P}}_2 \bar{\bar{R}}_{20} \right)^{-1} \bar{\bar{P}}_2 \bar{\bar{R}}_{23} \bar{\bar{P}}_2 \bar{\bar{T}}_{02}. \quad (4.22)$$

## 4.2 Guided Modes in a Planar Wave Guide

Fano resonances appear as earlier described, when waves of continuous and discrete states couple. In the case of the photonic crystal structure examined in this project the continuous external wave incident on the structure is able to couple to discrete bounded in-plane propagating waves. To get an idea of where the Fano resonances are to be found, the propagation constant for the guided modes will be compared to the propagation constant for the diffracted field related to the periodic layer. The waveguide that will be described consists of the outer layers consisting of air ( $\varepsilon_1 = \varepsilon_4 = 1$ ), surrounding two middle layers, one being silicon ( $\varepsilon_3 = 3.4^2$ ) and the other, representing the periodic layer having a permittivity given as  $\varepsilon_2 = \frac{a^2 \varepsilon_3 + (\Lambda^2 - a^2) \varepsilon_1}{\Lambda^2}$  for the 2D periodic structure and  $\varepsilon_2 = \frac{a \varepsilon_3 + (\Lambda - a) \varepsilon_1}{\Lambda}$  in the 1D periodic case.

### 4.2.1 Single Interface Fresnel Transmission and Reflection

The first thing that is needed to calculate the electromagnetic wave through the structure is to find the Fresnel transmission and reflection coefficients at the interfaces between layers with permittivity,

$$\varepsilon(\mathbf{r}) = \begin{cases} \varepsilon_i, & z > 0 \\ \varepsilon_j, & z < 0 \end{cases} \quad (4.23)$$

For S-polarization  $\mathbf{E}(\mathbf{r}) = \hat{x}E(y, z)$ , the electric field can be written as

$$E(\mathbf{r}) = \begin{cases} E_0 \left( e^{-k_{zi}z} + r^{(s)}(k_y) e^{ik_{zi}z} \right) e^{ik_y y}, & z > 0 \\ E_0 t^{(s)}(k_y) e^{-ik_{zj}z} e^{ik_y y}, & z < 0 \end{cases} \quad (4.24)$$

where  $k_{zi} = \sqrt{k_0^2 \varepsilon_i - k_y^2}$ . Using the boundary conditions for the tangential part of the electric and the magnetic field at the boundary  $z = 0$  given as  $E_{yi} = E_{yj}$  and  $-\frac{\partial \mathbf{B}}{\partial t} = \nabla \times \mathbf{E} \rightarrow \frac{\partial E_{xi}}{\partial z} = \frac{\partial E_{xj}}{\partial z}$ , leaves two boundary conditions to be,

$$1 + r^{(s)} = t^{(s)} \quad (4.25)$$

$$-ik_{zi}(1 - r^{(s)}) = -ik_{zj}t^{(s)}, \quad (4.26)$$

Where  $r^{(s)}$  and  $t^{(s)}$  are the Fresnel reflection and transmission coefficients respectively. From these two equations the reflection and transmission coefficients for the interface can be found as

$$t^{(s)} = \frac{k_{zi}}{k_{zj}}(1 - r^{(s)}) \quad (4.27)$$

$$= \frac{k_{zi}}{k_{zj}}(1 - (t^{(s)-1})) \quad (4.28)$$

$$\Rightarrow t^{(s)} \left( 1 + \frac{k_{zi}}{k_{zj}} \right) = 2 \frac{k_{zi}}{k_{zj}} \quad (4.29)$$

$$\Rightarrow t^{(s)} = \frac{2k_{zi}}{k_{zj} + k_{zi}} \quad (4.30)$$

and

$$r^{(s)} = \frac{k_{zi} - k_{zj}(1 + r^{(s)})}{k_{zi}} \quad (4.31)$$

$$\Rightarrow r^{(s)} \left( 1 + \frac{k_{zj}}{k_{zi}} \right) = \frac{k_{zi} - k_{zj}}{k_{zi}} \quad (4.32)$$

$$\Rightarrow r^{(s)} = \frac{k_{zi} - k_{zj}}{k_{zi} + k_{zj}}. \quad (4.33)$$

For P-polarization the reflection coefficient can be found in the same manner to be

$$r^{(p)} = \frac{\varepsilon_j k_{zi} - \varepsilon_i k_{zj}}{\varepsilon_j k_{zi} + \varepsilon_i k_{zj}}, \quad (4.34)$$

and the transmission coefficient can be found from Equation (4.25).

## 4.2.2 Many Layered Waveguide

As the photonic crystal is divided into four layers, and to describe the light through the structure, matrices for the interfaces, as well as the individual layers, should be constructed. For the structure being  $h$  thick, the magnetic field can be described outside the crystal as

$$E(\mathbf{r}) = e^{ik_0 n_m y} \begin{cases} E_1^+ e^{-ik_{z,1}z} + E_1^- e^{ik_{z,1}z}, & z > 0 \\ E_4^+ e^{-ik_{z,4}(z+h)} + E_4^- e^{ik_{z,4}(z+h)}, & z < -h \end{cases} \quad (4.35)$$

The boundary between layers at  $z = z_b$  the field on each side of the boundary can be written as

$$E(\mathbf{r}) = e^{ik_0 n_m y} \begin{cases} E_i^+ e^{-ik_{z,i}(z-z_b)} + E_i^- e^{ik_{z,i}(z-z_b)}, & h_i > z - z_b > 0 \\ E_j^+ e^{-ik_{z,j}(z-z_b)} + E_j^- e^{ik_{z,j}(z-z_b)} & 0 > z - z_b > -h_j \end{cases} \quad (4.36)$$

By the boundary conditions for the electric field, it is possible to relate the fields on each side by a matrix  $\bar{\bar{T}}_{ij}$

$$E_j^+ = E_i^+ t_{ij} + E_j^- r_{ji} \quad (4.37)$$

$$\Rightarrow E_i^+ = \frac{1}{t_{ij}} (E_j^+ + E_j^- r_{ij}) \quad (4.38)$$

$$E_j^- = E_i^- t_{ij} + E_j^+ r_{ji} \quad (4.39)$$

$$\Rightarrow E_i^- = \frac{1}{t_{ij}} (E_j^+ r_{ij} + E_j^-) \quad (4.40)$$

$$\Rightarrow \begin{bmatrix} E_i^+ \\ E_i^- \end{bmatrix} = \frac{1}{t_{ij}} \begin{bmatrix} 1 & r_{ij} \\ r_{ij} & 1 \end{bmatrix} \begin{bmatrix} E_j^+ \\ E_j^- \end{bmatrix} = \bar{\bar{T}}_{ij} \begin{bmatrix} E_j^+ \\ E_j^- \end{bmatrix} \quad (4.41)$$

utilising  $r_{12} = -r_{21}$ . Inside a single layer, the field can be described relative to the top or bottom of the layer, letting  $z_b$  be the top layer, as follows

$$E(\mathbf{r}) = e^{ik_0 n_m y} \begin{cases} E_i^+ e^{-ik_{z,i}(z-z_b)} + E_i^- e^{ik_{z,i}(z-z_b)} & -h_i < z - z_b < 0 \\ \tilde{E}_i^+ e^{-ik_{z,i}(z-(z_b-h_i))} + \tilde{E}_i^- e^{ik_{z,i}(z-(z_b-h_i))} & 0 < z - (z_b - h_i) < h_i \end{cases} \quad (4.42)$$

By this way of writing the same field, it is clear that the coefficients are related by the following matrix

$$\begin{bmatrix} E_i^+ \\ E_i^- \end{bmatrix} = \begin{bmatrix} e^{-ik_{z,i}h_i} & 1 \\ 1 & e^{ik_{z,i}h_i} \end{bmatrix} \begin{bmatrix} \tilde{E}_i^+ \\ \tilde{E}_i^- \end{bmatrix} = \overline{\overline{\mathbf{L}}}_i \begin{bmatrix} \tilde{E}_i^+ \\ \tilde{E}_i^- \end{bmatrix} \quad (4.43)$$

This makes for a resulting matrix relating the field on both sides of the structure to be

$$\begin{bmatrix} E_1^+ \\ E_1^- \end{bmatrix} = \overline{\overline{\mathbf{T}}}_{1,2} \overline{\overline{\mathbf{L}}}_2 \overline{\overline{\mathbf{T}}}_{2,3} \overline{\overline{\mathbf{L}}}_3 \overline{\overline{\mathbf{T}}}_{3,4} \begin{bmatrix} E_4^+ \\ E_4^- \end{bmatrix} = \begin{bmatrix} m_{11} & m_{12} \\ m_{21} & m_{22} \end{bmatrix} \begin{bmatrix} E_4^+ \\ E_4^- \end{bmatrix}. \quad (4.44)$$

To have guided modes in the structure it is required that  $E_1^+ = E_4^- = 0$ . By this requirement  $m_{11}$  must be 0 as well.  $m_{11}$  is a function of the mode index which means the guides mode indices will be found by finding the indices where  $m_{11}(n_m) = 0$ . [32]



# Chapter 5

## Results

The results presented in this chapter will first be about the various FMM formulations and how they converge. After this, it is investigated if the Fano resonances found from the structure relate to the guided modes of the crystal. Then the light incident on the crystal is varied in angle and lastly, a multitude of tests is presented, examining how the physical parameters of the structure affect the transmittance spectrum.

In all calculations done with the FMM presented in this chapter, the lattices chosen have periods  $\Lambda_x$  and  $\Lambda_y$  of equal length, and for simplicity,  $\Lambda = \Lambda_x = \Lambda_y$ . Furthermore,  $M$  and  $N$  are also chosen to be the same and will be referred to as  $N$ . The spectra will be plotted against the linear frequency given by  $f = \frac{c}{\lambda_0}$ .

### 5.1 The Two-Dimensional Photonic Crystal

The first tests to be done will involve the 2D FMM such that it can be checked for convergence and thereafter compared to the 3D FMM for a one-dimensional periodic structure such as the one illustrated in Figure 2.5.

#### 5.1.1 Convergence Test of the 2D FMM

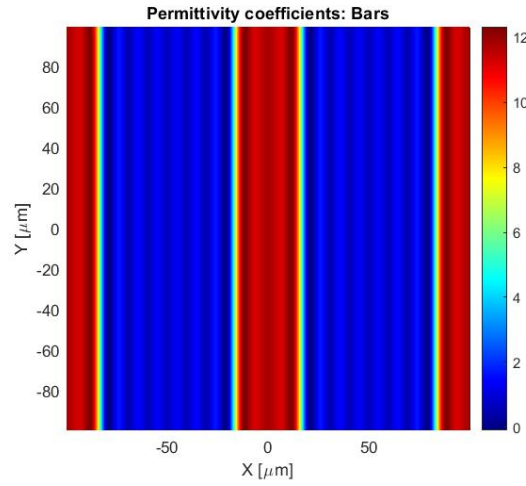
First off, the transmission of the S-polarized light is checked for convergence. Plots of the transmittance spectrum for 0.9 - 2.4 THz in  $L_f = 1000$  points for  $N = 1, 3, 5$  and 7 can be seen in Figure 5.2. The calculation was done for the structure B2 described in Table 2.1. In Figure 5.1, the permittivity coefficients of the structure are plotted for the  $x$ - and  $y$ -axis going from  $-\Lambda$  to  $+\Lambda$ . Furthermore, the absolute average difference for consecutive transmittance spectra  $\{t_i\}_k$  with an increasing amount of plane waves is plotted, where the  $x$ -axis represents

$N$  for the  $k$ 'th spectra in the calculation

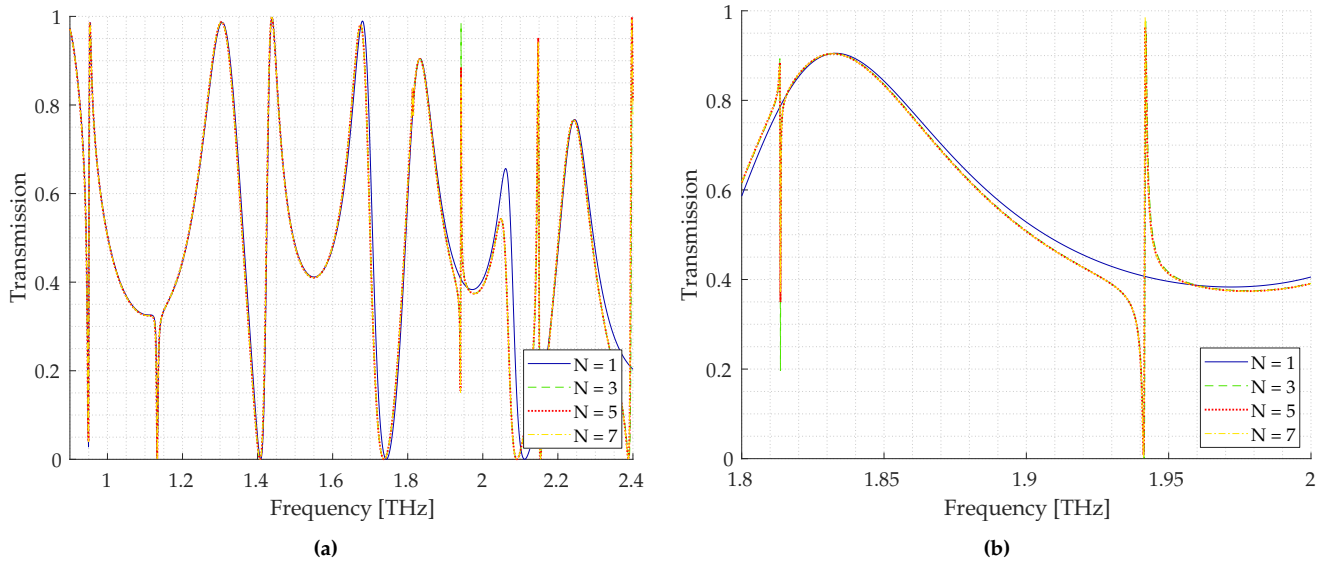
$$Error = \sum_i \frac{|\{t_i\}_{k+1} - \{t_i\}_k|}{L_f} \quad (5.1)$$

, which can be seen in Figure 5.5c.

As it can be seen in all figures, the model converges very well and is already stable at  $N = 4$ , meaning 9 plane waves. In Figure 5.2 it can be noted that from  $N = 1$  to  $N = 3$  new sharp peaks appear throughout the spectrum, which is the only apparent difference. From  $N = 3$  to  $N = 5$  and for  $N = 7$  the spectrum is indistinguishable and the calculations have fully converged to an acceptable degree.

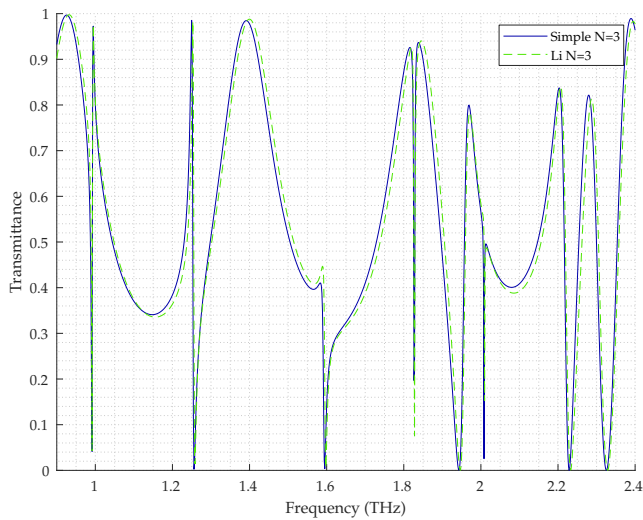
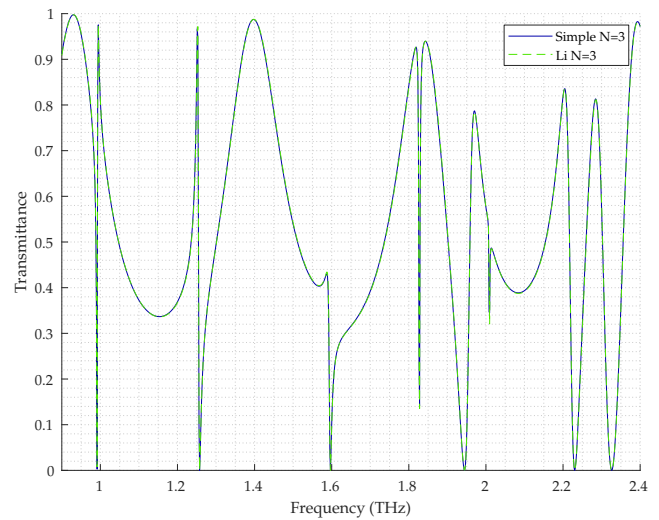


**Figure 5.1:** Permittivity coefficients for the periodic bar structure, B2 in Table 2.1, calculated for  $N = 10$ .



**Figure 5.2:** Transmittance spectrum (a) 0.9 – 2.4 THz and (b) 1.8 – 2 THz for S-polarized light calculated using the simple FMM for the B2 structure found in Table 2.1 with  $N = 1, 3, 5$  and 7. The frequency was discretized into 1000 points.

For P-polarized light, the calculations were done for the two different models at  $N = 3$  and  $N = 30$  with the same configurations as before. This was done to find out if the models converged to the same spectrum. The plots can be seen in Figure 5.3 where it can be verified that the two models converge. In Figure 5.4 the simple and Li's model with  $N = 3$  are compared to Li's at  $N = 30$ . From this plot, it can be seen that Li's model is closer to the fully converged plot at  $N = 3$  than the simple model and the two models converge toward each other.

(a) The calculations were done with  $N = 3$ .(b) The calculations were done with  $N = 30$ .

**Figure 5.3:** Transmittance spectrum calculated from a 2D FMM using the simple model and using Lifeng Li's factorization rules. The spectra were calculated for the B2 structure, found in Table 2.1. This is for P-polarized light.

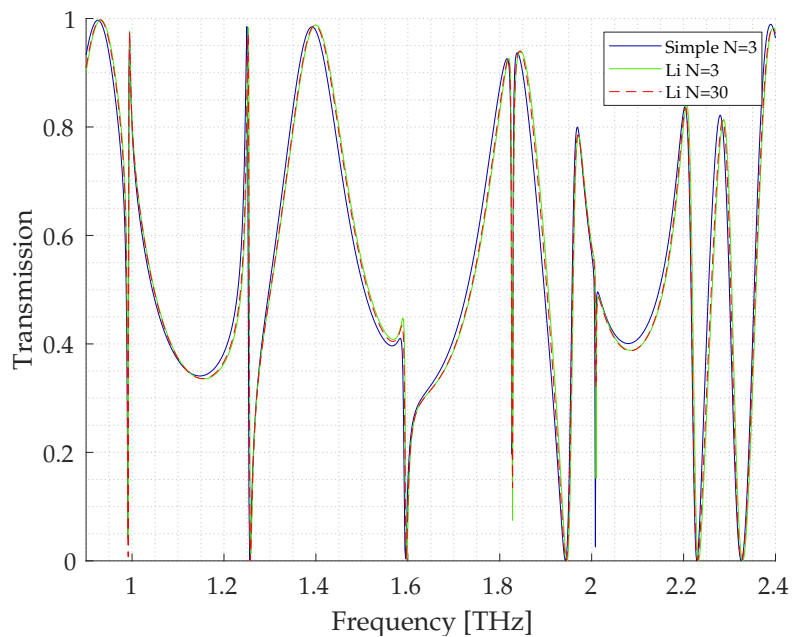


**Figure 5.4:** Transmittance spectrum for the B2 structure found in Table 2.1 calculated for P-polarized light using a simple model at  $N = 3$  as well as using the Li model with  $N = 3, 30$ .

The two ways of calculating the transmittance of the P-polarized light were checked for

convergence in the same way as for S-polarization. This test can be seen in Figures 5.5a and 5.5b. Both versions show to be converging as expected and as it could be noted Li's version of expressing the permittivity does converge better. Though the simple version has a smaller difference between each run at first, it takes a longer time before it has fully converged, still fluctuating slightly at  $N = 14$ . In Figure 5.6 a closer look at a peak at 1.24 THz is plotted for 5 different amounts of plane waves for Li's formulation. The resonance shifts slightly to the right when going from  $N = 1$  to  $N = 3$  but does not shift much after.

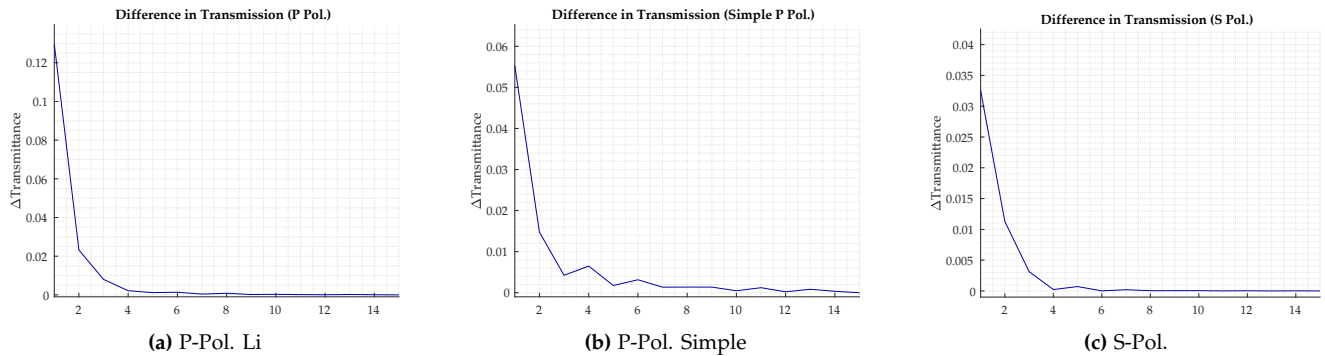


**Figure 5.5:** Absolute mean difference for the transmittance calculated for different plane waves where the  $x$ -axis shows the value of  $i$  in (5.1). a) shows the convergence for P-polarized light calculated using Lifeng Li's rules. b) is for the simple method. c) shows how the calculations for S-polarized light converge. The structure calculated was B2 found in Table 2.1.

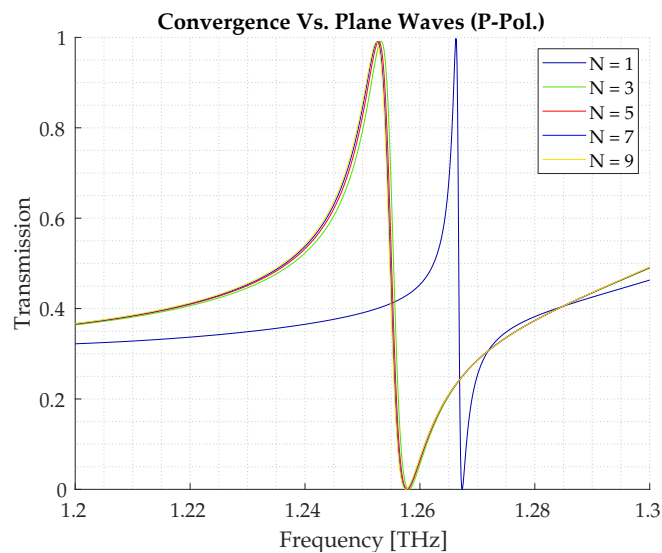


**Figure 5.6:** Transmittance spectrum for the B2 structure for P-polarized light, see Table 2.1 of a single resonance calculated for a number of plane waves between 1 and 9 for a 2D FMM. Lifeng Li's factorization rules were used.

### 5.1.2 Comparison of 2D/3D FMM

The 2D FMM converged well and is now ready to be compared to the calculations of the same structure calculated using the 3D FMM. As for the tests of the 2D model, the spectrum is calculated for frequencies between 0.9 and 2.4 THz discretized in 1000 elements. For S-polarization, the spectrum calculated for  $N = 5$  is seen in Figure 5.7. The results are almost identical with an average absolute deviation of  $1.1 \times 10^{-16}$ , which can be explained solely by computational rounding error.

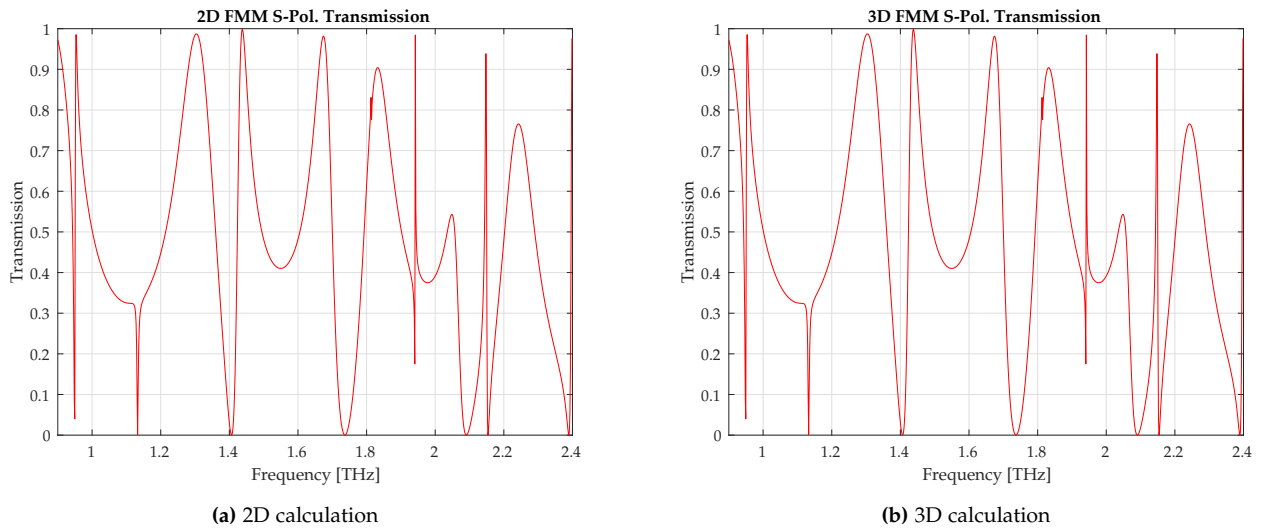


**Figure 5.7:** Transmission spectrum for the B2 structure found in Table 2.1 calculated using a 2D FMM and a 3D FMM, with the simple formulation with  $N = 5$ .

For P-polarization, there are once again two different methods used to calculate the spectrum for the three-dimensional FMM. In Figure 5.8 the spectrum is calculated between 1.2 - 1.7 THz for the two methods, with and without Li's factorization rule and using 2D FMM as well as 3D. The calculation was made with  $N = 3$  and for 1000 frequencies. The two methods returned P-polarized spectra where the 2D and 3D model were identical with and without using Li's rules but was not equal to each other. The spectrum between 0.9 and 2.4 THz can be seen in Figure 5.9 where the same is true. At a larger amount of plane waves the two different methods do converge as was seen for for the 2D FMM.

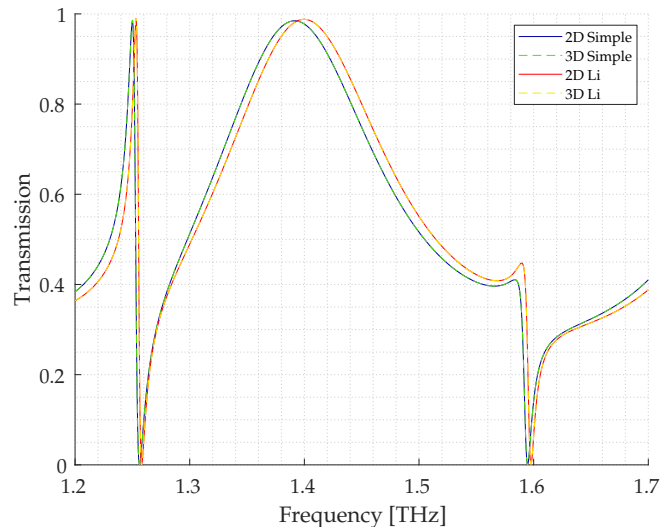


**Figure 5.8:** Transmittance spectrum for P-polarized light for the B2 structure found in Table 2.1 calculated using a 2D FMM and a 3D FMM with and without using Li's rules. The calculations were made with  $N = 3$ .

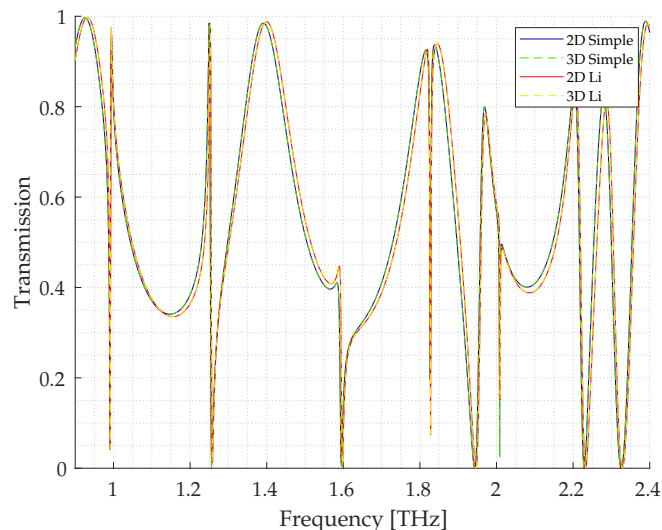


**Figure 5.9:** Transmittance spectrum for the B2 structure found in Table 2.1 calculated for P-polarized light using a 2D FMM and a 3D FMM with and without using Li's rules. The calculations were made with  $N = 3$ .

As the two methods in the 2D model give almost identical spectra, these were compared to the 3D model using Li's rules, by subtracting the result of the 3D model from the two 2D models for  $N = 5$  (Figure 5.10). This shows a greater agreement between the two models utilizing Li's rules where the average absolute deviation for the model without Li's rules is 0.0222 and with Li's rules decreasing to  $1.258 \times 10^{-5}$ . The deviation is greatest at the resonances, which is explained by small deviations at steep peaks creating a large difference.

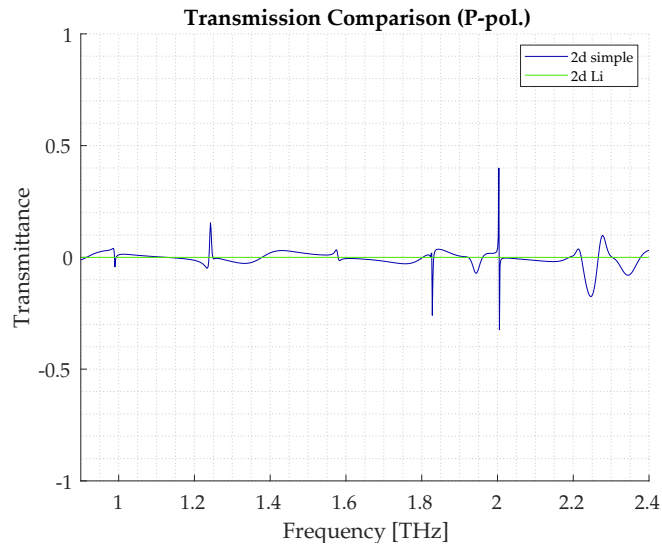
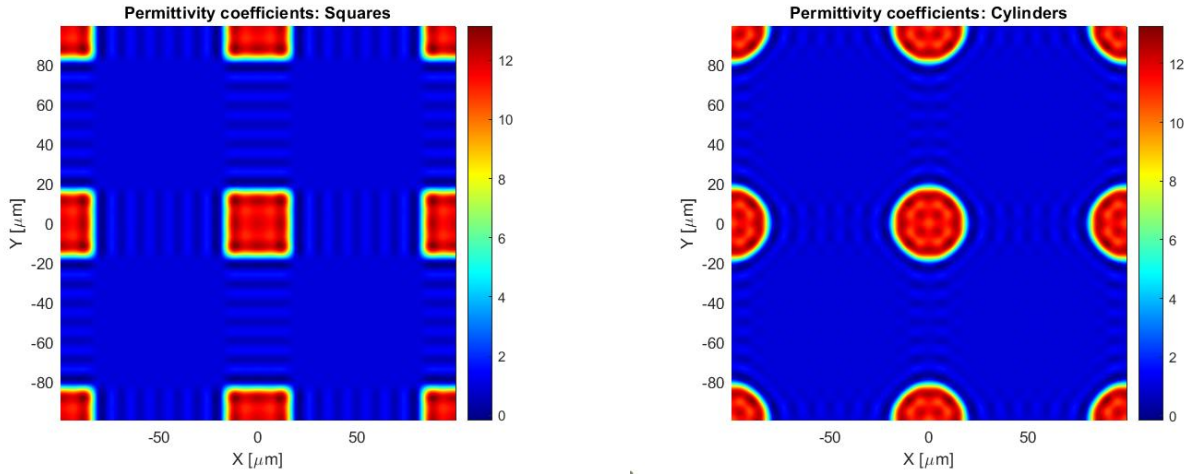


**Figure 5.10:** The difference between the transmission spectrum calculated for P-polarized light by Li's formulation for 3D FMM and a 2D calculation with and without Li's rules both with  $N = 5$  for the B2 structure found in Table 2.1.

## 5.2 Comparing Different 3D FMMs

In this section, the convergence vs. number of plane waves of the three different FMM formulations are tested and compared, for a single resonance. This comparison was made for two different structures. First for a square rod structure (SRS1), as described in Chapter 2. The calculated permittivity of the periodic structure is seen in Figure 5.11a. Secondly, for cylindrical rods in a square grid structure (SRC1), also described in Chapter 2 as well, see Figure 5.11b.



(a) Permittivity coefficients calculated for the square rods with  $N=10$ . Physical parameters can be found in Table 2.1.

(b) Permittivity coefficients calculated for the cylindrical rods with  $N=10$ . Physical parameters can be found in Table 2.2.

**Figure 5.11:** The calculated permittivity coefficients plotted in a  $2\Lambda \times 2\Lambda$  grid for the square and cylindrical rods.

For both the convergence tests and comparisons, a single resonance was considered, located between 1.545 THz and 1.57 THz, and the frequency resolution of these tests was maximized, while still keeping the computational cost as low as needed, with these considerations the test was done for 150 discrete frequencies.

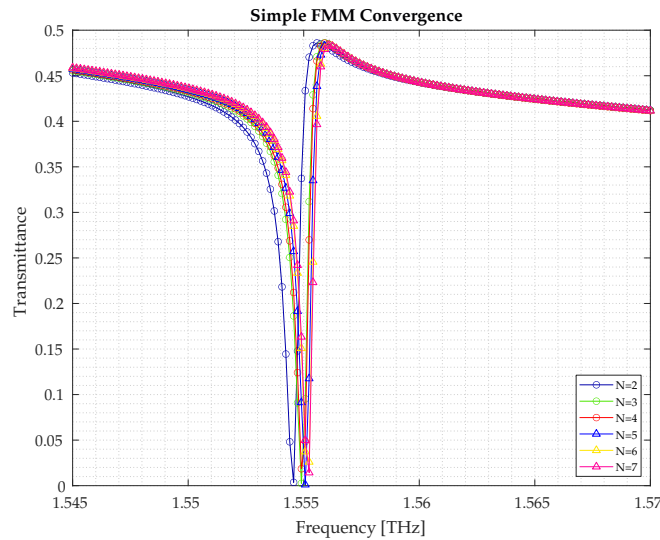


**Figure 5.12:** Transmittance spectra for 6 different numbers of plane waves with the parameter  $N$  ranging from 2 to 7, simulated with the simple FMM formulation. The simulated samples are SRS1 described in Table 2.1. Each spectrum consists of 150 discrete frequencies.

The convergence of the simple FMM formulation was tested for  $N = 2$  to  $N = 7$ , and the result can be seen in Figure 5.12. The spectra for every number of plane waves give resonances at  $f_0 = 1.555 \pm 0.002$  THz, while a higher number of plane waves shifts  $f_0$  to a higher frequency, except for  $N = 3$  to  $N = 4$  and  $N = 6$  to  $N = 7$ , at which  $f_0$  does not vary.

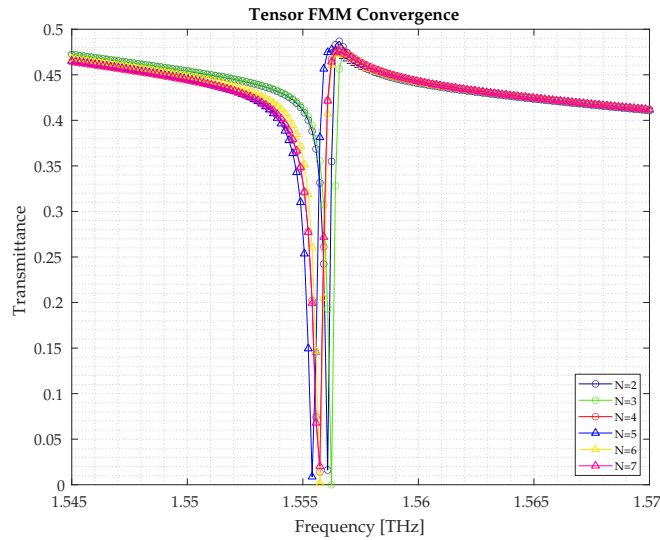


**Figure 5.13:** Transmittance spectra for 6 different numbers of plane waves with the parameter  $N$  ranging from 2 to 7, simulated with the tensor FMM formulation. The simulated samples are SRS1 described in Table 2.1. Each spectrum consists of 150 discrete frequencies.

The convergence of the tensor FMM formulation was tested for the same number of plane waves as the simple formulation, and the spectra can be seen in Figure 5.13. Similarly, all spectra had  $f_0 = 1.557 \pm 0.002$  THz, however with this formulation the resonance did not shift uniformly as the number of plane waves increased. Instead,  $f_0$  shifted to a higher frequency for  $N = 2$  to  $N = 3$ , from  $N = 3$  to  $N = 5$  the resonance shifted to a lower frequency, then for  $N = 5$  to  $N = 6$  the shift is to a higher frequency again, and lastly no shift from  $N = 6$  to  $N = 7$ .

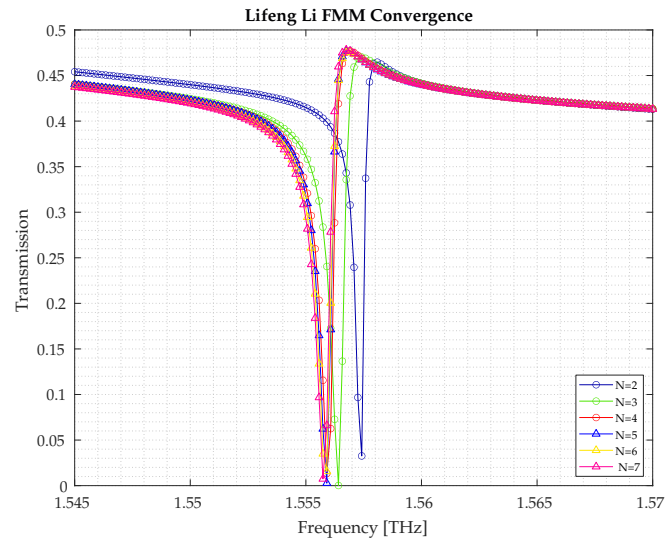


**Figure 5.14:** Transmittance spectra for 6 different numbers of plane waves with the parameter  $N$  ranging from 2 to 7, simulated with the Lifeng Li FMM formulation. The simulated samples are SRS1 described in Table 2.1. Each spectrum consists of 150 discrete frequencies.

The last formulation was tested for  $N = 2$  to  $N = 7$  as well and the resulting spectra can be observed in Figure 5.14. Firstly, for this formulation, the resonance converged at  $f_0 \approx 1.556$  THz after  $N = 3$ , however also had the largest deviation for the few plane waves.

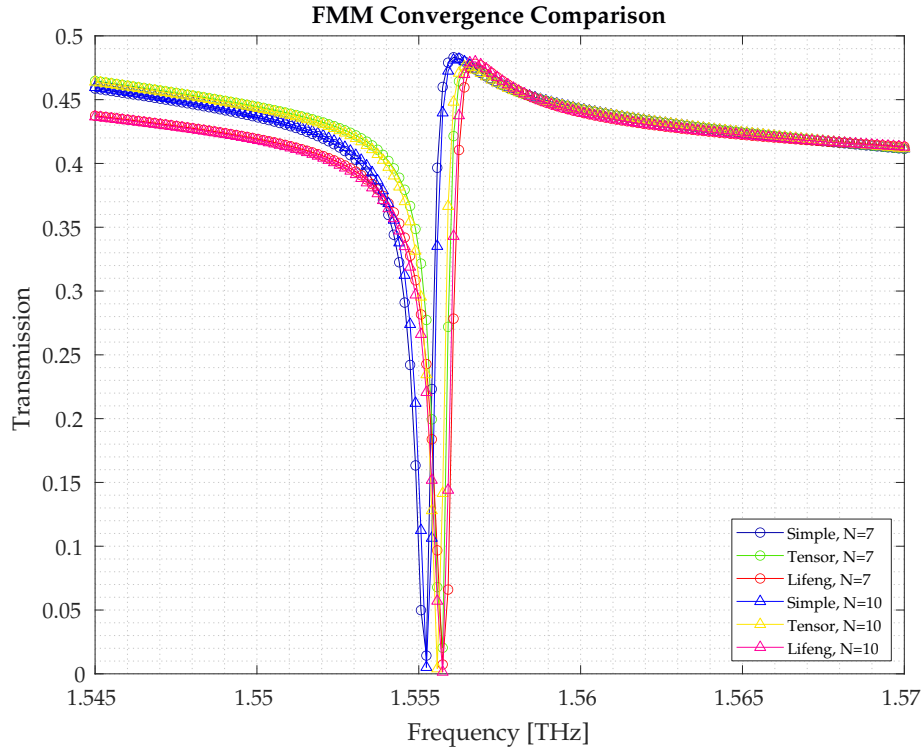


**Figure 5.15:** Transmittance spectra comparing the three different formulations at  $N = 7$  and  $N = 10$ . Each spectrum is for sample SRS1 2.1 and 150 frequencies.

Lastly, for the square rod structure, the three formulations were compared for  $N = 7$  and  $N = 10$ . All three formulations at  $N = 10$  give resonances at approximately  $f_0 = 1.555$  with deviations of at most 1 GHz with Li's formulation being at the highest frequency. Regarding the convergence, the simple and Lifeng spectra show no shift in  $f_0$  from  $N = 7$  to  $N = 10$ . The tensor spectra do shift by  $< 1$  GHz, towards a lower frequency. The fitted values of shape factor  $q$ , linewidth  $\Gamma$ , resonance frequency  $f_0$  for each formulation and  $N = 10$  can be seen in Table 5.1. The linewidth for the simple and tensor formulations are 550.6 and 509.2 MHz respectively, while it is significantly wider at 737.5 MHz for the Lifeng Li. For the square rod structure, the tensor formulation gives the most symmetric resonance at  $q = 0.280$ , while the Lifeng Li gives the most asymmetric at  $q = 0.3345$ .

FMM Type	$q$	$\Gamma$ [MHz]	$f_0$ [THz]	$R^2$
Simple	0.3268 (0.3208, 0.3328)	550.6 (544.1, 557.2)	1.555 (1.555, 1.555)	0.9977
Lifeng	0.3345 (0.3212, 0.3478)	737.5 (718.6, 756.5)	1.556 (1.556, 1.556)	0.9883
Tensor	0.2860 (0.2707, 0.3012)	509.2 (494.0, 524.4)	1.555 (1.555, 1.555)	0.9845

**Table 5.1:** Table containing the three parameters, shape factor  $q$ , linewidth  $\Gamma$  and resonance frequency  $f_0$ , of the Fano formula fitted to the  $N = 10$  spectra for each formulation along with 95% confidence interval for each parameter and the  $R^2$  for each fit.

The convergence and comparison test for the SRS1 structure have likewise been conducted for the SRC1 structure. SRC1 have the same parameters as SRS1, except for  $a_{cyl} = 18.3362 \mu\text{m}$ , which were chosen such that the cross-section area of the cylinders and square rods are the same. The same number of plane waves and the same frequency vector have been used, since the same requirement for computational cost and resolution apply here.

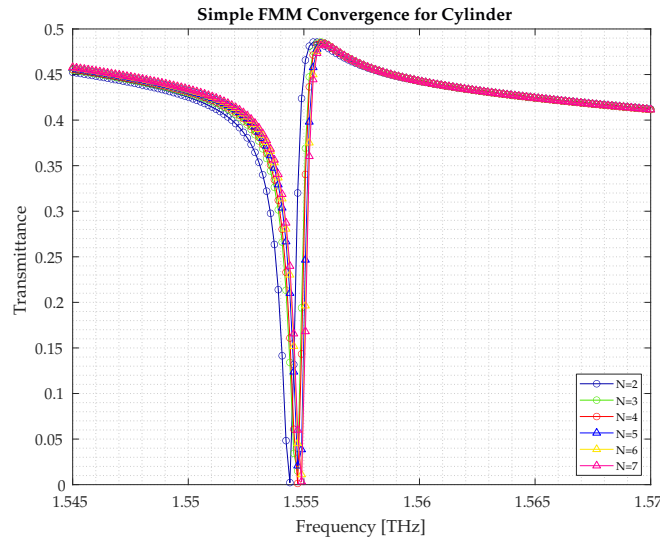


**Figure 5.16:** Transmittance spectra for 6 different numbers of plane waves with the parameter  $N$  ranging from 2 to 7, simulated with the simple FMM formulation. The simulated samples are SRC1 described in Table 2.2. Each spectrum consists of 150 discrete frequencies.

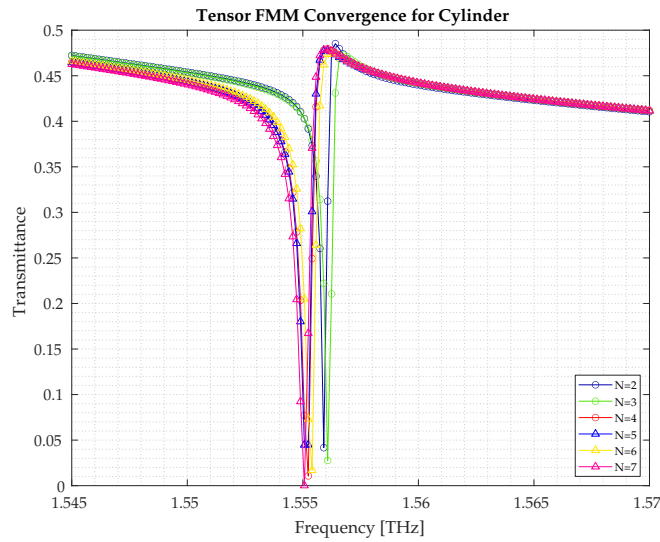


**Figure 5.17:** Transmittance spectra for 6 different numbers of plane waves with the parameter  $N$  ranging from 2 to 7, simulated with the tensor FMM formulation. The simulated samples are SRC1 described in Table 2.2. Each spectrum consists of 150 discrete frequencies.

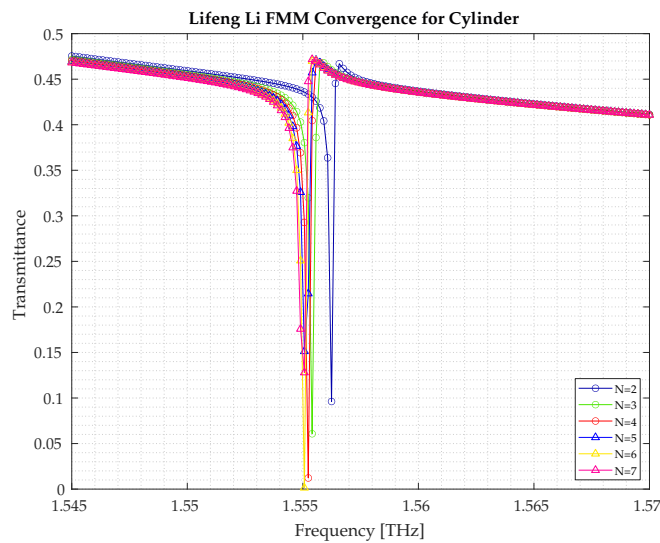


**Figure 5.18:** Transmittance spectra for 6 different numbers of plane waves with the parameter  $N$  ranging from 2 to 7, simulated with the Lifeng Li FMM formulation. The simulated samples are SRC1 described in Table 2.2. Each spectrum consists of 150 discrete frequencies.

The convergence of the simple, tensor and Lifeng Li FMM formulations on the SRC1 structure, for  $N = 2$  to  $N = 7$ , can be seen in Figure 5.16, 5.17 and 5.18 respectively. All three spectra for all three formulations converge to a resonance frequency of  $f_0 \approx 1.555$  THz. For

the simple formulation, all spectra resonance frequencies are within 2 GHz of 1.555 THz. The tensor formulation has one spectrum,  $N = 3$ , which deviates more than 2 GHz from  $N = 7$ , while the same is true for  $N = 2$  in the Lifeng Li formulation spectrum.

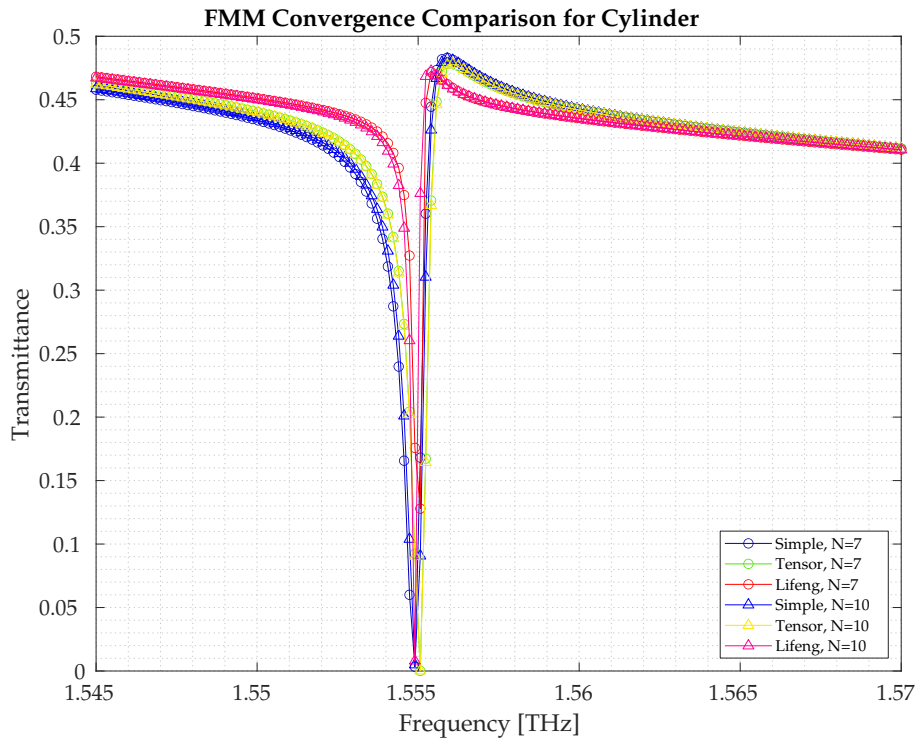


**Figure 5.19:** Transmission spectra comparing the three different formulations at  $N = 7$  and  $N = 10$ . Each spectrum is for sample SRC1 as seen in 2.2 and 150 frequencies.

Other than the convergence for each formulation, the three formulations were also compared for  $N = 7$  and  $N = 10$ , which can be observed in Figure 5.19, furthermore the fitted parameters for the profiles can be found in Table 5.2 for  $N = 10$ . For each formulation, there is no apparent shift in resonance frequency between  $N = 7$  and  $N = 10$  and only a slight change in profile, while there is  $< 1$  GHz change in resonance frequency between the formulations. For the circular-shaped rods, the resonance from the Lifeng Li formulation is the narrowest and the spectral width is less than half compared to either of the other formulations. On the other hand, here the Lifeng Li formulation is the most symmetric and the simple the most asymmetric.

FMM Type	$q$	$\Gamma$ [MHz]	$f_0$ [THz]	$R^2$
Simple	0.3163 (0.3140, 0.3186)	581.3 (578.7, 583.9)	1.555 (1.555, 1.555)	0.9997
Lifeng	0.2634 (0.2507, 0.2760)	234.7 (229.4, 239.9)	1.555 (1.555, 1.555)	0.9922
Tensor	0.2946 (0.2894, 0.2998)	528.3 (522.9, 533.7)	1.555 (1.555, 1.555)	0.9983

**Table 5.2:** Table containing the three parameters, shape factor  $q$ , linewidth  $\Gamma$  and resonance frequency  $f_0$  of the Fano formula fitted to the  $N = 10$  spectra for each formulation along with 95% confidence interval for each parameter and the  $R^2$  for each fit.

### 5.3 Coupling to Guided Modes

The modes were found by calculating  $m_{11}$  from Section 4.2 for  $n_m$  between 1 and 3.4 for wavelengths between 120 and 340  $\mu\text{m}$  and then finding where  $m_{11} = 0$ . In these calculations the simulated structure were the B1 structure found in Table 2.1. The calculations were done for S and P polarized light and the results can be seen as the blue lines in Figure 5.20 where the propagation constant is plotted against the vacuum wavelength. In the plots the first three diffraction orders of the periodic layer  $\frac{m2\pi}{\Lambda}$  where  $m = 1, 2, 3$  is plotted as the green dashed lines as well and where these lines cross the guided mode line is where it would be expected to find a Fano resonance.

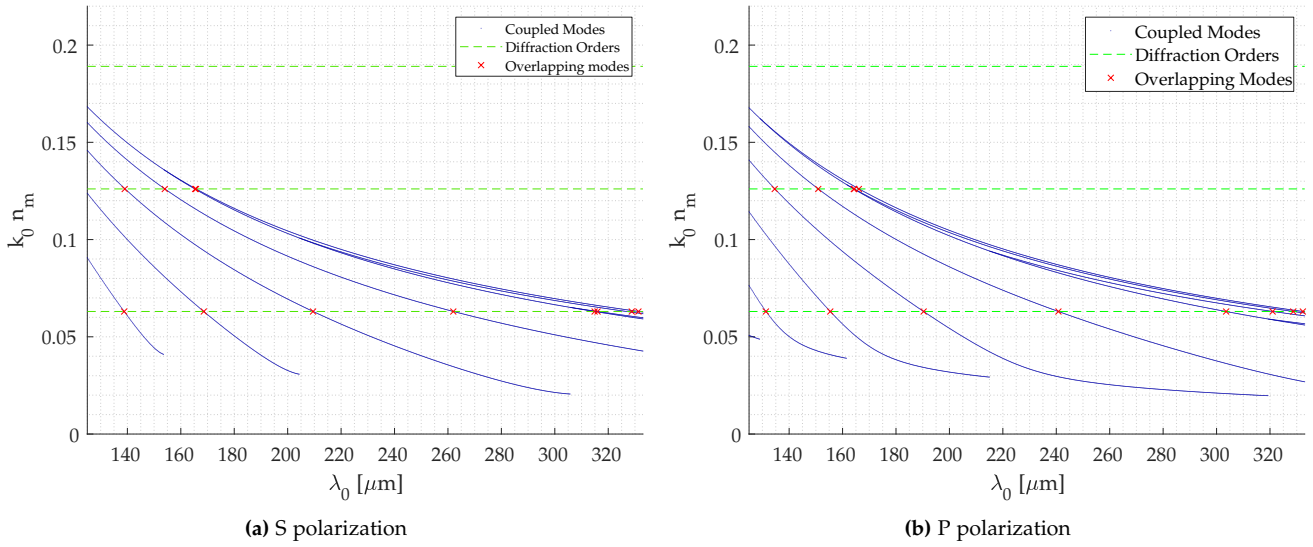


**Figure 5.20:** Calculated propagation constants for the structure of four layers with permittivity  $\varepsilon_1 = 1$ ,  $\varepsilon_2 = \frac{a\varepsilon_3 + (\Lambda - a)\varepsilon_1}{\Lambda}$ ,  $\varepsilon_3 = 3.4^2$  and  $\varepsilon_4 = 1$ . This was calculated for wavelengths between 125-333  $\mu\text{m}$  (0.9-2.4 THz). The green dotted lines represent the diffraction orders ( $m2\pi/\Lambda$ ) for  $m = 1, 2, 3$ . At the intersection where the diffraction order is equal to the guided mode propagation constant a Fano resonance is to be expected and is marked with a red x. The simulated structure were B1.

It was found that the guided mode indices equals the diffraction order for the wavelengths found in Table 5.3. Now these values can be compared to the resonances found through FMM. For the 1-dimensional periodic structure the transmittance for  $N = 5$  subtracted for  $N = 0$ , for S- and P-polarization is plotted in Figure 5.21 with the frequencies where the diffraction line equals the guided modes for the wave guide.

Overlapping Propagation $\lambda_0$ [ $\mu\text{m}$ ]			
S-pol.	P-pol.	S-pol.	P-pol.
(m=1)		(m=2)	
142.5	131.3	139.8	134.6
171.9	155.4	154.4	150.9
212.5	190.4	165.4	164.2
264.1	240.8	166.7	164.4
315.7	303.6		166.1
326.4	321.0		
331.15	328.7		
	332.3		

**Table 5.3:** Calculated wavelengths in  $\mu\text{m}$  where the first two diffraction orders for a wave incident on a periodic silicon-air structure given as  $\frac{m2\pi}{\Lambda}$ , is equal to the propagation constants of guided modes of a waveguide consisting of a layer of silicon and a layer of periodic silicon-air surrounded by layers of air.

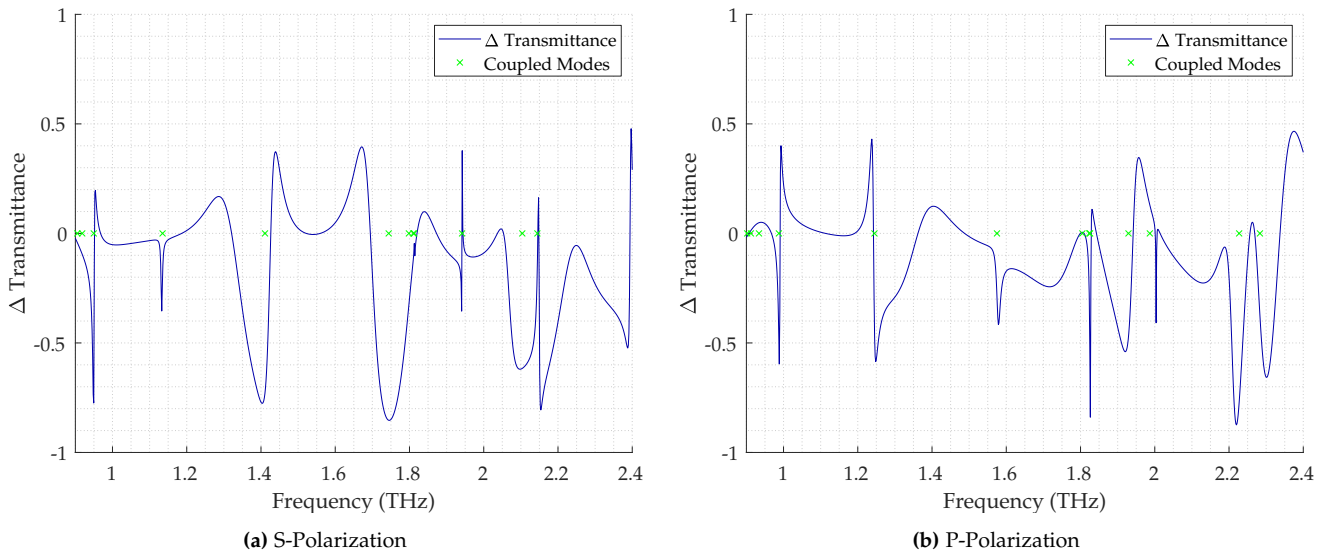


**Figure 5.21:** The  $\Delta$ -transmittance line is the respective transmittance calculated for  $N = 0$  subtracted from the transmittance for  $N = 5$ . The green 'x's represent the frequencies where a guided modes, lies at the same frequency as a diffraction order. These results are for the 1D-periodic air-Si/air-Si-air structure, B1, with  $\epsilon_1 = \epsilon_4 = 1$ ,  $\epsilon_2 = \frac{a\epsilon_3 + (\Lambda - a)\epsilon_1}{\Lambda}$ ,  $\epsilon_3 = 3.4^2$ .

For the 2D periodic structure the coupled modes were still calculated using the same model with the only exception being how  $\varepsilon_2$  was found. Then as before, the transmittance was calculated for  $N = 0$  where from the  $N = 5$  transmittance is subtracted and the coupled modes for both S and P-polarization were found as well (Figure 5.22). It can again be noted that all coupled modes lies right at a resonance peak however not all resonance peaks sees a coupled mode.

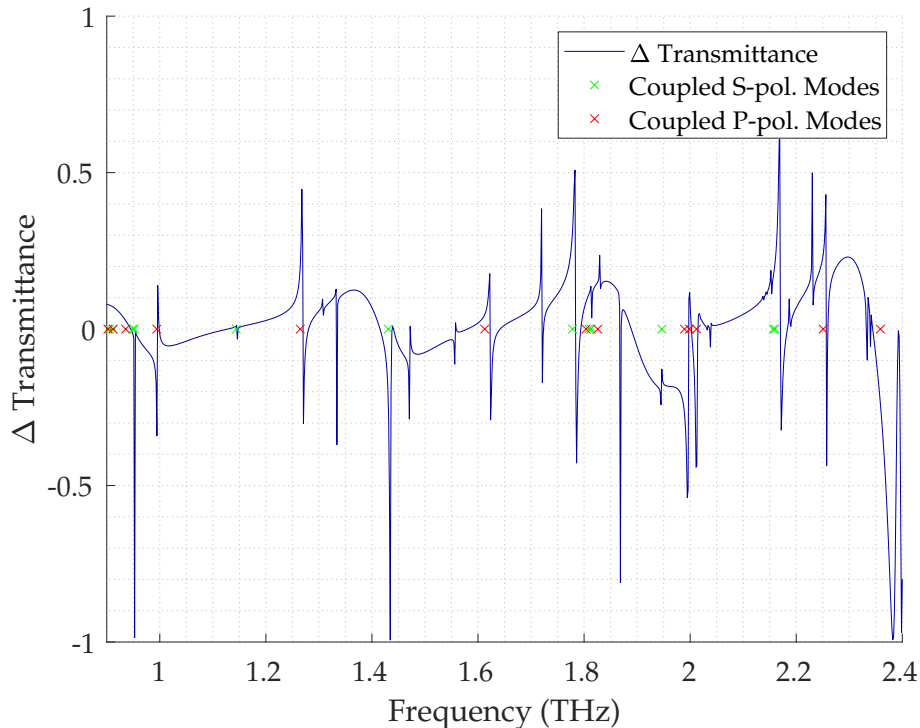


**Figure 5.22:**  $\Delta$ -transmission line is the transmittance calculated for  $N = 0$  subtracted from the transmittance for  $N = 5$  for the 2D-periodic structure, SRS1, consisting of layers air-Si/air-Si-air. The green and red x's represent the frequencies where guided modes lies at the same frequency as a diffraction order, calculated for a 1D periodic structure, B1, for S and P-polarization.

## 5.4 Square or Cylindrical Rods

In reality the periodic structure of the photonic crystal would not be made of square rods but of cylindrical shapes instead<sup>[33]</sup>. Two different dimensional choices where the square structure would match the cylindrical structure in behavior was thought to be, either when the cross-sectional area of the rods would be the same, meaning that the radius of the cylinders would be  $r = \frac{a}{\sqrt{\pi}}$  where  $a$  is the side length of the square rod or when the diameter of the cylinder would match  $a$ . The two different cylinders were constructed and the spectra were

computed and in Figure 5.23 a resonance is seen for all three structures. Non of the three peaks is exactly similar but is at most 1 GHz apart however the cylinder with  $r = \frac{a}{\sqrt{\pi}}$  is the closest to the square calculations being under 0.1 GHz apart for both  $N = 3$  and 5. The calculated coefficients for the permittivity of a single rod is plotted for a square rod and for cylinder where  $a = 2r$  and  $a = \sqrt{\pi}r$  in Figure 5.24 for  $N = 3, 5, 10$ .

The spectra for cylindrical and square rods for  $a = r\sqrt{\pi}$  was calculated between 0.9-2.4 THz (Figure 5.25). Here it is clear that apart from the height of the resonances, simply due to the resolution of the frequency and because the peaks are not exactly in the same position, there are no distinct difference in the two spectra.

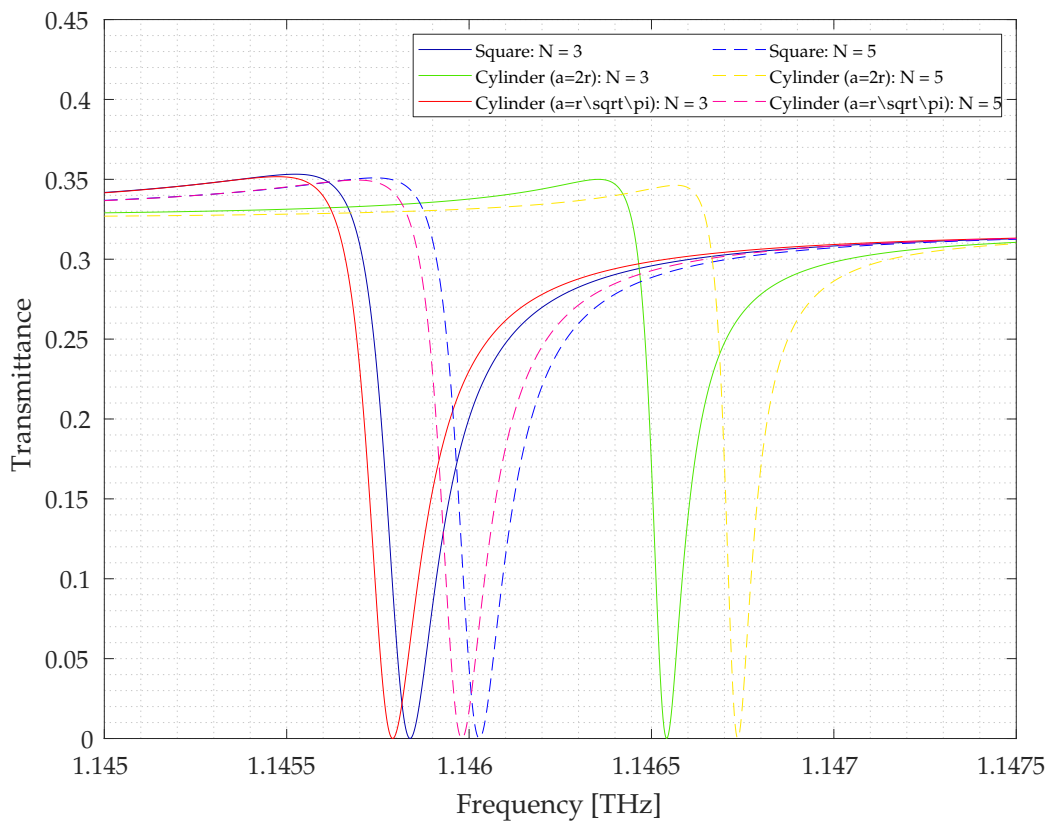


**Figure 5.23:** A single resonance in transmission calculated for square rods (SRS1) and two cylindrical rods (SRC1, SRC2) where either the area or the side length and diameter are equal. Calculated for  $N = 3, 5$ .

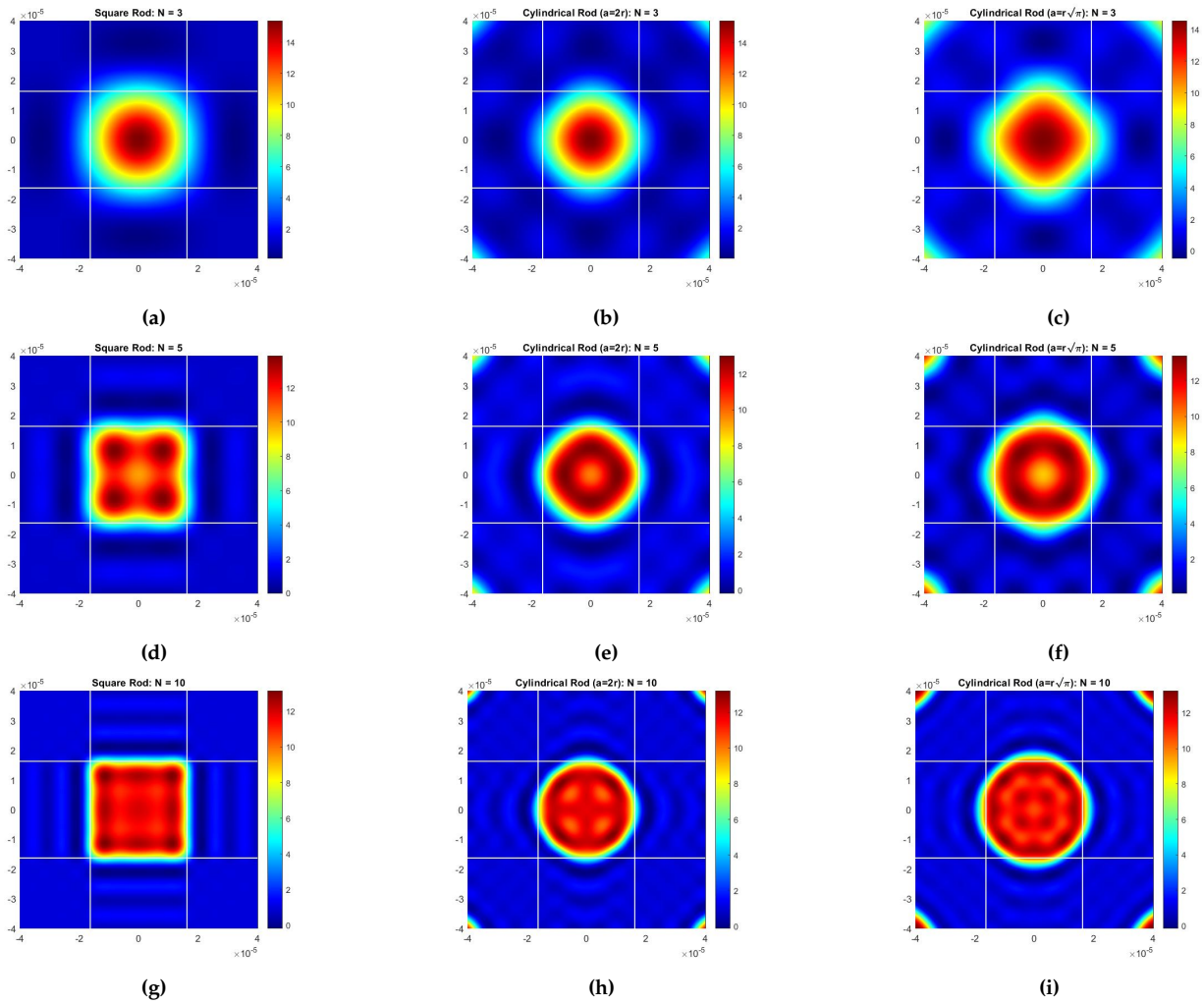


**Figure 5.24:** The calculated permittivity coefficients of the rods calculated for a square (SRS1) and for cylinders with radius  $r = \frac{a}{2}$  (SRC2) and  $r = \frac{a}{\sqrt{\pi}}$  (SRC1) for  $N=3, 5, 10$ . The white lines is at  $\pm 16.25\mu\text{m}$  for both axes.  $x$ - and  $y$ -axis are plotted in  $\text{m}$

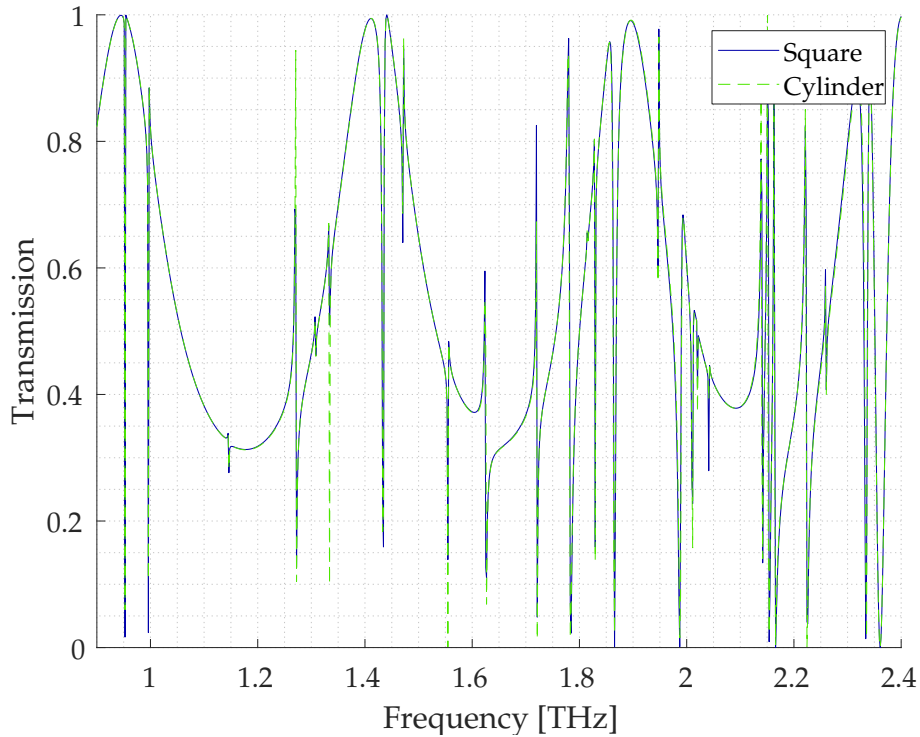


**Figure 5.25:** Transmission spectrum calculated for rods being either square (SRS1) or cylindrical (SRC1) where the area of the rods is equal for both calculations.  $N = 3$

## 5.5 Transmittance for Angled Incidence Field

In this test the angle of the incident light was varied. This was done for square rods (SRS1), cylindrical rods (SRC1) and for the one-dimensional periodic bar structure (B1). In [23] this test was performed for bars but since 2D FMM was used, only the angle perpendicular to the direction of the bars could be varied. Using the 3D FMM, it is now possible to vary the incident light in any direction i.e. varying  $\theta$  and  $\varphi$  in spherical coordinates. In Figure 5.26 the angle  $\theta$  was varied between 0 and 14 degrees for B1. In 5.26a and 5.26b the angle was varied along the bars while in 5.26c and 5.26d the angle was varied perpendicular to the bars.

Since the field is rotated 90 degrees between the 5.26a - 5.26b and the 5.26c - 5.26d the resonances found in 5.26a and 5.26d are the same, and the resonances found in 5.26b and 5.26c are the same. The 5.26a and 5.26d simulations feature seven distinct resonances. In the  $\varphi = 0^\circ$  case, where the field was angled along the bars, the resonances all seem unaffected by the field angling. In the  $\varphi = 90^\circ$  case, where the field was angled against the bars, all seven resonances split into two each. The splits increases with  $\theta$  and two pairs of resonances overlap and interfere before  $\theta = 14^\circ$ , namely the  $f_{1.8}, f_2$  pair and the  $f_{2.2}, f_{2.4}$  pair. For the

5.26b and 5.26c simulations, similar but slightly shifted resonances are observed where again the equivalent resonances interfere as before.

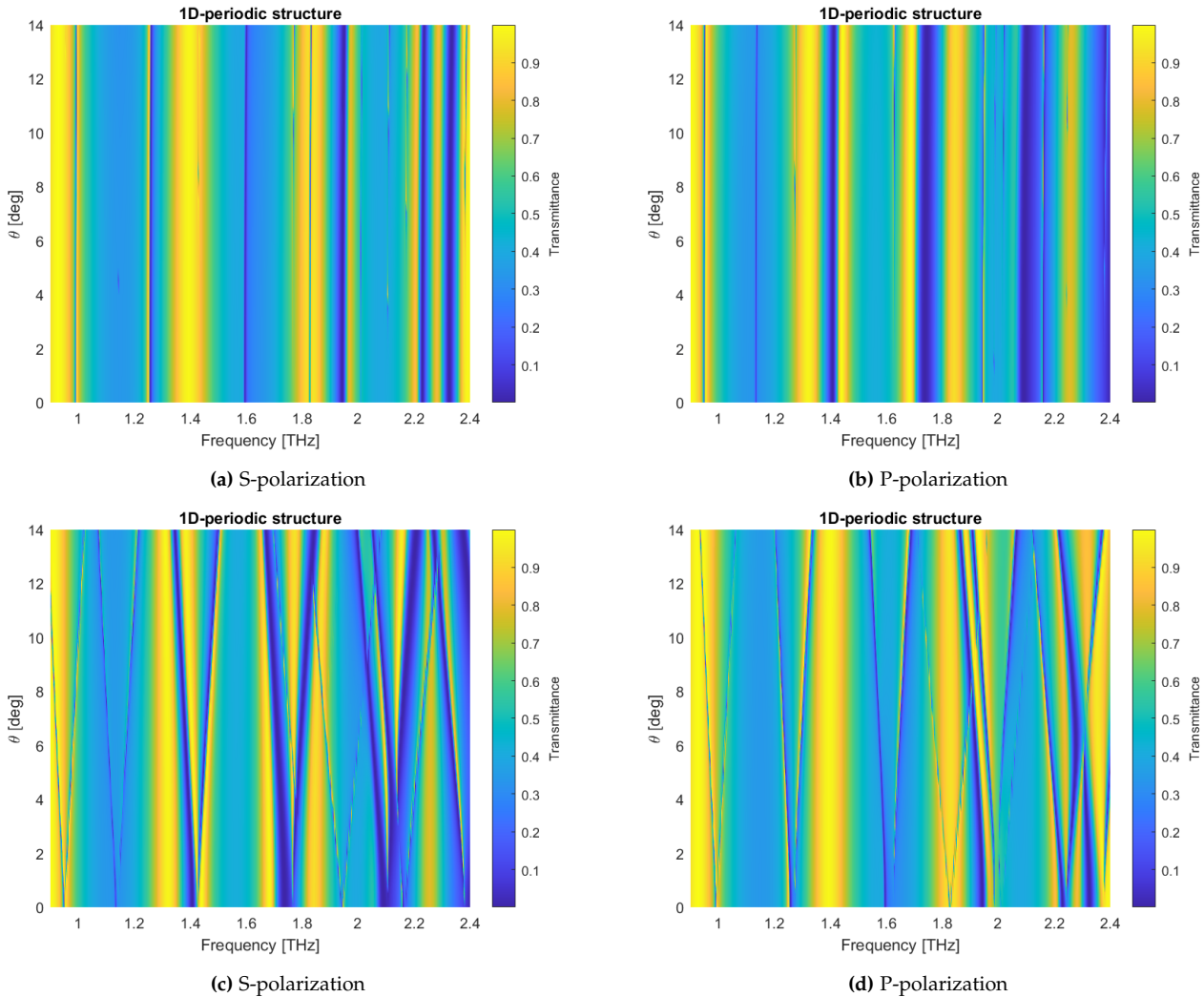


**Figure 5.26:** Transmittance for the one-dimensional periodic structure (B1) at angles  $\theta = 0 : 14$  in increments of 0.5. In (a) and (b)  $\phi = 0$  and in (c) and (d)  $\phi = 90$ . Calculations for  $N = 5$  and 500 discrete frequencies from 0.9 to 2.4 THz.

For the same angles as before the same test was done for squares as well as cylindrical rods using the simple formulation. Figure 5.27 shows the result for the square rods while Figure 5.28 shows the results for cylinders for S- and P-polarization. (The same plots done for  $\phi = 90^\circ$  are in Appendix B). For both S- and P-polarized light and for both structures some of the resonances split once again while others do not. Comparing the results for the square rods with figures 5.26 some of the split resonances appear to repeat for either S- or

P-polarization. As an example, the resonance  $f_{1.3}$  splits for P-polarization and not for S-pol. for the squares. This resonance can be found for P but not S-polarization for the bars. On the other hand,  $f_{1.4}$  can be seen splitting for S-polarization for both bars and rods. In the 3D model some resonances split for both polarizations such as  $f_{1.9}$ . This resonance does not seem to be observed in either case for the bar structure.

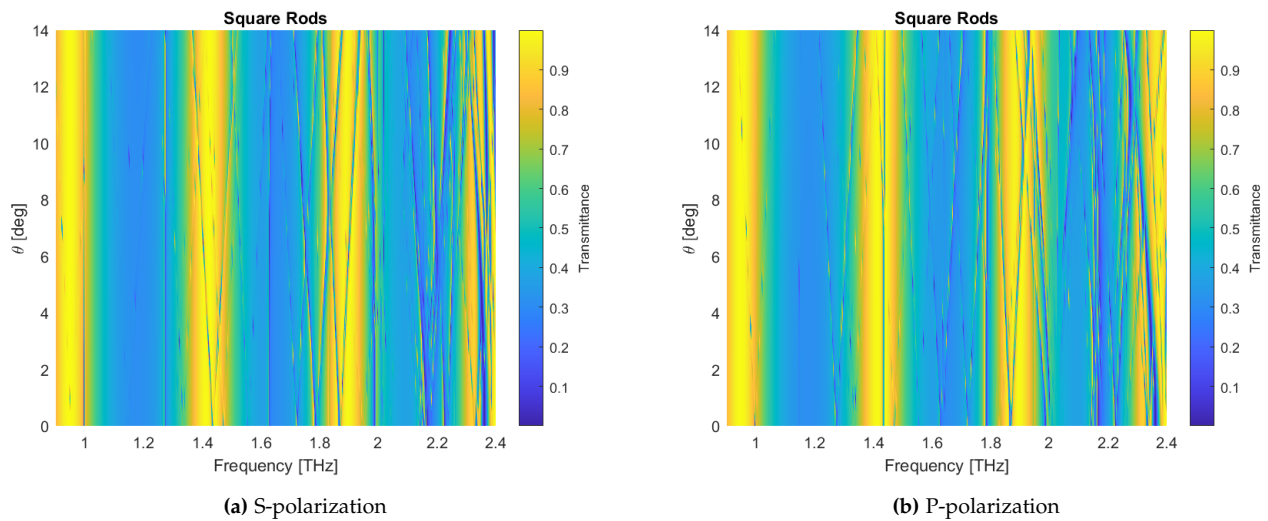


**Figure 5.27:** Transmittance of the SRS1 structure for  $\theta = 0 : 14$  deg in increments of 0.5 with  $\varphi = 0$  deg. Calculations done with  $N = 5$  and 500 discrete frequencies from 0.9 to 2.4 THz.

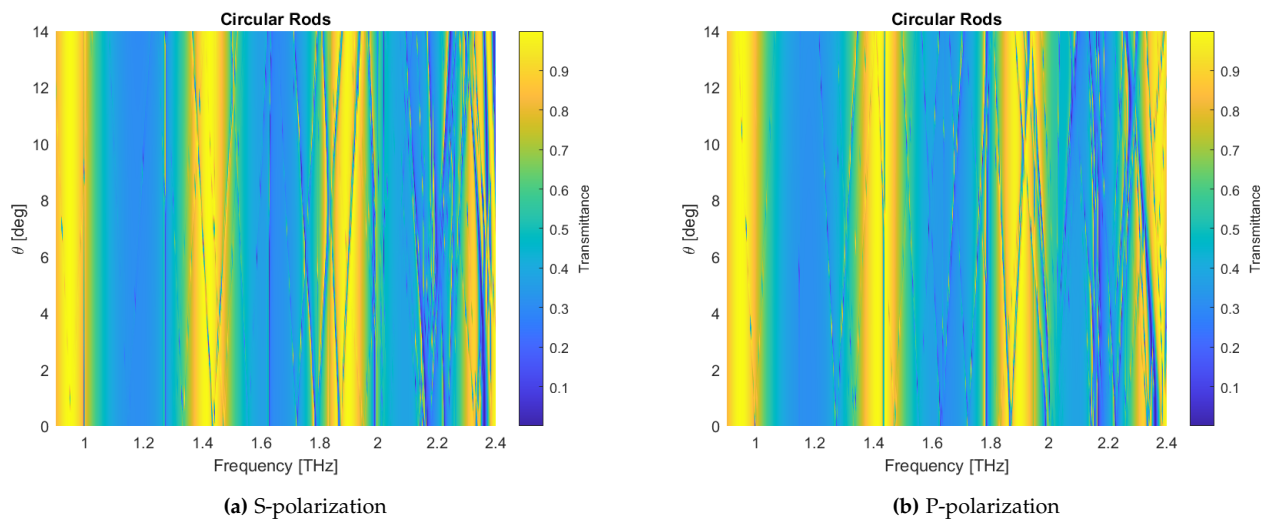


**Figure 5.28:** Transmittance of the SRC1 structure for  $\theta = 0 : 14$  deg in increments of 0.5 with  $\varphi = 0$  deg. Calculations done with  $N = 5$  and 500 discrete frequencies from 0.9 to 2.4 THz.

The simple 3D FMM model was also used to show the effect of the change in  $\varphi$  on the transmittance from the structure. Figure 5.29 shows the transmittance plotted vs. frequencies from 0.9 to 2.4 THz for  $\varphi$  from 0 to 45 degrees with constant  $\theta = 10$  deg. The structure calculated is the SRS1 with the parameter  $N = 5$ . The same effect that is seen when varying  $\theta$  is present in these cases. Some of the resonance frequencies will split. Since  $\theta = 10$  deg, the resonances at  $\varphi = 0$  are already split, relative to the ones for a normal incident field.

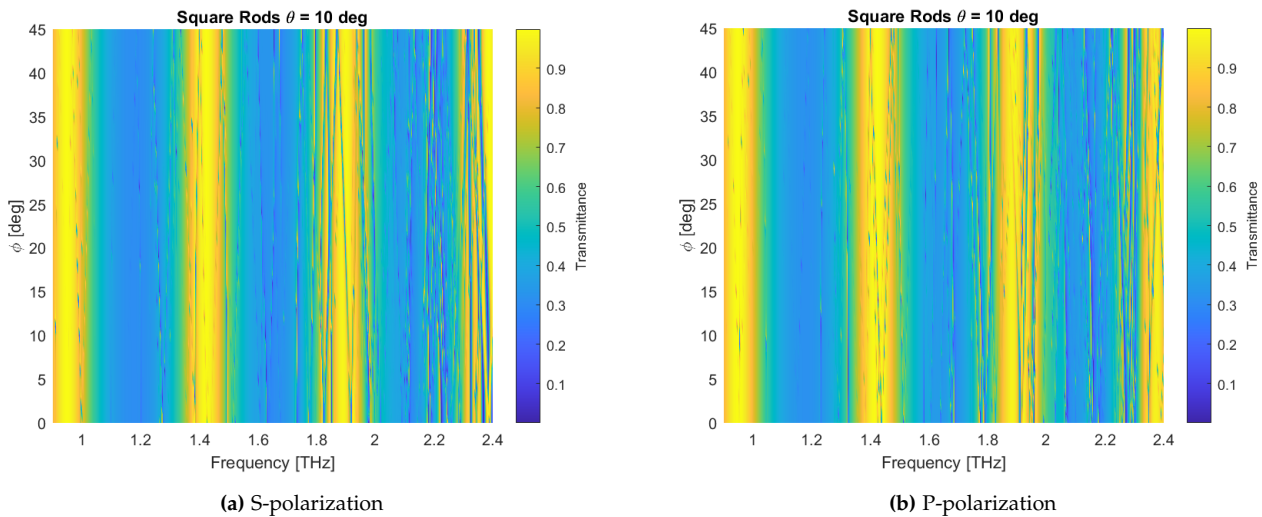


**Figure 5.29:** Transmittance of the SRS1 structure for  $\varphi = 0 : 45$  deg in increments of 1 with  $\theta = 10$  deg. Calculations were done with  $N = 5$  and 500 discrete frequencies from 0.9 to 2.4 THz.

## 5.6 Effect of the Structural Variables

The construction of the photonic crystal plays a part in what specific frequencies will be reflected and transmitted in the structure. To get an idea of which parameters could be used for tuning of the crystal as well as testing if the model behaves in a way that can be physically explained, the different physical parameters will be varied one at a time in this section.

### 5.6.1 Resonator Quality vs. Structure Height

Since the Fano resonances are caused by a coupling between the discrete modes in the periodic layer, and the continuous modes of the incident light, the periodic layer acts like a resonator<sup>[3]</sup>. The quality factor (Q-factor) of the simulated systems will be dependent on the height of the periodic layer, since lower layer height removes the effective diffraction grating of the system, making more difficult to couple with the guided modes of the system.

In Figure 5.30 a single resonance is plotted for various heights of the rods varying from 2.9 to 12.9  $\mu\text{m}$ . The Q-factor can be calculated by the full width at half maximum  $\Delta f_{1/2}$  of a resonance peak as  $Q = \frac{f}{2\Delta f_{1/2}}$  where  $\nu$  is the frequency at the peak<sup>[34]</sup>. In Figure 5.30 it is clear for taller rods the peak becomes wider relating to a smaller Q-factor. The Q-factor can also be calculated from the decay rate  $\gamma$  of the energy of the light stored in the cavity lost through transmission and absorption as  $Q \approx \frac{f}{\gamma}$ <sup>[34]</sup>. A way to accurately determine the linewidth  $\Gamma$  and resonance frequency  $f_0$  of each spectra were to fit each spectra to the Fano formula<sup>[3]</sup> presented in Chapter 1,

$$\sigma = \frac{(\epsilon + q)^2}{\epsilon^2 + 1}, \quad (5.2)$$

where  $\epsilon = 2(f - f_0)/\Gamma$  and  $q$  is the shape parameter.

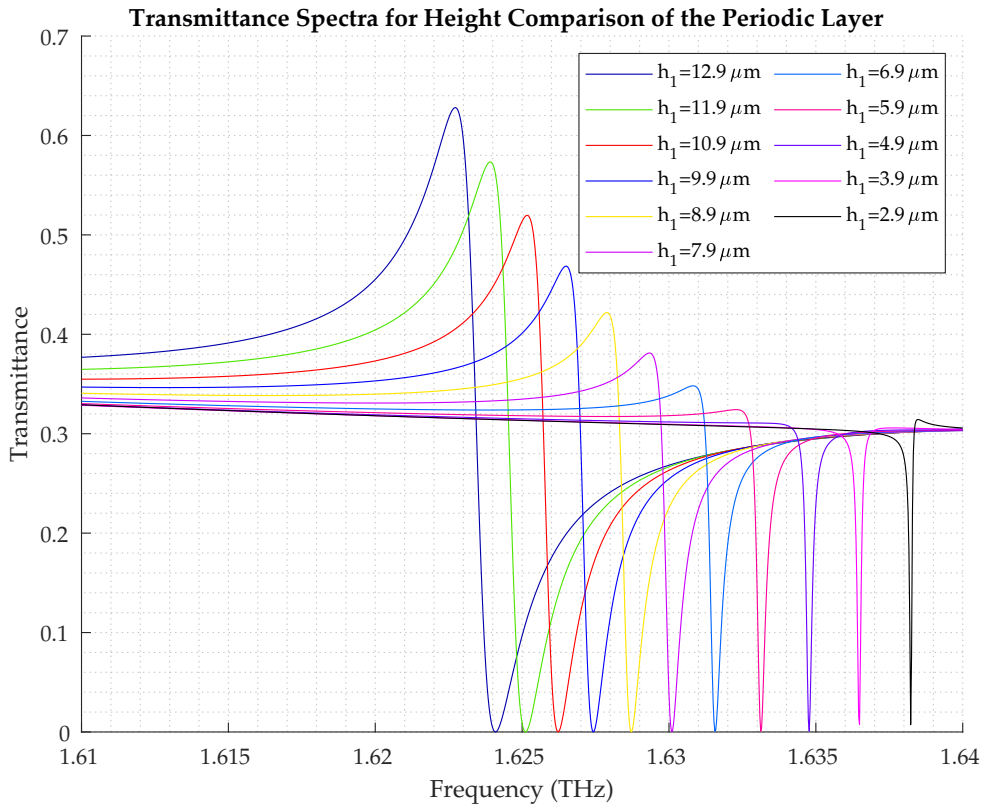


**Figure 5.30:** Transmittance spectra for different periodic layer heights, while otherwise keeping the parameters as in the SRS1 structure. The calculations were done for 400 frequencies and  $N = 5$ , with the simple FMM formulation.

The Q-factor calculated from the fitted parameter can be observed in Figure 5.31. Just as the spectral linewidth gets smaller as the height decreases, the Q-factor increases uniformly

as the height decreases.

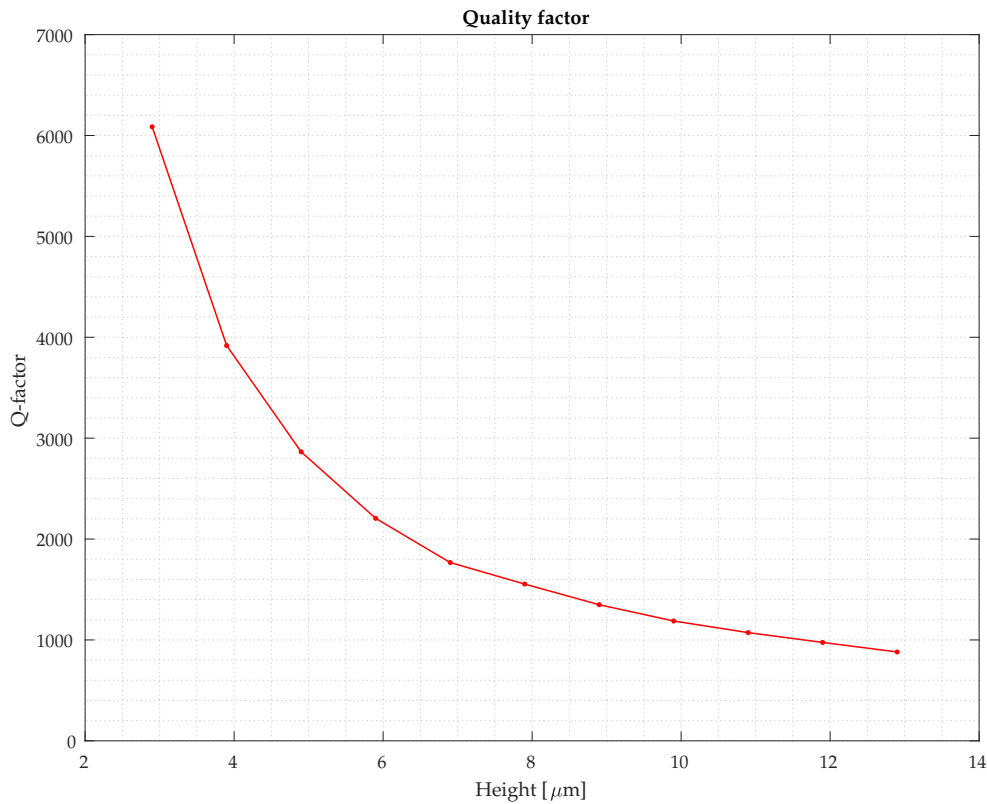


**Figure 5.31:** Plot of Q-factor vs. periodic layer height calculated from the fits of the spectra observed in Figure 5.30.

### 5.6.2 Changing $a$

For the next test the side length of the silicon square rods in the periodic layer was varied. The test was done using the 3D FMM using the simple formulation for the permittivity matrix. In Figure 5.32 the transmission for frequencies between 0.99 and 1 THz with 1000 steps is plotted. The calculations were then done for the side length of the silicon rods in the periodic layer being from 10-90% of the period. What can be noticed is how the resonance moves to lower frequencies when the amount of silicon in the periodic layers increases. The resonance frequency of the resonance for the different structures can be seen in Table 5.4. Another interesting feature is the change in the shape of the peak. At 0.1 and 0.9  $\Lambda$  the peak is sharper while it becomes wider when  $a \approx 0.5\Lambda$ . This gives rise to the Q-factor changing with  $a$  and the Q-factors for the various resonances is plotted in Figure 5.33. The Q-factor is obtained from the spectra in the same fashion as the result in Section 5.6.1. This results shows

that the Q-factor is minimum at  $a/\Lambda = 0.5$  and increases as the material ratio approaches either fully air or fully Si.

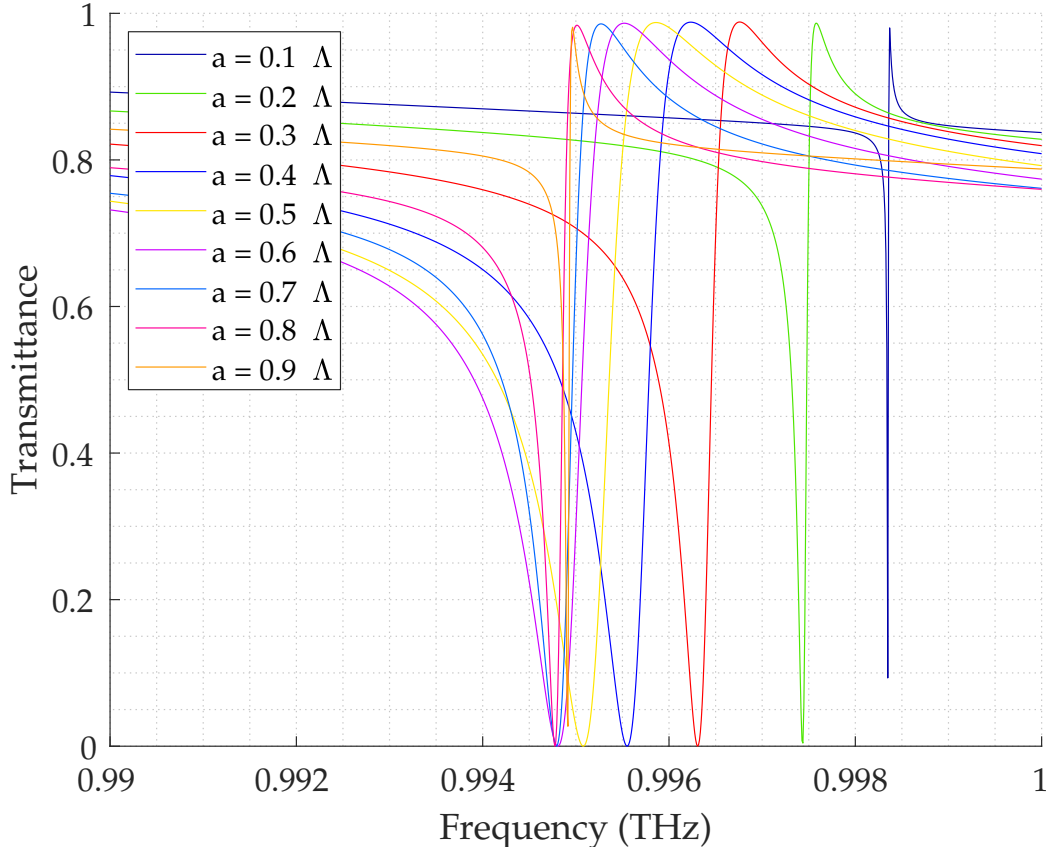


**Figure 5.32:** Transmittance spectrum for 0.99 - 1 THz for the air-Si/air-Si-air periodic square structure. The side length  $a$  of the silicon squares is chosen between 10-90% of the period with intervals of 10% where parameters were otherwise kept the same as SRS1 and  $N = 3$ .

$a$ [ $\Lambda$ ]	0.1	0.2	0.3	0.4	0.5	0.6	0.7	0.8	0.9
Peak Pos. Freq. [THz]	0.998	0.997	0.996	0.996	0.995	0.995	0.995	0.995	0.994

**Table 5.4:** The position of a specific peak in the transmittance spectrum (Figure 5.32) calculated for different values of the side length of the rods of the periodic layer of the crystal. First row gives the side length  $a$  in parts of the period  $\Lambda$ . Second row gives the position in frequency of the peak.

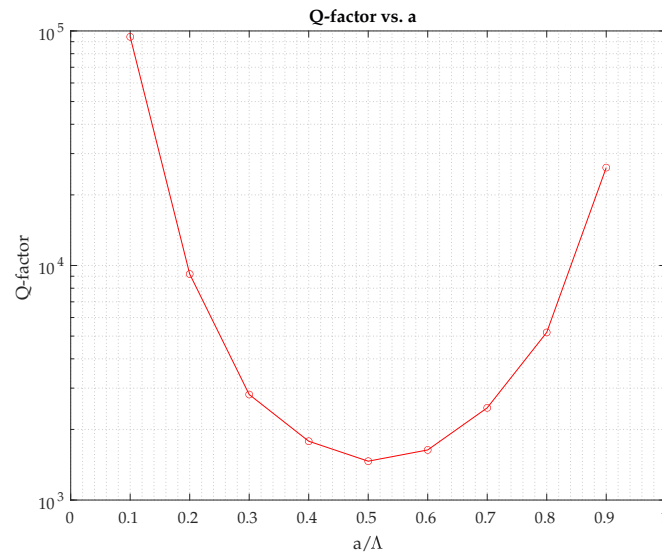


**Figure 5.33:** Q-factor calculated for the result seen in Figure 5.32 found between 0.99-1 THz for different values of  $a$ , going from  $0.1\Lambda$  to  $0.9\Lambda$ . The y-axis is a logarithmic scale.

The same frequency spectrum (0.99 THz - 1.00 THz) were also tested for  $a = 35 \mu\text{m}$  to  $a = 45 \mu\text{m}$ , in  $2.5 \mu\text{m}$  increments and otherwise equal parameters. The results, which can be seen in Figure 5.34, feature resonances that again shift to lower frequencies as  $a$  grows wider (and thus effective permittivity increases) while simultaneously growing wider with increased  $a$ .

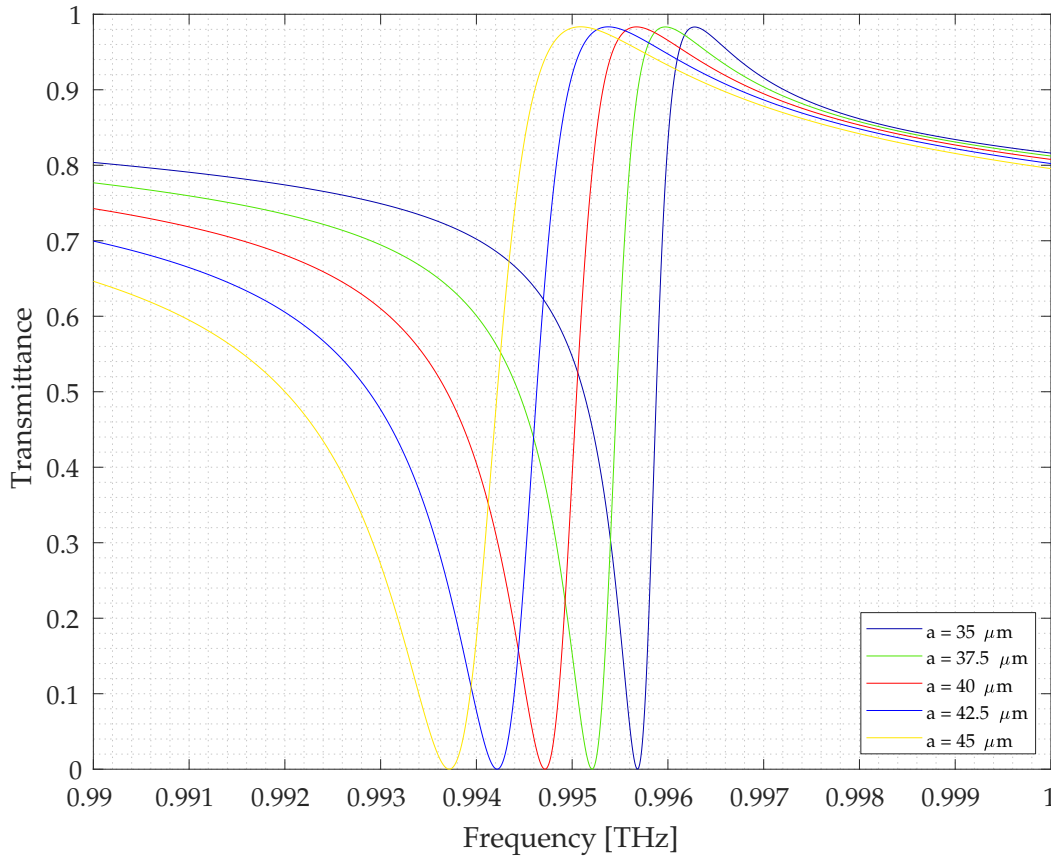


**Figure 5.34:** Transmission spectrum of the air-Si/air-Si-air periodic square structure for different values of side lengths of the silicon squares between 35 and 45  $\mu\text{m}$ , and otherwise the SRS1 parameters, calculated using the simple formulation.

a [ $\mu\text{m}$ ]	35	37.5	40	42.5	45
Peak Pos. Freq. [THz]	0.9957	0.9952	0.9947	0.9942	0.9937

**Table 5.5:** The frequency values for the resonance found between 0.99 and 1.00 THz for different values of the side length of the rods (Figure 5.34).

### 5.6.3 Changing $h_2$

For this test the homogeneous layer of silicon is varied in thickness, between 90  $\mu\text{m}$  and 95  $\mu\text{m}$  in 1  $\mu\text{m}$  increments. The other structure parameters were the same as SRS1, the plane wave parameter  $N = 5$  and the calculations were done for 400 frequencies. The spectra, shown in Figure 5.35, shifts towards lower frequencies as  $h_2$  increases. At the same time, the

resonance gets sharper. There is variation in maximum and minimum of the resonances as well as the rest of the spectrum, where  $h_2 = 90$  gives the largest transmission.

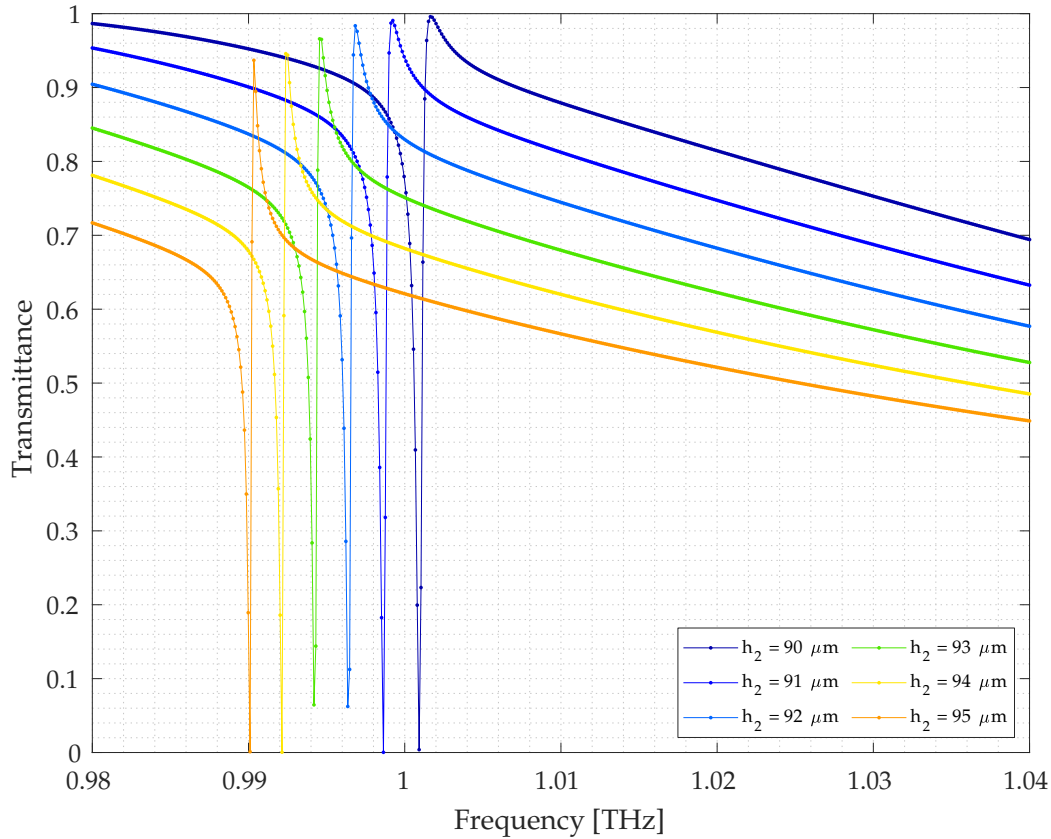


**Figure 5.35:** Transmittance spectra for the square periodic structure with layers air-Si/air-Si-air. The calculations were computed using the simple formulation, for  $N=5$  and with SRS1 except with  $h_2$  varying between 90-95  $\mu\text{m}$ .

#### 5.6.4 Changing $\Lambda$

Another parameter investigated were the distance between the rods, i.e changing  $\Lambda$  while keeping  $a$  constant at 32.5  $\mu\text{m}$ . It is expected that the resonances shift in frequency as the ratio, between Si and air change, resulting in the effective permittivity in the middle layer changing. This effect is seen in Figure 5.36 where a Fano resonances is found between 0.955 and 1.0 THz. The spectrum is plotted for  $\Lambda$  between 100 and 105  $\mu\text{m}$  where it is seen that the larger period relates to a shift in resonance to lower frequencies.

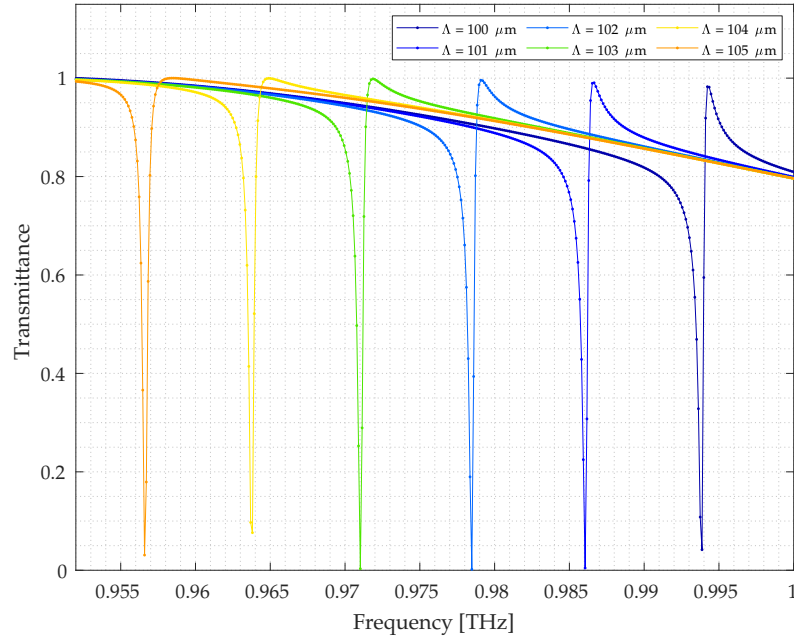


**Figure 5.36:** Transmittance spectra calculated with the simple FMM formulation for the SRS1, except for  $\Lambda$ ,  $N = 5$  and 500 frequencies between 0.94 and 1.00 THz. The period  $\Lambda$  were varied between 100 and 105  $\mu\text{m}$ .

## 5.7 Discussion

The discussion for all results will be done in this section in the same order as they were presented in the project. The first results presented were the convergence test of the 2-dimensional FMM. For S-polarization the factorization rules of Lifeng Li give that the permittivity coefficients should be treated as is, which of course then gives no cause for further investigation as the calculation converges almost immediately. For P-polarization the problem can be expressed with and without using Li's rules and fully as expected Li's formulation does converge better (Figure 5.5c) however Li's formulation does start further away from the converged spectrum. As seen in figures 5.3, 5.4, and 5.6 using Li's rules actually over corrects the result, moving the results up in transmission, up in frequency and appear to make the resonances too sharp for a small number of plane waves. Then when converging the simple and Li's formulations approach each other and meet in the middle when  $N$  increases.

In Section 5.1.2 once again it is shown that for S-polarization there is no problem in finding the same spectra for the 2D and 3D FMM. It was then shown that for P-polarization there was a difference in the result for the transmittance if Li's factorization rules were used or not for a small number of plane waves, as before. However, as the amount of plane waves increases the result converges to the same spectrum.

The test for the three different formulations gave similar results. For the square rods, the

tensor formulation and Lifeng Li's appear to be in best agreement for the peak frequency with the simple formulation seemingly converging at a lower frequency for  $N = 7$  to  $N = 10$  as seen in Figure 5.15. However, the frequency is close to each other with a resonance frequency being no longer than 1 GHz apart. On the other hand, the simple model and the tensor model are closer to each other in linewidth being 41.4 MHz apart while Li's and the simple model are 186.9 MHz from each other. Lastly, for the asymmetry factor  $q$ , the simple and Li's model was closest with values of 0.3268 and 0.3345, respectively. The tensor model peak was the most symmetric at 0.2860.

For the circular-shaped rods, all models once again converged to the same frequency. The simple model had the least deviation between each run, as was seen for the 2D model as well, while the tensor model had the highest amount of plane waves before converging, still fluctuating slightly at  $N = 7$ . For  $N = 2$  Li's formulation deviates the most but it is mostly converged at  $N = 3$ . For the cylinders the resonance frequency was the same for all models however this time Li's formulations deviated in the other direction for the linewidth, being the narrowest of the three with  $\Gamma = 234$  MHz being under half of the linewidth of the other formulations. Now Li's model appeared the most symmetric while the simple model was the most asymmetric. Given that these are numerical models being compared to each other, the deviations in the linewidth are of the order of MHz, the inconsistency in the symmetry and the similar  $f_0$ , it is not possible to determine which model is most correct.

No formulation showed to be superior when looking at resonance position and shape, however, Li's formulation did appear to converge faster vs.  $N$  for the two-dimensional periodic structure as well. The tensor formulation makes jumps both up and down in frequency when increasing the number of plane waves. This is believed to be because of the way the tensor averaging is calculated in real space, making some numbers of plane waves more favorable than others. For the correct amount of plane waves no averaging for the parallel and perpendicular permittivity is needed. This happens when the ratio  $\Lambda/a$  approximately evenly divide the number of plane waves along each direction.  $\Lambda = 99.7 \mu\text{m}$  and  $a = 32.5 \mu\text{m}$  then dictates that the number of plane waves along each direction is divisible by three. This means  $N = 4, 7, 10, \dots$  should give more accurate simulations than other values of  $N$ . This was indeed seen in Figure 5.13 where  $N = 4$  was closer to  $N = 7$  than  $N = 5$ .

Now that all the convergence tests are done for all FMM formulations various properties of the photonic crystal and of the Fano resonances were examined. The reason for the first of these tests was both to show that the Fano resonances indeed is a product of the continuous incident light coupling to the guided modes existing in the structure as well as possibly acquiring a way of finding out which frequencies would exhibit resonances. For the 1D periodic structure there appears to be a good correlation between the coupled modes and the position of the peaks for both S and P-polarization with clear resonances appearing at or close to all the coupled mode frequencies except for the the low frequency end for both polarization. For the 2D periodic structure most of the peaks found are still accompanied by a

guided mode however a few extra peaks appear. These extra peaks seen in the transmittance could be due to S and P polarization waves coupling in the structure, which is not accounted for in the wave guide calculations or they could appear because of the sharp edges that appear in the 2D periodic case. However the model of using guided modes to find out where to look for Fano resonances is a viable solution as there is a clear relation, which also gives credence to the reason for the Fano resonances.

To be able to calculate the transmittance for a structure of cylindrical rods by using the permittivity of a square, it was to be found out in which way the dimensions for the rods should relate. This gave rise to the next calculations where a cylindrical rod was constructed where  $a = 2r$  or  $a = \sqrt{\pi}r$ . In Figure 5.23 it could easily be seen that the best fit would be a square with the same area as the cylinder. It is seen that for fewer plane waves the cylinder with  $a = 2r$  is close to the square rod resonance, but as the number of plane waves increases it gets farther away from the results. Looking at Figure 5.24 at the same time it can be realized that for  $N = 3$  cylindrical rods with  $a = 2r$  is approximated too small and with  $a = \sqrt{\pi}r$  possibly slightly too big compared to the square rod. When increasing the plane waves  $a = 2r$  keeps being too small while  $a = \sqrt{\pi}r$  looks to match the square well and would be ideal. Which agrees with the effective medium theory.

The test for various angles showed some different properties. It was shown that the angle of the light had no apparent effect along the bars and it was shown that, when angled perpendicular to the bars, the resonances affected often split in two, one going to higher and one to lower frequencies. This split will come from the fact that the plane waves is described by the wave vectors in equations (3.13) and (3.14). For normal incidence light then the condition for modes to couple to the guided modes in the wave guide, is that the propagation constant for the guided mode  $\pm\beta = \pm nG$ . This would of course only give one specific resonance where this is true. However when the incidence light is angled then the condition becomes  $\pm\beta = k_{x,y} \pm nG_{x,y}$ . This results in two different solutions depending on which path the light takes in the structure. When changing the angle  $\varphi$  in Figure 5.29 the line simply split or not depending if the resonance split for on polarization and not the other. If the resonances found in figures 5.27 and 5.28 is compared to the guided modes from Figure 5.22 it is found that the resonances split for S-polarization but not for P-polarization, such as the resonance found just above 1.4 THz or 1.8 THz are found as guided modes for the S-polarization. On the other hand, the resonances only splitting for P-polarization, such as the resonance just under 1.3 THz, were found as guided modes for the P-polarization. Looking at peaks that split for both polarizations, such as the resonance between 1.8 and 1.9 THz, they were not found as guided modes for one or the other polarization. This could be explained by these resonances coming from a superposition of the two polarizations, which would create resonances that are not inherently found for P- nor S-polarized light.

The split seen for the two-dimensional periodic structure and for the 1-dimensional periodic structure when the angle is perpendicular to the bars would be an interesting topic for

real-life purposes as the light incident on the crystal could cancel out the Fano resonances found for a parallel beam if a Gaussian beam is used. This could happen when the resonance moves enough to no longer overlap for different angles found in the beam. For smaller angle variations, the peak would instead be widened and the transmittance increased.

It was shown that changing the height of the rods of the structure had an impact on the spectrum as smaller rods led to a lowering of peak transmission, a shift to higher frequencies for the peak position and lastly led to the peak becoming more narrow (Figure 5.30). The thickness of the homogeneous silicon layer was kept constant and the position of the peak would be explained by the entire structure becoming more thick, leading to larger wavelengths guided modes and therefore a peak position at lower frequency. The narrowness of the peak could be attributed to the modes being tougher to couple into and out of for smaller rods, leading to more specific wavelengths being reflected. Relating the linewidth to the Q-factor of the structure shows that an increasing height of the rods results in a smaller Q-factor and a faster decaying field in the structure (Figure 5.31). This would indicate that it is equally difficult to couple out of the guided modes. The smaller Q-factor could also explain the larger transmittance for the taller rods.

The next structural parameter change tests the effect of the size of the cross section of the rods. In Figure 5.32 the side length was varied for different percentages of the period from 10% to 90%. What was seen is that, for the smaller and larger rods, the resonance becomes the narrowest while around 50% the peak is the widest. Once again this could be explained by how easy the light couples. As the periodic layer gets closer to being entirely air or silicon the Fano resonance will become more narrow until the light will not be able to couple anymore. Furthermore, as the silicon rods become larger the position of the peak moves to shorter wavelengths but less for the bigger rods. This movement is explained by the periodic layer having a larger effective permittivity meaning that the wavelength for the guided modes is larger and the frequency smaller.

The size of the homogeneous silicon layer was varied between 90 and 95  $\mu\text{m}$  in intervals of 1  $\mu\text{m}$  (Figure 5.35). The overall transmission is at its highest when  $h_2$  matches  $\lambda = \frac{m\lambda_0}{2n}$  for  $m \in \mathbb{N}$ . For  $\lambda_0 \approx 300 \mu\text{m}$  and  $n = 3.4$ , the wavelength  $\lambda \approx 88 \mu\text{m}$  explains the lowering of transmittance as  $h_2 \rightarrow 95 \mu\text{m}$ . Furthermore, the larger layer of silicon has a resonance with the lowest frequency. Once again this is explained by the larger area with a higher permittivity leading to a higher effective refractive index that again leads to a higher guide mode wavelength

The last parameter to check for is  $\Lambda$ . It is to be expected that the change in  $\Lambda$  would have a similar effect as changing  $a$  as changing the period effectively adds more air to the structure which lowers the effective index. In contradiction to this, in Figure 5.36 it can be seen that a higher period relates to a lower frequency which is the opposite effect as for changing  $a$ . The reason for this lies in the calculation of the diffraction order for the diffracted light.

When changing  $a$  the effective permittivity changes which means that as  $k_0\sqrt{\varepsilon} = \beta$  and the permittivity gets larger for a larger  $a$ , then to couple  $\beta$  has to stay the same meaning  $k_0$  gets smaller. This, then in relation means that the frequency gets smaller, which is what is seen for the change in  $a$ . It could be believed that the same effect would be seen when making  $\Lambda$  larger, however as the diffraction orders are calculated as  $\frac{n2\pi}{\Lambda}$  these get lower for a larger  $\Lambda$ , having the opposite effect. The decrease of the diffraction order is greater than the decrease of the effective permittivity, making it possible for the position of the peak moving to smaller frequencies. Plots of the calculated guided modes and diffraction order can be seen in Appendix C for  $\Lambda = 100$  and  $105 \mu\text{m}$ .

# Chapter 6

## Conclusion

The first two sections (5.1.1 and 5.1.2) were made to verify that the more complex 3D FMM model would give the same transmittance spectrum as the 2D FMM model for a 1D periodic layer. It was found that the 2D FMM was converged to a point of almost no change after  $N = 7$  with a change in result for more plane waves being under 0.001 for P-polarization when formulating the eigenvalue problem using Lifeng Li's rules for the Fourier expansion of the permittivity. To get this result without using Li's rules,  $N = 10$  was needed, however, the change went over 0.001 again for  $N = 11$  at 0.0012. At  $N = 12$  and above the results stayed under. For S-polarization, only the direct permittivity is used, which means only one formulation is constructed. For the change to be under 0.001,  $N = 4$  is needed. These results show that the formulation constructed by Lifeng Li in [16] is converging faster with respect to  $N$ . When comparing the results for the 2D and 3D FMM with and without Li's rules for the one-dimensional structure, it was found to give the same results, which gave credibility to the 3D model.

The next test consisted of a convergence test for the three 3D models constructed for a specific peak found at 1.555 THz, both for square- and circular-shaped rods. The three models in question are the simple, Li's and the tensor formulation. All three formulations converged to the same point and only varied slightly in linewidth  $\Gamma$  as well as asymmetry factor  $q$ . It is not clear which model is the best, however, it was found that Li's formulation converged the fastest vs.  $N$  while  $N$  for the tensor formulations had to be chosen carefully. For the square-shaped rods, the tensor formulation had the potential to converge faster if the amount of plane waves is divisible by  $\Lambda/a$  since this avoids tensor averaging. This is observed for  $N = 4$  in Figure 5.13. The slower and uniform convergence observed for the cylinder-shaped rods (Figure 5.17) further supports this phenomenon being geometric in origin.

It was found that a useful way of locating the Fano resonances was by computing the guided mode indices in a waveguide, constructed as the structure, but with an effective

geometric mean permittivity for the periodic layer and comparing these to different diffraction orders of the periodic layer. This method of locating the Fano resonances is very accurate for the one-dimensional periodic crystal and fairly accurate when using it for the two-dimensional periodic structure. Here it was found that all the coupled modes found using this method did indeed correspond to a resonance found through FMM, however, not all resonances found had a corresponding calculated coupled mode.

The effect of changing the angle of the incidence light was also tested. For the 1-dimensional periodic structure and a change in incident angle perpendicular to the bars of the structure, showed the resonance peaks splitting in two when increasing the angle. This result was compared to a similar calculation done in [23] and the resemblance is satisfactory. When changing the angle along the bars no apparent shift in the resonances was seen. For the 2D periodic structure similar features was found again with some of the resonances moving to both lower and higher frequencies while others did not change. This showed to have a relation with which guided modes were found for either S- or P- polarization. Some resonances were found to split for both polarizations however these were not found as guided modes, which could be explained by the mode being a superposition of both polarizations.

Various structural dependencies were also investigated. First off it was found through the calculation of the Q-factor that the height of the periodic layer could change how easy it is to couple to the guided modes in the crystal with the lowest height, giving the sharpest resonance peak and being the toughest to couple to. Another way to change the Q-factor of the crystal is by varying the side length of the silicon rods. By either making the rods very small or by making them very big, effectively making the period consist of very small grooves, would increase the Q-factor as well. To get the broadest resonance the ratio between air and silicon should be at, or close to  $\frac{1}{2}$ .

To move the position of the peak, multiple variables could be used to adjust. First off, by changing the thickness of the structure ( $h_1$  or  $h_2$ ) where a larger waveguide would give rise to guided modes with larger wavelengths i.e. shorter frequency resonances. By increasing  $a$  the peak moved to lower frequencies as well. This was explained by an increase in effective permittivity, while the diffraction orders of the periodic layer were kept constant, leading to a decrease in  $k_0$  and, by extension, the frequency again. When instead increasing the period and therefore decreasing the effective permittivity the resonance frequency was seen decreasing again, contrary to what might be expected. However, this effect is due to the diffraction orders decreasing even more than the effective permittivity, making it possible for the frequency to increase as well. By adjusting the parameters of the PhCs in combination, it is in theory possible to design filters of specific frequencies and bandwidth within the terahertz regime.

# Bibliography

- [1] R. W. Wood. On a remarkable case of uneven distribution of light in a diffraction grating spectrum. *Proc. Phys. Soc*, 1902.
- [2] Lord Rayleigh. On the dynamical theory of gratings. *The Royal Society*, 1907.
- [3] Andrey E. Miroshnichenko & Sergej Flach & Yuri S. Kivshar. Fano resonances in nanoscale structures. *Reviews of Modern Physics*, Volume 82:2257–2298, Aug 2010.
- [4] Ugo Fano. Sullo spettro di assorbimento dei gas nobili presso il limite dello spettro d'arco. *Nuovo Cimento*, 1935.
- [5] Ugo Fano. Effects of configuration interaction on intensities and phase shifts. *Physical review*, Volume 124, 1961.
- [6] Sergey V. Gaponenko. *Introduction to NanoPhotonics*. Cambridge University Press, 2010.
- [7] Weidong Zhou & Deyin Zhao & Yi-Chen Shuai & Hongjun Yang & Santhad Chuwongin & Arvinder Chadha & Jung-Hun Seo & Ken X. Wang & Victor Liu & Zhenqiang Ma & Shanhui Fan. Progress in 2d photonic crystal fano resonance photonics. *Progress in Quantum Electronics*, 2014.
- [8] M Galli, SL Portalupi, M Belotti, LC Andreani, L O'Faolain, and TF Krauss. Light scattering and fano resonances in high-q photonic crystal nanocavities. *Applied Physics Letters*, 94(7):071101, 2009.
- [9] Rik Harbers, Selim Jochim, Nikolaj Moll, Rainer F Mahrt, Daniel Erni, John A Hoffnagle, and William D Hinsberg. Control of fano line shapes by means of photonic crystal structures in a dye-doped polymer. *Applied physics letters*, 90(20):201105, 2007.
- [10] Weidong Zhou, Zhenqiang Ma, Hongjun Yang, Zexuan Qiang, Guoxuan Qin, Huiqing Pang, Li Chen, Wei-quan Yang, Santhad Chuwongin, and Deyin Zhao. Flexible photonic-crystal fano filters based on transferred semiconductor nanomembranes. *Journal of Physics D: Applied Physics*, 42(23):234007, 2009.

- [11] Zexuan Qiang, Hongjun Yang, Li Chen, Huiqing Pang, Zhenqiang Ma, and Weidong Zhou. Fano filters based on transferred silicon nanomembranes on plastic substrates. *Applied Physics Letters*, 93(6):061106, 2008.
- [12] Hongjun Yang, H Pang, Z Qiang, Zhenqiang Ma, and Weidong Zhou. Surface-normal fano filters based on transferred silicon nanomembranes on glass substrates. *Electronics letters*, 44(14):858–860, 2008.
- [13] Shanhui Fan & J. D. Joannopoulos. Analysis of guided resonances in photonic crystal slabs. *Physical Review B*, Volume 65, Jun 2002.
- [14] Shanhui Fan, Wonjoo Suh, and John D Joannopoulos. Temporal coupled-mode theory for the fano resonance in optical resonators. *JOSA A*, 20(3):569–572, 2003.
- [15] Kazuki Koshino. Analytic approach to the optical response of one-dimensional photonic crystal slabs. *Physical Review B*, 67(16):165213, 2003.
- [16] Lifeng Li. Use of fourier series in the analysis of discontinuous periodic structures. *J. Opt. Soc. Am. A*, 1996.
- [17] Davide Bucci & Bruno Martin & Alain Morand. Application of the three-dimensional aperiodic fourier modal method using arc elements in curvilinear coordinates. *Journal of Optical Society of America*, Mar 2012.
- [18] Natalia S. Salakhova & Ilia M. Fradkin. Fourier modal method for moiré lattices. *Physical Review B*, Aug 2021.
- [19] Dmitry A. Bykov & Leonid L. Doskolovich. On the use of fourier modal method for calculation of localized eigenmodes of integrated optical resonators. *Computer Optics*, 2015.
- [20] J. Čtyroký & P. Kwiecien & J. Richter. Analysis of hybrid dielectric-plasmonic slot waveguide structures with 3d fourier modal methods. *Journal of European Optical Society*, Mar 2013.
- [21] Teppo Häyrynen & Andreas Dyhl Osterkryger & Jakob Rosenkrantz de Lasson & Niels Gregersen. Modeling open nanophotonic systems using the fourier modal method: Generalization to 3d cartesian coordinates. *Journal of the optical society of America A*, Aug 2017.
- [22] T. Vallius & M. Honkanen. Reformulation of the fourier modal method with adaptive spatial resolution: application to multilevel profiles. *Optics Express*, Jan 2002.

- [23] Anders Westerkam & Jesper L. W. Sonne & Karl G. Danielsen & Esben Skovsen & Thomas M. Søndergaard. All-dielectric one-dimensional gratings exhibiting fano resonances in the terahertz region. *Journal of the Optical Society of America B*, Jun 2022.
- [24] Lifeng Li. New formulation of the fourier modal method for crossed surface-relief gratings. *J. Opt. Soc. Am. A*, 1997.
- [25] Steven G. Johnson & J. D. Joannopoulos. Block-iterative frequency-domain methods for maxwell's equation in a planewave basis. *Optics Express*, Jan 2001.
- [26] K. T. Chao. *Theory of Differential Equations in Engineering and Mechanincs*, chapter 3: Ordinary Differential Equations. CRC Press, 2018.
- [27] Christopher A. Klausmeier. Floquet theory: a useful tool for understanding nonequilibrium dybamics. *Theoretical Ecology*, Sep 2008.
- [28] Hwi Kim & Junghyun Park & ByoungHo Lee. *Fourier Modal Method and its Applications in Computational Nanophotonics*, chapter 3: Fourier Modal Method. CRC Press, 2012.
- [29] N. M. Temme. *Special Functions: An introduction to the classical functions of mathematical physics*, chapter 9: Bessel Functions. Wiley, 1996.
- [30] Alan Jeffrey and Hui-Hui Dai. *Handbook of Mathematical Formulas and integrals*, chapter 17: Bessel Functions. Elsevier Academic Press, 4th edition, 2008.
- [31] Andrei V. Lavrinenko & Jesper Lægsgaard & Niels Gregersen & Frank Schmidt & Thomas Søndergaard. *Numerical Methods in Photonics*, chapter 6: Modal Method. CRC Press, 2017.
- [32] Thomas M. Søndergaard. *Green's Function Integral Equation Methods in Nano-Optics*, chapter Appendix F: Calculating Guided Modes of Planar Waveguides. CRC Press, 2019.
- [33] M. A. Butt & S. N. Khonina & N. L. Kazanskiy. Recent advances in photonic crystal optical devices: A review. *Elsevier*, May 2021.
- [34] Frank L. Pedrotti & Leno M. Pedrotti & Leno S. Pedrotti. *Introduction to Optics: Third Edition*, chapter 8: Optical Interferometry. Cambridge University Press, 2018.



# Appendix A

## Full Transmission: Different Structures

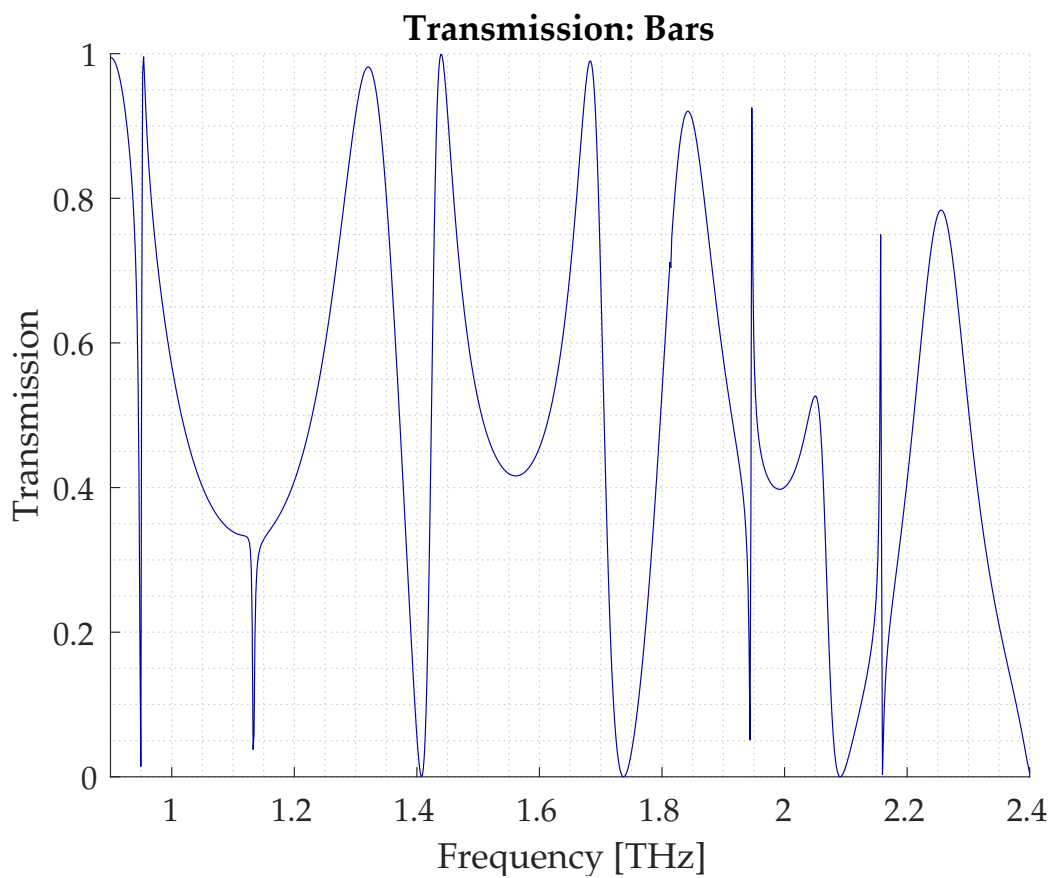
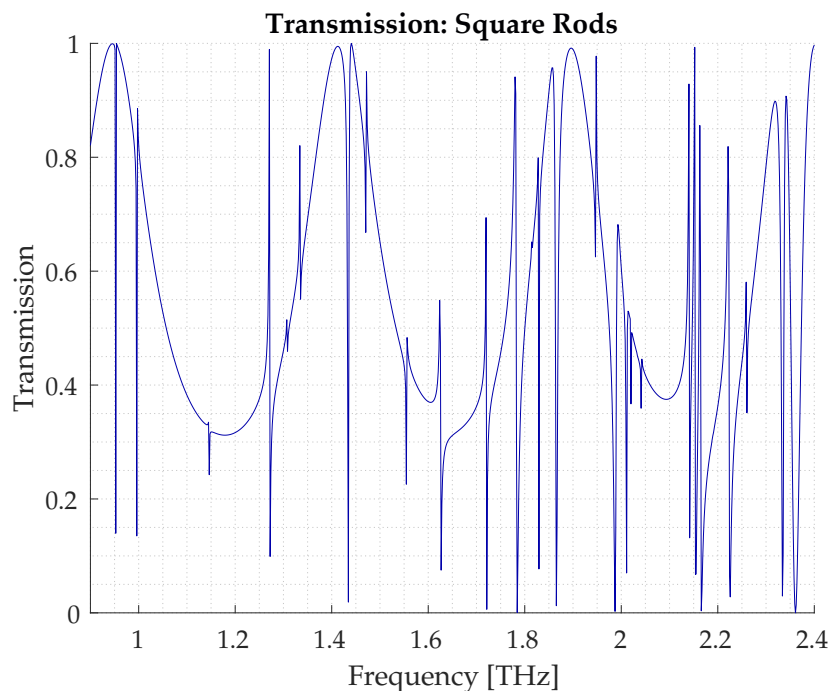
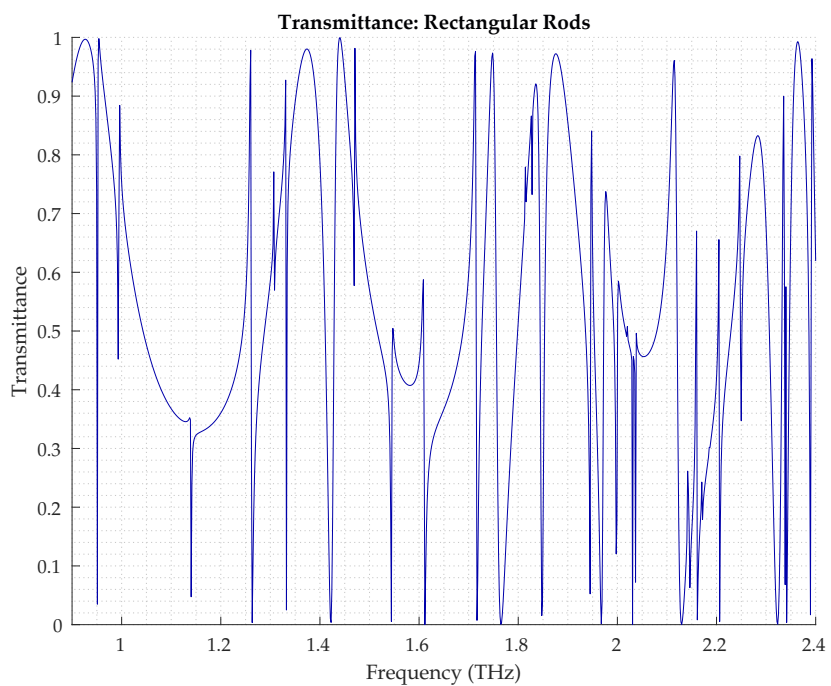


Figure A.1: S-polarization.  $N = 3$ . B1 structure



**Figure A.2:**  $N = 3$ . SRS1.



**Figure A.3:**  $N = 3$ . SRS1 however the sidelength of the rod in the  $x$ -direction is set to  $2a$ .

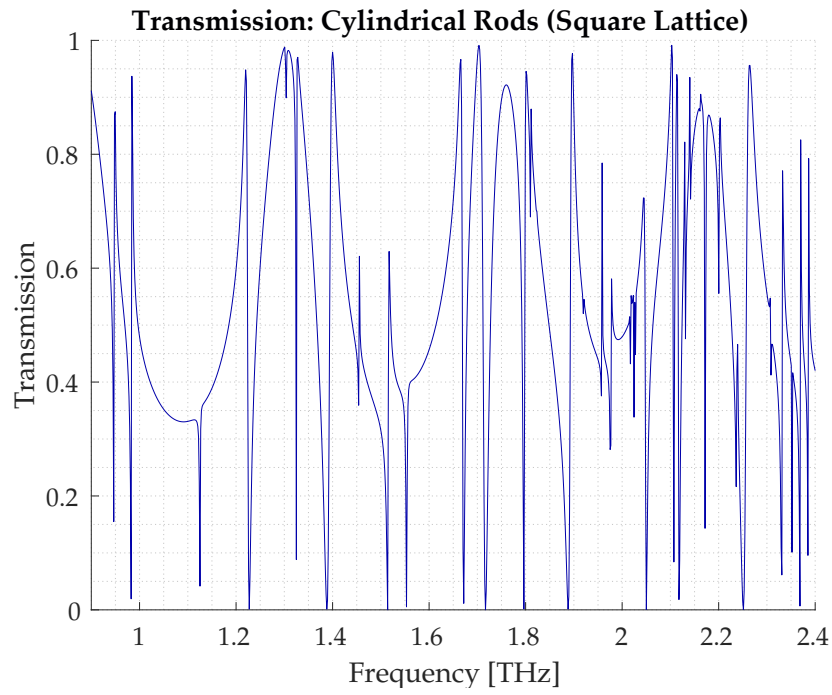


**Figure A.4:** N=3, SRC1.

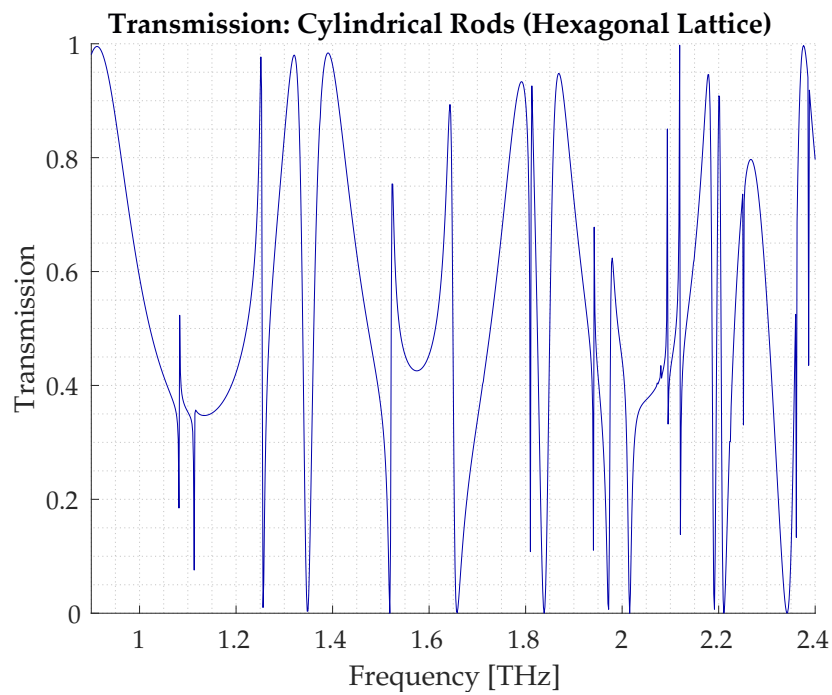


**Figure A.5:** N=3, HRC1.

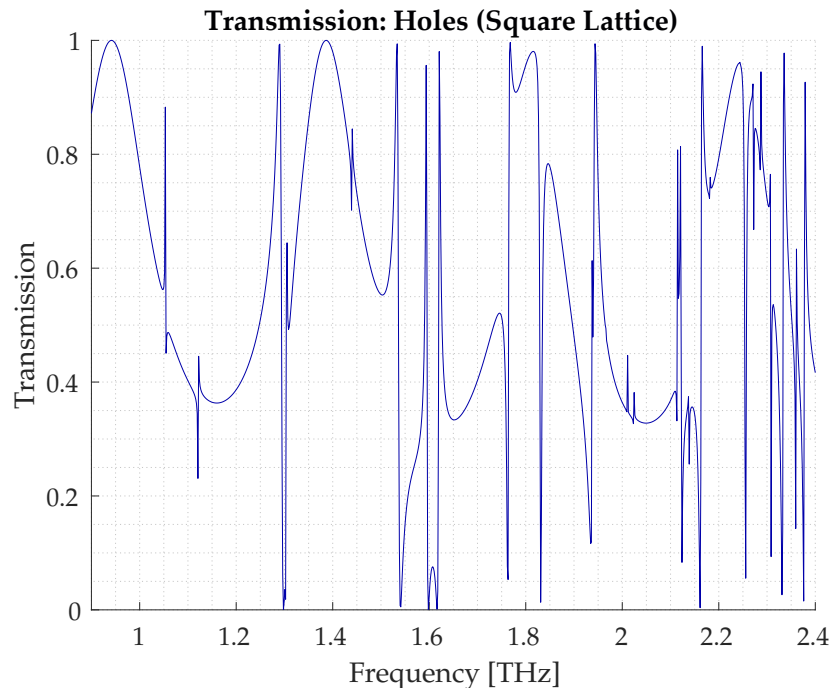


**Figure A.6:** N=3, SHS1.

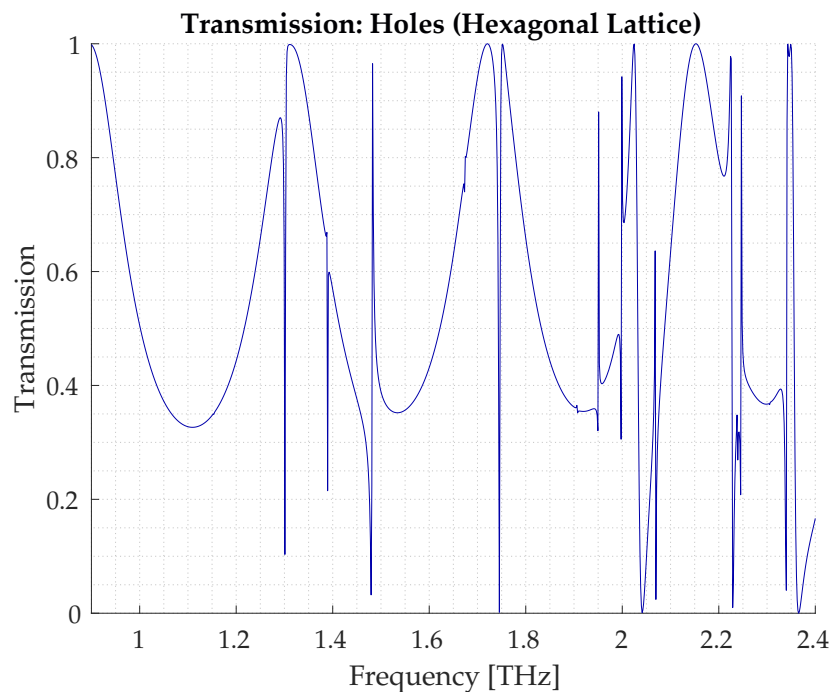


**Figure A.7:** N=3, HHC.

# Appendix B

## Plots for Varying Angles

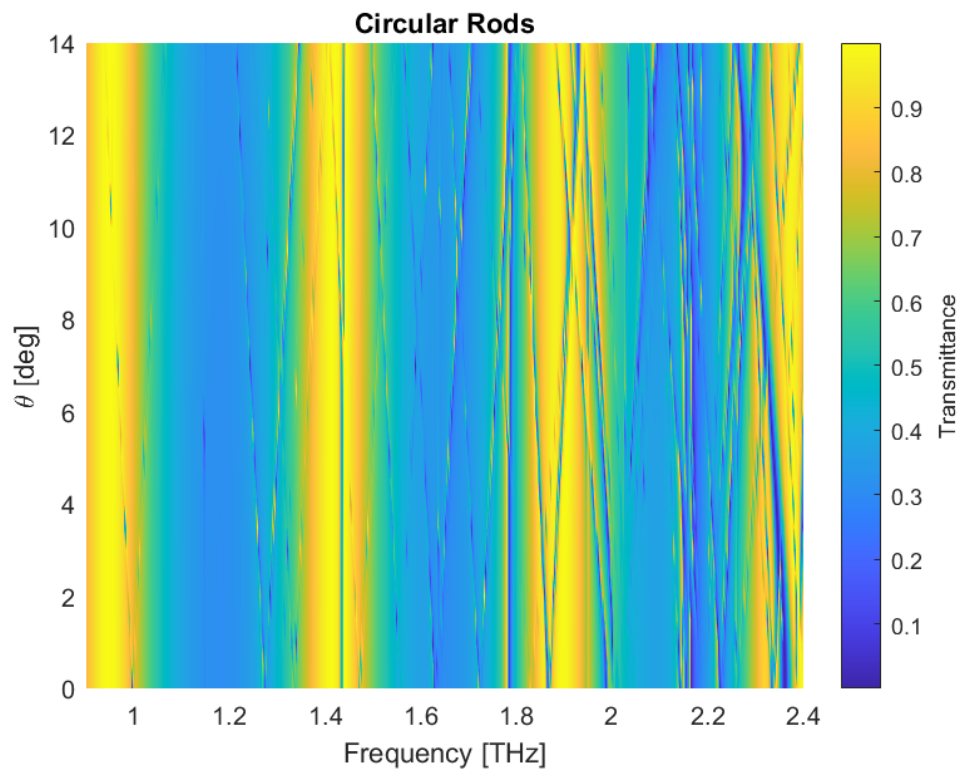


**Figure B.1:** Transmittance of the SRC1 structure for  $\theta = 0 : 14$  degrees in increments of 0.5 for  $\phi = 90$  for P-polarization and  $N = 5$ .

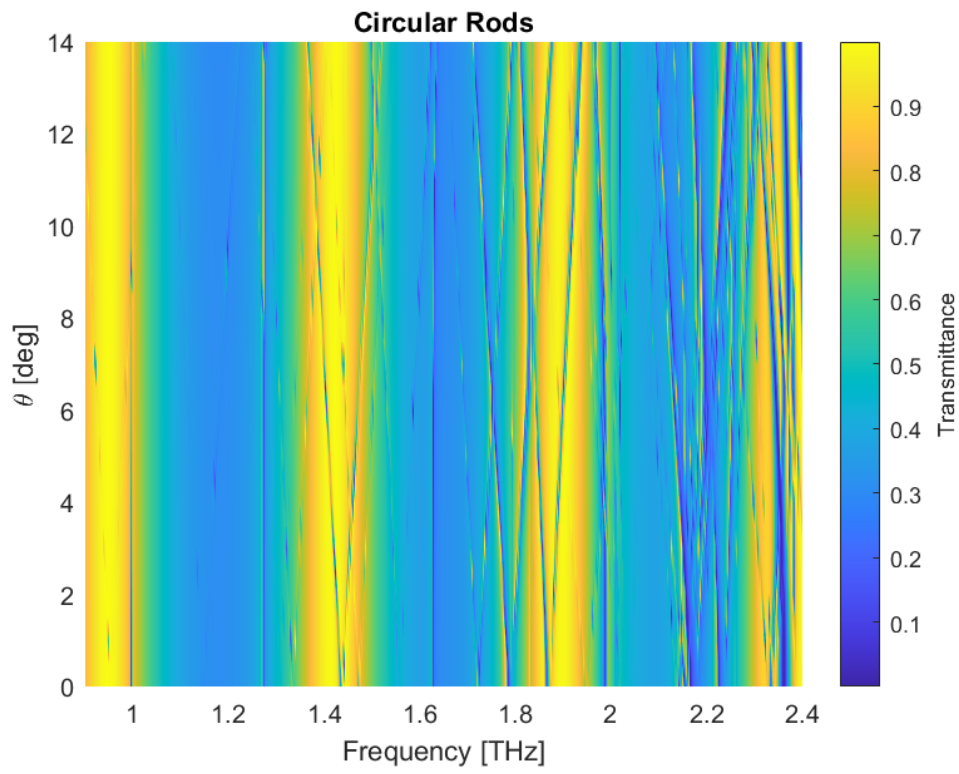


**Figure B.2:** Transmittance of the SRC1 structure for  $\theta = 0 : 14$  degrees in increments of 0.5 for  $\phi = 90$  for S-polarization and  $N = 5$ .

# Appendix C

## Coupled Modes for Different $\Lambda$

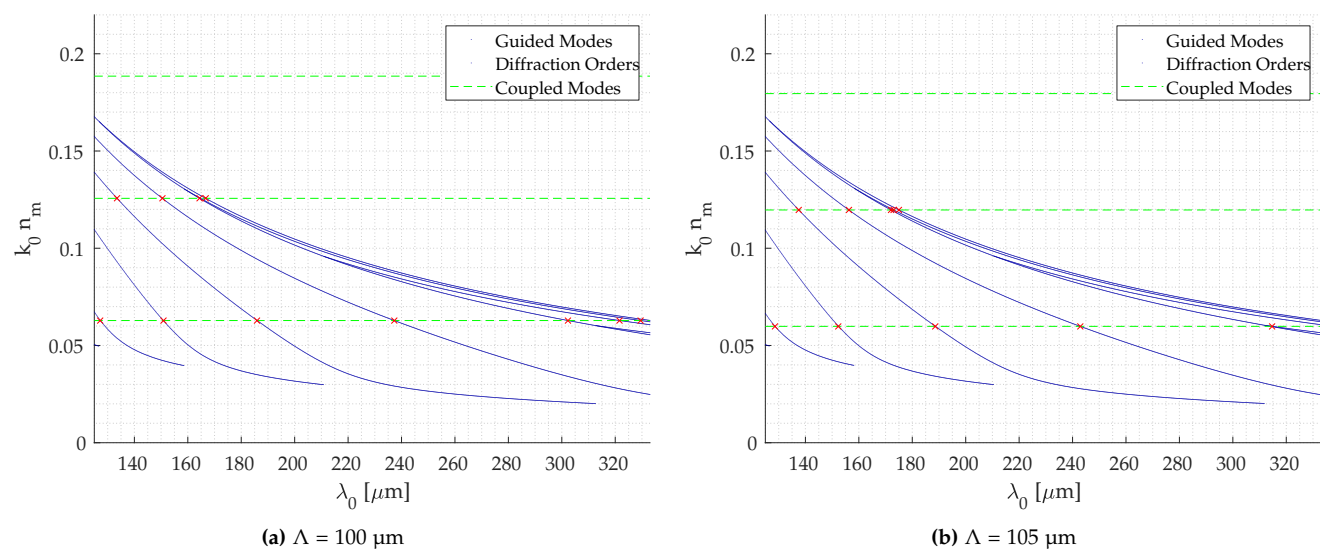


**Figure C.1:** Guided modes plotted as the blue lines and the first three diffraction orders plotted in green. Where these overlap at the red x's a coupled mode would be expected. The calculations was done for P-polarization





# Appendix D

## Other Lattices/Rods

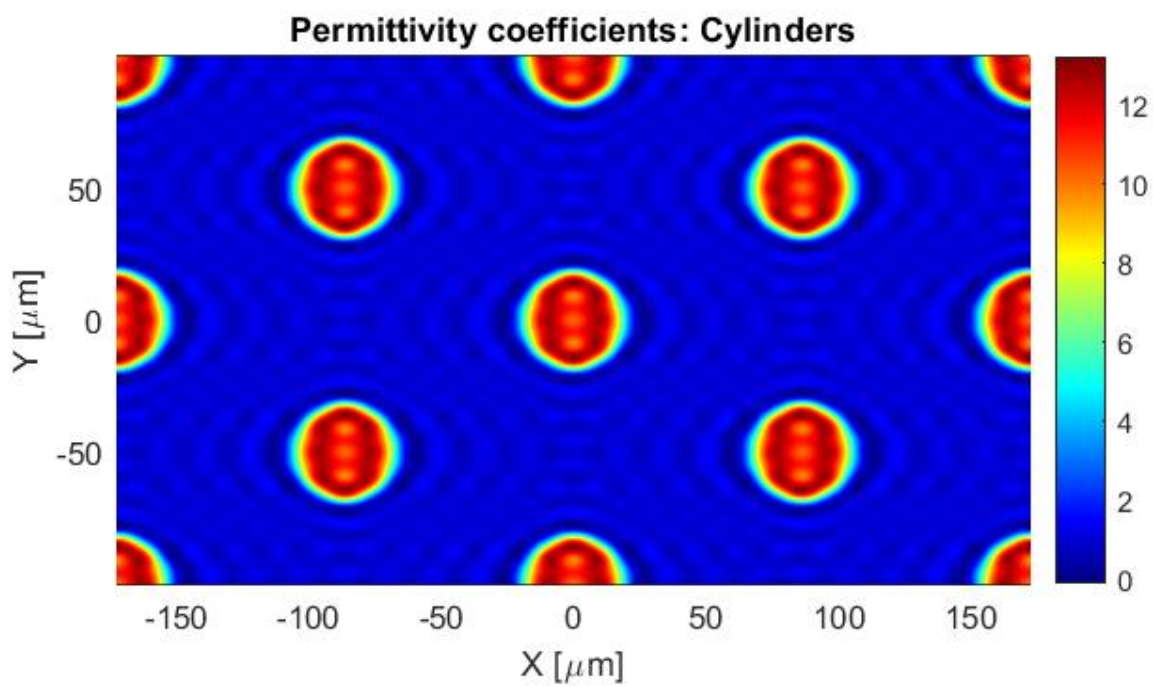


**Figure D.1:** The permittivity coefficients calculated for a hexagonal lattice.  $a = 32.5\mu\text{m}$ ,  $\Lambda_y = 99.7 \mu\text{m}$  and  $\Lambda_x = \sqrt{3}\Lambda_y$ .  $N = 10$

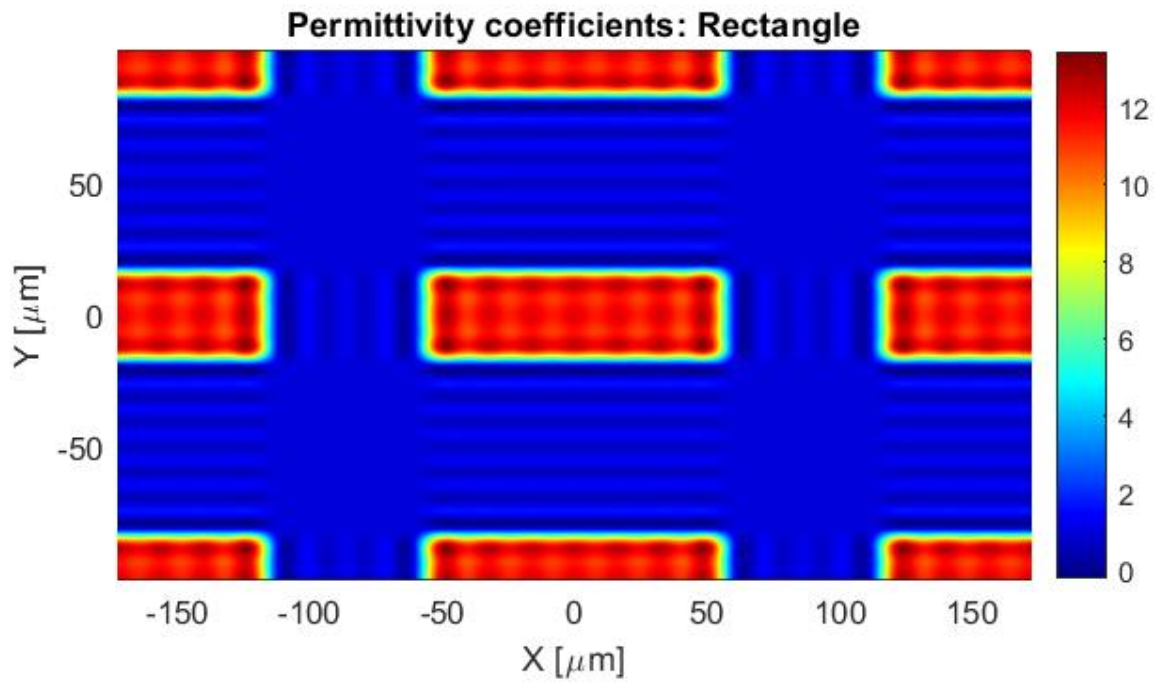


**Figure D.2:** The permittivity coefficients calculated for a rectangular rod for  $N = 10$ . The structure is the SRS1 but with the sidelength in the  $x$ -direction being  $2a$



# Appendix E

## Scripts

### E.1 3D FMM

#### E.1.1 Simple Formulation

```
1 %clear
2 %% Constants:
3 % incoming = 'Y';
4 incoming = input('Normal Incident [Y/N]? ', 's');
5 if incoming == 'N'
6     normal = false;
7     theta = input('theta [deg] = ');
8     phi = input('phi [deg] = ');
9 else
10    normal = true;
11    theta = 0;
12    phi = 0;
13 end
14 N = input('Number of plane waves? ');
15 % l = 125:300;
16 start = input('start frequency [THz]? ');
17 slut = input('end frequency [THz]? ');
18 freq = linspace(start, slut, 1000)*1e12;
19 % freq = linspace(0.9, 2.4, 200)*1e12;
20 c = physconst('LightSpeed'); % [m/s]
21 l = c./freq;
22 eps0 = 8.8542e-12; % [F/m]
23
24 %Structure:
25 eps1 = 1; %relative permittivity 1st layer
26 eps2 = 3.4^2; %relative permittivity 2nd layer
```

```

27 htot = 105e-6; %[m] total height of the structure
28 h2 = input('square rod/guldbar height [micro m]? ') * 1e-6; %12.9e-6; %[m] height of
    the square-cylinder
29 h3 = htot - h2; %92.1e-6; %[m] height of the Si layer
30 Lam = 99.7e-6; %[m] period (x,y)-plane
31
32 a = 32.5 * 10^-6; %42.5e-6; %32.5e-6; %[m] width nr1 of the square-cylinder
33
34
35 gemT = [];
36 gemR = [];
37 %Choosing E or H eigenvalue problem:
38 choose = input('[H/E]? ', 's');
39 if choose == 'H'
40     hfield = true;
41 else
42     hfield = false;
43 end
44 choose = input('Square [Y/N]? ', 's');
45 if choose == 'Y'
46     b = a;
47 else
48     b = Lam; %guldbar
49 end
50
51 pol = input('Polarization [S/P]? ', 's');
52 layers = input('Number of Layers [2/3/4]? ');
53
54 for i = 1:length(l)
55     l(i)
56     lambda = l(i); %[m] wavelength %125 mum = 2.4 THz 333 mum = 0.9 THz (THz =
    10^12 Hz)
57     k0 = 2 * pi / lambda; %[1/m] wavenumber
58     mu0 = 1 / (c^2 * eps0); %[N/A^2] but for micro
59     omega = k0 * c; %[1/s]
60     theta = theta * pi / 180;
61     phi = phi * pi / 180;
62     kx0 = k0 * cos(phi) * sin(theta);
63     ky0 = k0 * sin(phi) * sin(theta);
64     %Building K-matrices:
65     [Kx, Ky] = KMatrix(N, kx0, ky0, Lam);
66     kz1 = sqrt(k0^2 * eps1 * eye((2 * N + 1)^2) - Kx^2 - Ky^2);
67     kz3 = sqrt(k0^2 * eps2 * eye((2 * N + 1)^2) - Kx^2 - Ky^2);
68     %Normalizing Constants:
69     temp = sqrt(Kx^2 + Ky^2);
70     temp(ceil(end/2), ceil(end/2)) = 1;

```

```

71 norm1 = inv(temp);
72 temp = sqrt(Kx^2+Ky^2 + inv(kz1)*(Kx^2+Ky^2)^2);
73 temp(ceil(end/2),ceil(end/2)) = 1;
74 norm2 = inv(temp);
75 temp = sqrt(Kx^2+Ky^2 + inv(kz3)*(Kx^2+Ky^2)^2);
76 temp(ceil(end/2),ceil(end/2)) = 1;
77 norm3 = inv(temp);
78
79 %Building E-matrix 1st layer:
80 e11 = -norm1*Ky;
81 e21 = norm1*Kx;
82 e12a = norm2*Kx;
83 e22a = norm2*Ky;
84 if normal == true
85     e11(((2*N+1)^2+1)/2,((2*N+1)^2+1)/2) = 1;
86     e22a(((2*N+1)^2+1)/2,((2*N+1)^2+1)/2) = 1;
87 end
88 E1 = [e11 e12a;
89       e21 e22a];
90 %Building E-matrix 3rd layer:
91 e11 = -norm3*Ky;
92 e21 = norm3*Kx;
93 e12a = norm3*Kx;
94 e22a = norm3*Ky;
95 if normal == true
96     e11(((2*N+1)^2+1)/2,((2*N+1)^2+1)/2) = 1;
97     e22a(((2*N+1)^2+1)/2,((2*N+1)^2+1)/2) = 1;
98 end
99 E3 = [e11 e12a;
100       e21 e22a];
101
102 %Building H-matrix 1st and 3rd layers:
103 H1 = [-1/(omega*mu0)*Kx*Ky Kx*Kx/(omega*mu0)-omega*eps0*eps1*eye((2*N+1)^2);
104       -1/(omega*mu0)*Ky*Ky+omega*eps0*eps1*eye((2*N+1)^2) Ky*Kx/(omega*mu0)]*E1
105 * [kz1 zeros((2*N+1)^2); zeros((2*N+1)^2) kz1]^ -1;
106 H3 = [-1/(omega*mu0)*Kx*Ky Kx*Kx/(omega*mu0)-omega*eps0*eps2*eye((2*N+1)^2);
107       -1/(omega*mu0)*Ky*Ky+omega*eps0*eps2*eye((2*N+1)^2) Ky*Kx/(omega*mu0)]*E3
108 * [kz3 zeros((2*N+1)^2); zeros((2*N+1)^2) kz3]^ -1;
109
110 E4 = E1;
111 H4 = H1;
112 %Building permittivity-matrix periodic layer:
113 eps = permittivity(N,eps2,eps1,a,Lam,b);
114
115 epsBig = blkdiag(eps,eps);

```

```

115 %Eigenvalue problem:
116 KBigh = [Kx*Kx+eps*Ky*inv(eps)*Ky Kx*Ky-eps*Ky*inv(eps)*Kx; Ky*Kx-eps*Kx*inv(
117 eps)*Ky Ky*Ky+eps*Kx*inv(eps)*Kx];
118 KBige = [Ky*Ky+Kx*inv(eps)*Kx*eps Kx*inv(eps)*Ky*eps-Ky*Kx; Ky*inv(eps)*Kx*eps
119 -Kx*Ky Ky*inv(eps)*Ky*eps+Kx*Kx];
120 Mh = k0^2*epsBig-KBigh;
121 Me = k0^2*epsBig-KBige;
122 if hfield == true
123     [HCoeff,betasqh] = eig(Mh);
124     kz2 = sqrt(betasqh);
125 %Checking eigenvalues:
126 for idx = 1:length(diag(kz2))
127     if real(kz2(idx,idx))+imag(kz2(idx,idx))<0
128         kz2(idx,idx) = -kz2(idx,idx);
129     end
130 end
131 H2 = HCoeff;
132 E2 = [1/(omega*eps0)*Kx*inv(eps)*Ky (-1/(omega*eps0)*Kx*inv(eps)*Kx+omega*
133 mu0*eye((2*N+1)^2));
134 (1/(omega*eps0)*Ky*inv(eps)*Kx-omega*mu0*eye((2*N+1)^2)) -1/(omega*eps0)*
135 Ky*inv(eps)*Kx]*H2*kz2^-1;
136 else
137     [ECoeff,betasqe] = eig(Me);
138     kz2 = sqrt(betasqe);
139 %Checking eigenvalues:
140 for idx = 1:length(diag(kz2))
141     if real(kz2(idx,idx))+imag(kz2(idx,idx))<0
142         kz2(idx,idx) = -kz2(idx,idx);
143     end
144 end
145 E2 = ECoeff;
146 H2 = [-1/(omega*mu0)*Kx*Ky Kx*Kx/(omega*mu0)-omega*eps0*eps;
147 -1/(omega*mu0)*Ky*Ky+omega*eps0*eps Ky*Kx/(omega*mu0)]*E2*kz2^-1;
148 end
149 %Reflection matrices:
150 R12 = -1*(E2^-1*E1+H2^-1*H1)^-1*(E2^-1*E1-H2^-1*H1);
151 R21 = -1*(E1^-1*E2+H1^-1*H2)^-1*(E1^-1*E2-H1^-1*H2);
152 R23 = -1*(E3^-1*E2+H3^-1*H2)^-1*(E3^-1*E2-H3^-1*H2);
153 R32 = -1*(E2^-1*E3+H2^-1*H3)^-1*(E2^-1*E3-H2^-1*H3);
154 R43 = (E3^-1*E4+H3^-1*H4)^-1*(-E3^-1*E4+H3^-1*H4);
155 R34 = (E4^-1*E3+H4^-1*H3)^-1*(-E4^-1*E3+H4^-1*H3);
156 %Transmission matrices:
157 T12 = E2^-1*E1*(eye(2*(2*N+1)^2)+R12);
158 T21 = E1^-1*E2*(eye(2*(2*N+1)^2)+R21);

```

```

157 T23 = E3^-1*E2*(eye(2*(2*N+1)^2)+R23);
158 T32 = E2^-1*E3*(eye(2*(2*N+1)^2)+R32);
159 T34 = E4^-1*E3*(eye(2*(2*N+1)^2)+R34);
160 T43 = E3^-1*E4*(eye(2*(2*N+1)^2)+R43);
161
162 %Propagation matrices:
163 P1 = diag(exp(1i*diag(kz1)*h2));
164 P1 = [P1 zeros((2*N+1)^2);
165       zeros((2*N+1)^2) P1];
166 P2 = diag(exp(1i*diag(kz2)*h2));
167
168 P3 = diag(exp(1i*diag(kz3)*h3));
169 P3 = [P3 zeros((2*N+1)^2);
170       zeros((2*N+1)^2) P3];
171
172 %Total reflection and transmission:
173 T13 = T23*(eye(2*(2*N+1)^2)-P2*R21*P2*R23)^-1*P2*T12;
174 T31 = T21*(eye(2*(2*N+1)^2)-P2*R23*P2*R21)^-1*P2*T32;
175 R13 = R12+T21*((eye(2*(2*N+1)^2)-P2*R23*P2*R21)^-1)*P2*R23*P2*T12;
176 R31 = R32+T23*((eye(2*(2*N+1)^2)-P2*R21*P2*R23)^-1)*P2*R21*P2*T32;
177 T14 = T34*(eye(2*(2*N+1)^2)-P3*R31*P3*R34)^-1*P3*T13;
178 R14 = R13+T31*((eye(2*(2*N+1)^2)-P3*R34*P3*R31)^-1)*P3*R34*P3*T13;
179
180 a1 = zeros(2*(2*N+1)^2,1);
181 if pol == 'S'
182     a1(((2*N+1)^2+1)/2) = 1;
183 else
184     a1(((2*N+1)^2+1)/2+(2*N+1)^2) = 1;
185 end
186
187
188 if layers == 4
189     a2 = T14*a1;
190     b1 = R14*a1;
191     Ex_t = E4(1:end/2,:)*a2;
192     Ey_t = E4(end/2+1:end,:)*a2;
193     Hx_t = H4(1:end/2,:)*a2;
194     Hy_t = H4(end/2+1:end,:)*a2;
195 elseif layers == 3
196     a2 = T13*a1;
197     b1 = R13*a1;
198     Ex_t = E3(1:end/2,:)*a2;
199     Ey_t = E3(end/2+1:end,:)*a2;
200     Hx_t = H3(1:end/2,:)*a2;
201     Hy_t = H3(end/2+1:end,:)*a2;
202 else

```

```

203     a2 = T12*a1;
204     b1 = R12*a1;
205     Ex_t = E2(1:end/2,:) * a2;
206     Ey_t = E2(end/2+1:end,:) * a2;
207     Hx_t = H2(1:end/2,:) * a2;
208     Hy_t = H2(end/2+1:end,:) * a2;
209 end
210
211 I_t = Lam^2*sum(real(Ex_t.*conj(Hy_t)-Ey_t.*conj(Hx_t)));
212 Ex_i = E1(1:end/2,:) * a1;
213 Ey_i = E1(end/2+1:end,:) * a1;
214 Hx_i = H1(1:end/2,:) * a1;
215 Hy_i = H1(end/2+1:end,:) * a1;
216 I_i = Lam^2*sum(real(Ex_i.*conj(Hy_i)-Ey_i.*conj(Hx_i)));
217 T = I_t/I_i;
218
219 Ex_r = E1(1:end/2,:) * b1;
220 Ey_r = E1(end/2+1:end,:) * b1;
221 Hx_r = H1(1:end/2,:) * b1;
222 Hy_r = H1(end/2+1:end,:) * b1;
223 I_r = Lam^2*sum(real(Ex_r.*conj(Hy_r)-Ey_r.*conj(Hx_r)));
224 R = I_r/I_i;
225 gemT = [gemT T];
226 gemR = [gemR R];
227 end
228 Rand

```

## Permittivity Matrix: Square Rod

```

1 function eps=permittivity(N,eps2,eps1,a1,Lam,a2)
2 %% Code
3 epsk = zeros(2*N+1,2*N+1);
4 eps = zeros((2*N+1)^2,(2*N+1)^2);
5
6 for i = 1:2*N+1
7     epskV = zeros(1,2*N+1);
8     for j = 1:2*N+1
9         n = i-1;
10        m = j-1;
11        if i==1 && j==1
12            epskV(j) = eps2*a1*a2/Lam^2 + eps1*(Lam^2-a1*a2)/Lam^2;
13        elseif i==1 && j~=1
14            epskV(j) = (eps2-eps1)*a2*sin(m*pi*a1/Lam)/(m*pi*Lam);
15        elseif i~=1 && j==1
16            epskV(j) = (eps2-eps1)*a1*sin(n*pi*a2/Lam)/(n*pi*Lam);

```

```

17         else
18             epskV(j) = (eps2-eps1)*sin(n*pi*a2/Lam)*sin(m*pi*a1/Lam)/(n*m*pi
^2);
19         end
20     end
21     epskV = [flip(epskV) epskV(2:end)];
22     for k = 1:2*N+1
23         epsk(k,:) = epskV(2*N+1:end);
24         epskV = circshift(epskV,1);
25     end
26     if i==1
27         temp = repmat({epsk},1,2*N+1);
28         temp = blkdiag(temp{:});
29         eps = eps + temp;
30     else
31         temp = repmat({epsk},1,2*N+1);
32         temp = blkdiag(temp{:});
33         temp = triu(circshift(temp,[0 (i-1)*(2*N+1)]));
34         eps = eps + temp;
35         temp = repmat({epsk},1,2*N+1);
36         temp = blkdiag(temp{:});
37         temp = tril(circshift(temp,[0 -(i-1)*(2*N+1)]));
38         eps = eps + temp;
39     end
40 end
41 end

```

### Permittivity Matrix: Cylindrical Rod

```

1 function eps=cylinder(N,eps2,eps1,a,Lam)
2 %% Code
3     epsk = zeros(2*N+1,2*N+1);
4     eps = zeros((2*N+1)^2,(2*N+1)^2);
5
6     for i = 1:2*N+1
7         epskV = zeros(1,2*N+1);
8         for j = 1:2*N+1
9             n = i-1;
10            m = j-1;
11            if i==1 && j==1
12                epskV(j) = 1/Lam^2*(pi*a^2*eps2 + (Lam^2-a^2*pi)*eps1);
13            %
14            %elseif i==1 && j~=1
15            %    %epskV(j) = (eps2*a/Lam + eps1*(Lam-a)/Lam)/(m*pi)*sin(m*pi*a/
Lam);
16            %
17            %    epskV(j) = (eps2-eps1)*a2*sin(m*pi*a1/Lam)/(m*pi*Lam);

```

```

16 %           %epskV(j) = 1i*(eps2-eps1)*a*(exp(-1i*m*2*pi*a/Lam)-1)/(Lam*m*2*
    pi);
17 %           elseif i~=1 && j==1
18 %           %epskV(j) = (eps2*a/Lam + eps1*(Lam-a)/Lam)/(n*pi)*sin(n*pi*a/
    Lam);
19 %           epskV(j) = (eps2-eps1)*a1*sin(n*pi*a2/Lam)/(n*pi*Lam);
20 %           %epskV(j) = 1i*(eps2-eps1)*a*(exp(-1i*n*2*pi*a/Lam)-1)/(Lam*n*2*
    pi);
21           else
22               Gmn = 2*pi/Lam*sqrt(m^2+n^2);
23               epskV(j) = (eps2-eps1)/Lam^2*2*pi*a/Gmn*besselj(1,Gmn*a);
24 %           epskV(j) = (eps2-eps1)*sin(n*pi*a2/Lam)*sin(m*pi*a1/Lam)/(n*m*pi
    ^2);
25           %epskV(j) = (eps1-eps2)*(exp(-1i*n*2*pi*a/Lam)-1)*(exp(-1i*m*2*pi*
    a/Lam)-1)/(4*pi^2*n*m);
26           end
27       end
28       epskV = [flip(epskV) epskV(2:end)];
29       for k = 1:2*N+1
30           epsk(k,:) = epskV(2*N+1:end);
31           epskV = circshift(epskV,1);
32       end
33       if i==1
34           temp = repmat({epsk},1,2*N+1);
35           temp = blkdiag(temp{:});
36           eps = eps + temp;
37       else
38           temp = repmat({epsk},1,2*N+1);
39           temp = blkdiag(temp{:});
40           temp = triu(circshift(temp,[0 (i-1)*(2*N+1)]));
41           eps = eps + temp;
42           temp = repmat({epsk},1,2*N+1);
43           temp = blkdiag(temp{:});
44           temp = tril(circshift(temp,[0 -(i-1)*(2*N+1)]));
45           eps = eps + temp;
46       end
47   end
48 end

```

## K Matrix

```

1 function [Kx,Ky]=KMatrix(N,kx0,ky0,Lam)
2     for ii = 1:2*N+1
3         i = ii-N-1;
4         kxk{ii} = (kx0+2*pi*i/Lam)*eye(2*N+1);

```

```

5      kyk{ ii } = (ky0*eye(2*N+1)+2*pi*diag(-N:N)/Lam);eye(2*N+1);endKx =
      blkdiag(kxk:);Ky = blkdiag(kyk:);end

```

## E.1.2 Li's Formulation

```

1 %clear
2 tic
3 %% Contanst:
4 kx0 = 0; %normal-incident
5 ky0 = 0; %normal-incident
6 N = 3; %number of plane waves
7 Lam = 99.7*10^-6; %[m] period (x,y)-plane
8 a = 32.5e-6; %[m] width nr1 of the square-cylinder
9 b = Lam; %[m] width nr2 of the square-cylinder
10
11 mu0 = pi*4e-7; %[N*A^-2]
12 eps0 = 8.8542e-12; %[F/m]
13 c = 1/sqrt(mu0*eps0); %[m/s]
14 eps1 = 1; %relative permittivity 1st layer
15 eps2 = 3.4^2; %relative permittivity 2nd layer
16 %freq = linspace(0.9,2.4,1000)*1e+12;
17 freq = linspace(1.1,1.17,1000)*1e+12;
18 l = c./freq;
19
20 gemT = zeros(1,length(freq));
21 gemR = gemT;
22 %Choosing E or H eigenvalue problem:
23 choose = input('[H/E]? ','s');
24 if choose == 'H'
25     hfield = true;
26 else
27     hfield = false;
28 end
29 choose = input('Square [Y/N]? ','s');
30 if choose == 'Y'
31     epssquare = true;
32 else
33     epssquare = false;
34 end
35 pol = input('Polarization [S/P]? ','s');
36 layers = input('Number of Layers [2/3/4]? ');
37
38 parfor i = 1:length(l)
39     disp(i/length(l))

```

```

40 lambda = l(i); %[m] wavelength %125 mum = 2.4 THz 333 mum = 0.9 THz (THz =
10^12 Hz)
41 k0 = 2*pi/lambda; %[1/m] wavenumber
42 omega = k0*c; %[1/s]
43 %Building K-matrices:
44 [Kx,Ky] = KMatrix(N,kx0,ky0,Lam);
45 kz1 = sqrt(k0^2*eps1*eye((2*N+1)^2) - Kx^2 - Ky^2);
46 kz3 = sqrt(k0^2*eps2*eye((2*N+1)^2) - Kx^2 - Ky^2);
47 %Normalizing Constants:
48 temp = sqrt(Kx^2+Ky^2);
49 temp(ceil(end/2),ceil(end/2)) = 1;
50 norm1 = inv(temp);
51 temp = sqrt(Kx^2+Ky^2 + inv(kz1)*(Kx^2+Ky^2)^2);
52 temp(ceil(end/2),ceil(end/2)) = 1;
53 norm2 = inv(temp);
54 temp = sqrt(Kx^2+Ky^2 + inv(kz3)*(Kx^2+Ky^2)^2);
55 temp(ceil(end/2),ceil(end/2)) = 1;
56 norm3 = inv(temp);
57
58 %Building E-matrix 1st layer:
59 e11 = -norm1*Ky;
60 e21 = norm1*Kx;
61 e12a = norm2*Kx;
62 e22a = norm2*Ky;
63 e11(((2*N+1)^2+1)/2,((2*N+1)^2+1)/2) = 1;
64 e22a(((2*N+1)^2+1)/2,((2*N+1)^2+1)/2) = 1;
65 E1 = [e11 e12a;
66       e21 e22a];
67 %Building E-matrix 3rd layer:
68 e11 = -norm3*Ky;
69 e21 = norm3*Kx;
70 e12a = norm3*Kx;
71 e22a = norm3*Ky;
72 e11(((2*N+1)^2+1)/2,((2*N+1)^2+1)/2) = 1;
73 e22a(((2*N+1)^2+1)/2,((2*N+1)^2+1)/2) = 1;
74 E3 = [e11 e12a;
75       e21 e22a];
76
77 %Building H-matrix 1st and 3rd layers:
78 H1 = [-1/(omega*mu0)*Kx*Ky Kx*Kx/(omega*mu0)-omega*eps0*eps1*eye((2*N+1)^2);
79       -1/(omega*mu0)*Ky*Ky+omega*eps0*eps1*eye((2*N+1)^2) Ky*Kx/(omega*mu0)]*E1
80 * [kz1 zeros((2*N+1)^2); zeros((2*N+1)^2) kz1]^(-1);
81 H3 = [-1/(omega*mu0)*Kx*Ky Kx*Kx/(omega*mu0)-omega*eps0*eps2*eye((2*N+1)^2);
82       -1/(omega*mu0)*Ky*Ky+omega*eps0*eps2*eye((2*N+1)^2) Ky*Kx/(omega*mu0)]*E3
83 * [kz3 zeros((2*N+1)^2); zeros((2*N+1)^2) kz3]^(-1);

```

```

83 E4 = E1;
84 H4 = H1;
85 %Building permittivity-matrix periodic layer:
86 if epssquare == true % Dette er for firkanter
87     [epsLi1, epsLi2, Kx, Ky, eps] = permLi(N, eps2, eps1, a, Lam, kx0, ky0);
88 else % Dette er for striber/guldbar
89     [%epsLi1, epsLi2, Kx, Ky, eps] = permLiBar(N, eps2, eps1, a, Lam, Lam, kx0, ky0);
90     [epsLi1, epsLi2, Kx, Ky, eps] = permLiBar_TS(N, eps2, eps1, a, Lam, Lam, kx0, ky0);
91 end
92
93 %Eigenvalue problem:
94 IM = eye((2*N+1)^2);
95 F = [Kx*inv(eps)*Ky k0^2*IM-Kx*inv(eps)*Kx; Ky*inv(eps)*Ky-k0^2*IM -Ky*inv(eps)
96 ]*Kx];
97 G = [-Kx*Ky Kx^2-k0^2*epsLi2; k0^2*epsLi1-Ky^2 Kx*Ky];
98 Me = F*G;
99 Mh = G*F;
100
101 if hfield == true
102     [HCoeff, betasqh] = eig(Mh);
103     kz2 = sqrt(betasqh/k0^2);
104     %Checking eigenvalues:
105     for idx = 1:length(diag(kz2))
106         if real(kz2(idx, idx))+imag(kz2(idx, idx))<0
107             kz2(idx, idx) = -kz2(idx, idx);
108         end
109     end
110     H2 = HCoeff;
111     E2 = [1/(omega*eps0)*Kx*inv(eps)*Ky (-1/(omega*eps0)*Kx*inv(eps)*Kx+omega*
112 mu0*eye((2*N+1)^2));
113 (1/(omega*eps0)*Ky*inv(eps)*Ky-omega*mu0*eye((2*N+1)^2)) -1/(omega*eps0)*
114 Ky*inv(eps)*Kx]*H2*kz2^-1;
115 %E2 = 1/k0*F*H2*kz2^-1;
116 %E2 = 1/k0*kz2^-1*F*H2;
117 else
118     [ECoeff, betasqe] = eig(Me);
119     kz2 = sqrt(betasqe/k0^2);
120     %Checking eigenvalues:
121     for idx = 1:length(diag(kz2))
122         if real(kz2(idx, idx))+imag(kz2(idx, idx))<0
123             kz2(idx, idx) = -kz2(idx, idx);
124         end
125     end
126     E2 = ECoeff;
127     H2 = [-1/(omega*mu0)*Kx*Ky Kx*Kx/(omega*mu0)-omega*eps0*epsLi2;
128 -1/(omega*mu0)*Ky*Ky+omega*eps0*epsLi1 Kx*Ky/(omega*mu0)]*E2*kz2^-1;

```

```

126     %H2 = 1/k0*G*E2*kz2^-1;
127     %H2 = 1/k0*kz2^-1*G*E2;
128 end
129
130 %Reflection matrices:
131 R12 = -1*(E2^-1*E1+H2^-1*H1) ^ -1*(E2^-1*E1-H2^-1*H1) ;
132 R21 = -1*(E1^-1*E2+H1^-1*H2) ^ -1*(E1^-1*E2-H1^-1*H2) ;
133 R23 = -1*(E3^-1*E2+H3^-1*H2) ^ -1*(E3^-1*E2-H3^-1*H2) ;
134 R32 = -1*(E2^-1*E3+H2^-1*H3) ^ -1*(E2^-1*E3-H2^-1*H3) ;
135 R43 = (E3^-1*E4+H3^-1*H4) ^ -1*(-E3^-1*E4+H3^-1*H4) ;
136 R34 = (E4^-1*E3+H4^-1*H3) ^ -1*(-E4^-1*E3+H4^-1*H3) ;
137
138 %Transmission matrices:
139 T12 = E2^-1*E1*(eye(2*(2*N+1)^2)+R12);%2*inv(inv(E1)*E2+inv(H1)*H2) ;
140 T21 = E1^-1*E2*(eye(2*(2*N+1)^2)+R21);%2*inv(inv(E2)*E1+inv(H2)*H1) ;
141 T23 = E3^-1*E2*(eye(2*(2*N+1)^2)+R23);%2*inv(inv(E2)*E3+inv(H2)*H3) ;
142 T32 = E2^-1*E3*(eye(2*(2*N+1)^2)+R32);%2*inv(inv(E3)*E2+inv(H3)*H2) ;
143 T34 = E4^-1*E3*(eye(2*(2*N+1)^2)+R34);%2*inv(inv(E3)*E4+inv(H3)*H4) ;
144 T43 = E3^-1*E4*(eye(2*(2*N+1)^2)+R43);%2*inv(inv(E4)*E3+inv(H4)*H3) ;
145
146 %%Propagation matrices:
147 h2 = 12.9e-6; %[m] height of the square-cylinder
148 %h2 = 11.9e-6; %[m] height of the square-cylinder
149 h3 = 92.1e-6;
150
151 P1 = diag(exp(1i*diag(kz1)*h2));
152 P1 = [P1 zeros((2*N+1)^2);
153       zeros((2*N+1)^2) P1];
154 P2 = diag(exp(1i*diag(kz2)*h2));
155
156 P3 = diag(exp(1i*diag(kz3)*h3));
157 P3 = [P3 zeros((2*N+1)^2);
158       zeros((2*N+1)^2) P3];
159
160 %%Total reflection and transmission:
161 T13 = T23*(eye(2*(2*N+1)^2)-P2*R21*P2*R23) ^ -1*P2*T12;
162 T31 = T21*(eye(2*(2*N+1)^2)-P2*R23*P2*R21) ^ -1*P2*T32;
163 R13 = R12+T21*((eye(2*(2*N+1)^2)-P2*R23*P2*R21) ^ -1)*P2*R23*P2*T12;
164 R31 = R32+T23*((eye(2*(2*N+1)^2)-P2*R21*P2*R23) ^ -1)*P2*R21*P2*T32;
165 T14 = T34*(eye(2*(2*N+1)^2)-P3*R31*P3*R34) ^ -1*P3*T13;
166 R14 = R13+T31*((eye(2*(2*N+1)^2)-P3*R34*P3*R31) ^ -1)*P3*R34*P3*T13;
167
168 a1 = zeros(2*(2*N+1)^2,1);
169 if pol == 'S'
170     a1(((2*N+1)^2+1)/2) = 1;
171 else

```

```

172     a1(((2*N+1)^2+1)/2+(2*N+1)^2) = 1;
173 end
174
175
176 if layers == 4
177     a2 = T14*a1;
178     b1 = R14*a1;
179     Ex_t = E4(1:end/2,:)*a2;
180     Ey_t = E4(end/2+1:end,:)*a2;
181     Hx_t = H4(1:end/2,:)*a2;
182     Hy_t = H4(end/2+1:end,:)*a2;
183 elseif layers == 3
184     a2 = T13*a1;
185     b1 = R13*a1;
186     Ex_t = E3(1:end/2,:)*a2;
187     Ey_t = E3(end/2+1:end,:)*a2;
188     Hx_t = H3(1:end/2,:)*a2;
189     Hy_t = H3(end/2+1:end,:)*a2;
190 else
191     a2 = T12*a1;
192     b1 = R12*a1;
193     Ex_t = E2(1:end/2,:)*a2;
194     Ey_t = E2(end/2+1:end,:)*a2;
195     Hx_t = H2(1:end/2,:)*a2;
196     Hy_t = H2(end/2+1:end,:)*a2;
197 end
198
199 I_t = Lam^2*sum(real(Ex_t.*conj(Hy_t)-Ey_t.*conj(Hx_t)));
200 Ex_i = E1(1:end/2,:)*a1;
201 Ey_i = E1(end/2+1:end,:)*a1;
202 Hx_i = H1(1:end/2,:)*a1;
203 Hy_i = H1(end/2+1:end,:)*a1;
204 I_i = Lam^2*sum(real(Ex_i.*conj(Hy_i)-Ey_i.*conj(Hx_i)));
205 T = I_t/I_i;
206
207 Ex_r = E1(1:end/2,:)*b1;
208 Ey_r = E1(end/2+1:end,:)*b1;
209 Hx_r = H1(1:end/2,:)*b1;
210 Hy_r = H1(end/2+1:end,:)*b1;
211 I_r = Lam^2*sum(real(Ex_r.*conj(Hy_r)-Ey_r.*conj(Hx_r)));
212 R = I_r/I_i;
213 gemT(i) = T;
214 gemR(i) = R;
215 end
216 toc
217 Rand

```

```
218
219 plot(freq,gemT)
```

### Li's Permittivity Matrix: Square Rod

```
1 function [epsmixed1,epsmixed2,Kx,Ky,eps]=permLi(N,eps2,eps1,a,Lam,kx0,ky0)
2 M_la = zeros(2*N+1,2*N+1);
3 M_ga = zeros(2*N+1,2*N+1);
4 eps = zeros((2*N+1)^2,(2*N+1)^2);
5 Kx = eps;
6 Ky = eps;
7 epsmixed = eps;
8 epsmixed1 = eps;
9 epsmixed2 = eps;
10
11 u=1;
12 for m=-N:N
13     for n=-N:N
14         mv(u)=m;
15         nv(u)=n;
16         u=u+1;
17     end
18 end
19
20 for u=1:(2*N+1)^2
21     m=mv(u);
22     n=nv(u);
23     if m==n
24         M_la(m+N+1,n+N+1) = a/(eps2*Lam) + (Lam-a)/(eps1*Lam);
25         M_ga(m+N+1,n+N+1) = 1/eps1;
26     else
27         M_la(m+N+1,n+N+1) = sin(pi*(m-n)*a/Lam)*(1/eps2-1/eps1)/((m-n)*pi);
28         M_ga(m+N+1,n+N+1) = 0;
29     end
30 end
31 Minv_la = inv(M_la);
32 Minv_ga = inv(M_ga);
33 for u=1:(2*N+1)^2
34     for v=1:(2*N+1)^2
35         m=mv(u);
36         mm=mv(v);
37         n=nv(u);
38         nm=nv(v);
39         if n==mm
40             epsmixed1(u,v)=Minv_ga(m+N+1,mm+N+1)*a/Lam+Minv_la(m+N+1,mm+N+1)*(Lam-
```

```

a)/Lam;
41     elseif n~=nm
42         epsmixed1(u,v)=(Minv_ga(m+N+1,mm+N+1)-Minv_la(m+N+1,mm+N+1))*sin(pi*(n
-nm)*a/Lam)/(pi*(n-nm));
43     end
44     if m==mm
45         epsmixed2(u,v)=Minv_ga(n+N+1,rm+N+1)*a/Lam+Minv_la(n+N+1,rm+N+1)*(Lam-
a)/Lam;
46     elseif m~=mm
47         epsmixed2(u,v)=(Minv_ga(n+N+1,rm+N+1)-Minv_la(n+N+1,rm+N+1))*sin(pi*(m
-mm)*a/Lam)/(pi*(m-mm));
48     end
49     if m==mm && n==nm
50         eps(u,v)=eps2*a^2/Lam^2+eps1*(Lam^2-a^2)/Lam^2;
51     elseif m==mm && n~=nm
52         eps(u,v)=(eps2-eps1)*a*sin(pi*(n-nm)*a/Lam)/(pi*(n-nm)*Lam);
53     elseif m~=mm && n==nm
54         eps(u,v)=(eps2-eps1)*a*sin(pi*(m-mm)*a/Lam)/(pi*(m-mm)*Lam);
55     else
56         eps(u,v)=(eps2-eps1)*sin(pi*(m-mm)*a/Lam)*sin(pi*(n-nm)*a/Lam)/(pi^2*(
m-mm)*(n-nm));
57     end
58     if m==mm && n==nm
59         Kx(u,v)=kx0+m*2*pi/Lam;
60         Ky(u,v)=ky0+n*2*pi/Lam;
61     end
62 end
63 end

```

### Li's Permittivity Matrix: Cylindrical Rod

```

1 function [epsmixed1,epsmixed2,Kx,Ky,eps]=permLiCyl(N,eps2,eps1,a,Lam,kx0,ky0)
2 Ny = 50;
3 dy = 2*a/(Ny);
4
5 M_la = zeros(2*N+1,2*N+1);
6 M_ga = zeros(2*N+1,2*N+1);
7 eps = zeros((2*N+1)^2,(2*N+1)^2);
8 Kx = eps;
9 Ky = eps;
10 epsmixed1 = eps;
11 epsmixed2 = eps;
12
13 u=1;
14 for m=-N:N

```

```

15     for n=-N:N
16         mv(u)=m;
17         nv(u)=n;
18         u=u+1;
19     end
20 end
21 for idx = 0:Ny-1
22     ym(idx+1) = a-(idx+0.5)*2*a/Ny;
23 end
24 avec = 2*sqrt(a^2-ym.^2);
25
26 for idx = 1:Ny
27     for u=1:(2*N+1)^2
28         m=mv(u);
29         n=nv(u);
30         if m==n
31             M_la(m+N+1,n+N+1) = avec(idx)/(eps2*Lam) + (Lam-avec(idx))/(eps1*
Lam);
32             M_ga(m+N+1,n+N+1) = 1/eps1;
33         else
34             M_la(m+N+1,n+N+1) = sin(pi*(m-n)*avec(idx)/Lam)*(1/eps2-1/eps1)/((
m-n)*pi);
35             M_ga(m+N+1,n+N+1) = 0;
36         end
37     end
38     M{idx} = inv(M_la);
39 end
40 Minv_ga = inv(M_ga);
41 for u=1:(2*N+1)^2
42     disp(u/(2*N+1)^2)
43     for v=1:(2*N+1)^2
44         m=mv(u);
45         mm=mv(v);
46         n=nv(u);
47         nm=nv(v);
48         if n==nm
49             epsmixed1(u,v) = 1/Lam*(Minv_ga(m+N+1,mm+N+1)*(Lam-2*a));
50             for idx = 1:length(M)
51                 epsmixed1(u,v) = epsmixed1(u,v) + 1/Lam*M{idx}(m+N+1,mm+N+1)*dy;
52             end
53         elseif n~=nm
54             epsmixed1(u,v) = (Minv_ga(m+N+1,mm+N+1)-M{1}(m+N+1,mm+N+1))*sin(-pi*(n
-nm)*a/Lam)/(pi*(n-nm));
55             for idx = 1:(length(M)/2-1)
56                 epsmixed1(u,v) = epsmixed1(u,v) + (M{idx}(m+N+1,mm+N+1)-M{idx+1}(m
+N+1,mm+N+1))*sin(-pi*(n-nm)*(a-idx*dy)/Lam)/(pi*(n-nm));

```

```

57         end
58     end
59     if m==mm
60         epsmixed2(u,v)=1/Lam*(Minv_ga(n+N+1,mm+N+1)*(Lam-2*a));
61         for idx = 1: length(M)
62             epsmixed2(u,v) = epsmixed2(u,v) + 1/Lam*M{idx}(n+N+1,mm+N+1)*dy;
63         end
64     elseif m~mm
65         epsmixed2(u,v)= (Minv_ga(n+N+1,mm+N+1)-M{1}(n+N+1,mm+N+1))*sin(-pi*(m-
66 mm)*a/Lam)/(pi*(m-mm));
67         for idx = 1:(length(M)/2-1)
68             epsmixed2(u,v) = epsmixed2(u,v) + (M{idx}(n+N+1,mm+N+1)-M{idx+1}(n
69 +N+1,mm+N+1))*sin(-pi*(m-mm)*(a-idx*dy)/Lam)/(pi*(m-mm));
70         end
71     end
72     eps=cylinder(N,eps2,eps1,a,Lam,Lam);
73     if m==mm && n==nm
74         Kx(u,v)=kx0+m*2*pi/Lam;
75         Ky(u,v)=ky0+n*2*pi/Lam;
76     end
77 end
78 end

```

### E.1.3 Tensor Formulation

```

1 %clear
2 tic
3 eps2=3.4^2;
4 eps1=1;
5 P=99.7e-6; % Period along x and y
6 Lam = P;
7 theta = 0;
8 phi = 0;
9 kx0 = sin(theta)*cos(phi);
10 ky0 = sin(theta)*sin(phi);
11 mu0 = pi*4e-7; %[N*A^-2]
12 eps0 = 8.8542e-12; %[F/m]
13 c = 1/sqrt(mu0*eps0); %[m/s]
14 freq = linspace(0.9,2.4,1000)*1e+12;
15 l = c./freq;
16 gemT = zeros(1,length(freq));
17 gemR = gemT;
18 hfield = false;
19 pol = input('Polarization [S/P]? ','s');
20 layers = 4;

```

```

21
22 use_square_shaped_rod = true
23 a=32.5e-6; % side-length of square-shaped rod
24
25 use_round_rod = false
26 a_round=18.3362e-6; %radius of round rod
27
28 N=5; %number of plane waves (2*N+1)^2
29
30 u=1;
31 nv=zeros((2*N+1)^2,1);
32 mv=nv;
33
34 for n=-N:N
35     for m=-N:N
36         nv(u)=n;
37         mv(u)=m;
38         u=u+1;
39     end
40 end
41
42 epsM = permittivity(N,eps2,eps1,a,Lam);
43
44
45 %We first construct the dielectric constant in real space
46 dx=P/(2*N+1); dy=dx;
47 epsxxrM=zeros(2*N+1);
48 epsyyrM=epsxxrM; epsxyrM=epsxxrM; epsyxrM=epsxxrM;
49 for n=1:2*N+1
50     x=(n-0.5)*dx;
51     for m=1:2*N+1
52         y=(m-0.5)*dy;
53         epsperp=0;
54         epspar=0;
55         for nsub=1:100
56             xs=x-dx/2+dx*(nsub-0.5)/100;
57             for msub=1:100
58                 ys=y-dy/2+dy*(msub-0.5)/100;
59                 if use_square_shaped_rod == true
60                     eps=dielectric_constant_square_rod(xs,ys,P,a,eps1,eps2);
61                 end
62                 if use_round_rod == true
63                     eps=dielectric_constant_round_rod(xs,ys,P,a_round,eps1,eps2);
64                 end
65                 epspar=epspar+eps;
66                 epsperp=epsperp+1/eps;

```

```

67         end
68     end
69     epspar=epspar/10000;
70     epsperp=epsperp/10000; epsperp=1/epsperp;
71     if abs(epspar-epsperp)>1e-5
72         % A boundary exists within the cell
73         %We find the normal vector
74         foundedge=0;
75         for jedge=1:4
76             if jedge==1
77                 xa=x-dx/2; ya=y-dy/2; xb=x+dx/2; yb=ya;
78             end
79             if jedge==2
80                 xa=x+dx/2; xb=xa; ya=y-dy/2; yb=y+dy/2;
81             end
82             if jedge==3
83                 xa=x-dx/2; xb=x+dx/2; ya=y+dy/2; yb=ya;
84             end
85             if jedge==4
86                 xa=x-dx/2; xb=xa; ya=y-dy/2; yb=y+dy/2;
87             end
88             for j=1:10000
89                 x1=xa+(xb-xa)*(j-1)/10000; x2=xa+(xb-xa)*j/10000;
90                 y1=ya+(yb-ya)*(j-1)/10000; y2=ya+(yb-ya)*j/10000;
91                 if use_square_shaped_rod == true
92                     epsel1=dielectric_constant_square_rod(x1,y1,P,a,eps1,eps2);
93                     epsel2=dielectric_constant_square_rod(x2,y2,P,a,eps1,eps2);
94                 end
95                 if use_round_rod == true
96                     epsel1=dielectric_constant_round_rod(x1,y1,P,a_round,eps1,
97 eps2);
98                     epsel2=dielectric_constant_round_rod(x2,y2,P,a_round,eps1,
99 eps2);
100                 end
101                 if abs(epsel1-epsel2)>1e-4
102                     foundedge=foundedge+1;
103                     if foundedge==1
104                         xedge1=(x1+x2)/2; yedge1=(y1+y2)/2;
105                     else
106                         xedge2=(x1+x2)/2; yedge2=(y1+y2)/2;
107                     end
108                 end
109             end
110         end
111     end
112     if foundedge>2
113         errorout=99
114     end
115 end

```

```

111     end
112     txd=(xedge2-xedge1); tyd=(yedge2-yedge1);
113     tx=txd/sqrt(txd^2+tyd^2); ty=tyd/sqrt(txd^2+tyd^2);
114     nx=-ty; ny=tx;
115
116     epsxxrM(n,m)=epspar+nx*nx*(epsperp-epspar);
117     epsyyrM(n,m)=epspar+ny*ny*(epsperp-epspar);
118     epsxyrM(n,m)=nx*ny*(epsperp-epspar);
119     epsyxrM(n,m)=nx*ny*(epsperp-epspar);
120     epszxrM(n,m)=epspar;
121
122     etharM=[epsxxrM(n,m) epsxyrM(n,m) 0;epsyxrM(n,m) epsyyrM(n,m) 0;0 0
epszxrM(n,m)];
123     etharM=etharM^(-1);
124     ethaxxrM(n,m)=etharM(1,1); ethaxyM(n,m)=etharM(1,2);
125     ethayxrM(n,m)=etharM(2,1); ethayyrM(n,m)=etharM(2,2);
126     ethazxrM(n,m)=etharM(3,3);
127     else
128     epsxxrM(n,m)=epspar;
129     epsyyrM(n,m)=epspar;
130     epszxrM(n,m)=epspar;
131     epsxyrM(n,m)=0;
132     epsyxrM(n,m)=0;
133
134     etharM=[epsxxrM(n,m) epsxyrM(n,m) 0;epsyxrM(n,m) epsyyrM(n,m) 0;0 0
epszxrM(n,m)];
135     etharM=etharM^(-1);
136     ethaxxrM(n,m)=etharM(1,1); ethaxyM(n,m)=etharM(1,2);
137     ethayxrM(n,m)=etharM(2,1); ethayyrM(n,m)=etharM(2,2);
138     ethazxrM(n,m)=etharM(3,3);
139     end
140     epsparrM(n,m)=epspar;
141     epsperprM(n,m)=epsperp;
142
143     etha_parrM(n,m)=1/epsparrM(n,m);
144     etha_perprM(n,m)=1/epsperprM(n,m);
145     end
146 end
147 for u=1:(2*N+1)^2
148     E=zeros(2*N+1);
149     n=nv(u)+N+1; m=mv(u)+N+1;
150     E(n,m)=1; Efft=fft2(E);
151     % E represents Ex or Ey
152     Exxfft=ifft2(Efft.*ethaxxrM);
153     Exyfft=ifft2(Efft.*ethaxyM);
154     Eyxfft=ifft2(Efft.*ethayxrM);

```

```

155 Eyyfft=ifft2 ( Efft .* ethayyrM );
156 Ezzfft=ifft2 ( Efft .* ethazzrM );
157
158 Eparfft=ifft2 ( Efft .* etha_parrM );
159 Eperpfft=ifft2 ( Efft .* etha_parrM );
160 for v=1:(2*N+1)^2
161     nm=nv(v)+N+1; mm=mv(v)+N+1;
162     ethaxxM(u,v)=Exxfft (nm,mm) ;
163     ethaxyM(u,v)=Exyfft (nm,mm) ;
164     ethayxM(u,v)=Eyxfft (nm,mm) ;
165     ethayyM(u,v)=Eyyfft (nm,mm) ;
166     ethazzM(u,v)=Ezzfft (nm,mm) ;
167
168     ethaparM(u,v)=Eparfft (nm,mm) ;
169     ethaperpM(u,v)=Eperpfft (nm,mm) ;
170 end
171
172 Exxfft=ifft2 ( Efft .* epsxxrM );
173 Exyfft=ifft2 ( Efft .* epsxyrM );
174 Eyxfft=ifft2 ( Efft .* epsyxrM );
175 Eyyfft=ifft2 ( Efft .* epsyyrM );
176 Ezzfft=ifft2 ( Efft .* epsz zrM );
177 for v=1:(2*N+1)^2
178     nm=nv(v)+N+1; mm=mv(v)+N+1;
179     epsxxM(u,v)=Exxfft (nm,mm) ;
180     epsxyM(u,v)=Exyfft (nm,mm) ;
181     epsyxM(u,v)=Eyxfft (nm,mm) ;
182     epsyyM(u,v)=Eyyfft (nm,mm) ;
183     epszzM(u,v)=Ezzfft (nm,mm) ;
184 end
185 end
186
187 for i = 1:length(l)
188     disp(i/length(l))
189     lambda = l(i); %[m] (THz = 10^12 Hz)
190     k0 = 2*pi/lambda; %[1/m] wavenumber
191     kx = k0*kx0;
192     ky = k0*ky0;
193     omega = k0*c; %[1/s]
194     %Building K-matrices:
195     [Kx,Ky] = KMatrix(N,kx,ky,Lam) ;
196     kz1 = sqrt(k0^2*eps1*eye((2*N+1)^2) - Kx^2 - Ky^2);
197     kz3 = sqrt(k0^2*eps2*eye((2*N+1)^2) - Kx^2 - Ky^2);
198     %Normalizing Constants:
199     temp = sqrt(Kx^2+Ky^2);
200     temp(ceil(end/2),ceil(end/2)) = 1;

```

```

201 norm1 = inv(temp);
202 temp = sqrt(Kx^2+Ky^2 + inv(kz1)*(Kx^2+Ky^2)^2);
203 temp(ceil(end/2),ceil(end/2)) = 1;
204 norm2 = inv(temp);
205 temp = sqrt(Kx^2+Ky^2 + inv(kz3)*(Kx^2+Ky^2)^2);
206 temp(ceil(end/2),ceil(end/2)) = 1;
207 norm3 = inv(temp);
208
209 %Building E-matrix 1st layer:
210 e11 = -norm1*Ky;
211 e21 = norm1*Kx;
212 e12a = norm2*Kx;
213 e22a = norm2*Ky;
214 if kx0 == 0 | ky0 == 0
215     e11(((2*N+1)^2+1)/2,((2*N+1)^2+1)/2) = 1;
216     e22a(((2*N+1)^2+1)/2,((2*N+1)^2+1)/2) = 1;
217 end
218 E1 = [e11 e12a;
219       e21 e22a];
220 %Building E-matrix 3rd layer:
221 e11 = -norm3*Ky;
222 e21 = norm3*Kx;
223 e12a = norm3*Kx;
224 e22a = norm3*Ky;
225 if kx0 == 0 | ky0 == 0
226     e11(((2*N+1)^2+1)/2,((2*N+1)^2+1)/2) = 1;
227     e22a(((2*N+1)^2+1)/2,((2*N+1)^2+1)/2) = 1;
228 end
229 E3 = [e11 e12a;
230       e21 e22a];
231
232 %Building H-matrix 1st and 3rd layers:
233 H1 = [-1/(omega*mu0)*Kx*Ky Kx*Kx/(omega*mu0)-omega*eps0*eps1*eye((2*N+1)^2);
234       -1/(omega*mu0)*Ky*Ky+omega*eps0*eps1*eye((2*N+1)^2) Ky*Kx/(omega*mu0)]*E1
235 * [kz1 zeros((2*N+1)^2); zeros((2*N+1)^2) kz1]^(-1);
236 H3 = [-1/(omega*mu0)*Kx*Ky Kx*Kx/(omega*mu0)-omega*eps0*eps2*eye((2*N+1)^2);
237       -1/(omega*mu0)*Ky*Ky+omega*eps0*eps2*eye((2*N+1)^2) Ky*Kx/(omega*mu0)]*E3
238 * [kz3 zeros((2*N+1)^2); zeros((2*N+1)^2) kz3]^(-1);
239
240 E4 = E1;
241 H4 = H1;
242 %Building permittivity-matrix periodic layer:
243
244 %Eigenvalue problem:
245 Me = [k0^2*epsxxM-Ky^2-Kx*inv(epszzM)*Kx*epsxxM-Kx*inv(epszzM)*Ky*epsyxM k0^2*
epsxyM+Ky*Kx-Kx*inv(epszzM)*Kx*epsxyM-Kx*inv(epszzM)*Ky*epsyyM; k0^2*epsyxM-Ky*

```

```

244 inv(epszzM)*Kx*epsxxM-Ky*inv(epszzM)*Ky*epsyxM+Kx*Ky k0^2*epsyyM-Ky*inv(epszzM)
*Kx*epsxyM-Ky*inv(epszzM)*Ky*epsyyM-Kx^2];
245 [ECoeff, betasqe] = eig(Me);
246 kz2 = sqrt(betasqe);
247 %Checking eigenvalues:
248 for idx = 1:length(diag(kz2))
249     if real(kz2(idx, idx))+imag(kz2(idx, idx))<0
250         kz2(idx, idx) = -kz2(idx, idx);
251     end
252 end
253 E2 = ECoeff;
254 H2 = [-omega*eps0*epsxyM-1/(omega*mu0)*Kx*Ky -omega*eps0*epsyyM+1/(omega*mu0)*
Kx*Kx; omega*eps0*epsxxM-1/(omega*mu0)*Ky*Ky omega*eps0*epsxyM+1/(omega*mu0)*Ky
*Kx]*E2*kz2^-1;
255 %Reflection matrices:
256 R12 = -1*(E2^-1*E1+H2^-1*H1)^-1*(E2^-1*E1-H2^-1*H1);
257 R21 = -1*(E1^-1*E2+H1^-1*H2)^-1*(E1^-1*E2-H1^-1*H2);
258 R23 = -1*(E3^-1*E2+H3^-1*H2)^-1*(E3^-1*E2-H3^-1*H2);
259 R32 = -1*(E2^-1*E3+H2^-1*H3)^-1*(E2^-1*E3-H2^-1*H3);
260 R43 = (E3^-1*E4+H3^-1*H4)^-1*(-E3^-1*E4+H3^-1*H4);
261 R34 = (E4^-1*E3+H4^-1*H3)^-1*(-E4^-1*E3+H4^-1*H3);
262
263 %Transmission matrices:
264 T12 = E2^-1*E1*(eye(2*(2*N+1)^2)+R12);
265 T21 = E1^-1*E2*(eye(2*(2*N+1)^2)+R21);
266 T23 = E3^-1*E2*(eye(2*(2*N+1)^2)+R23);
267 T32 = E2^-1*E3*(eye(2*(2*N+1)^2)+R32);
268 T34 = E4^-1*E3*(eye(2*(2*N+1)^2)+R34);
269 T43 = E3^-1*E4*(eye(2*(2*N+1)^2)+R43);
270
271 %%Propagation matrices:
272 h2 = 12.9e-6; %[m] height of the square-cylinder
273 h3 = 92.1e-6;
274 P1 = diag(exp(1i*diag(kz1)*h2));
275 P1 = [P1 zeros((2*N+1)^2);
276     zeros((2*N+1)^2) P1];
277 P2 = diag(exp(1i*diag(kz2)*h2));
278
279 P3 = diag(exp(1i*diag(kz3)*h3));
280 P3 = [P3 zeros((2*N+1)^2);
281     zeros((2*N+1)^2) P3];
282
283 %%Total reflection and transmission:
284 T13 = T23*(eye(2*(2*N+1)^2)-P2*R21*P2*R23)^-1*P2*T12;
285 T31 = T21*(eye(2*(2*N+1)^2)-P2*R23*P2*R21)^-1*P2*T32;

```

```

286 R13 = R12+T21*((eye(2*(2*N+1)^2)-P2*R23*P2*R21)^-1)*P2*R23*P2*T12;
287 R31 = R32+T23*((eye(2*(2*N+1)^2)-P2*R21*P2*R23)^-1)*P2*R21*P2*T32;
288 T14 = T34*(eye(2*(2*N+1)^2)-P3*R31*P3*R34)^-1*P3*T13;
289 R14 = R13+T31*((eye(2*(2*N+1)^2)-P3*R34*P3*R31)^-1)*P3*R34*P3*T13;
290
291 a1 = zeros(2*(2*N+1)^2,1);
292 if pol == 'S'
293     a1(((2*N+1)^2+1)/2) = 1;
294 else
295     a1(((2*N+1)^2+1)/2+(2*N+1)^2) = 1;
296 end
297
298
299 if layers == 4
300     a2 = T14*a1;
301     b1 = R14*a1;
302     Ex_t = E4(1:end/2,:)*a2;
303     Ey_t = E4(end/2+1:end,:)*a2;
304     Hx_t = H4(1:end/2,:)*a2;
305     Hy_t = H4(end/2+1:end,:)*a2;
306 elseif layers == 3
307     a2 = T13*a1;
308     b1 = R13*a1;
309     Ex_t = E3(1:end/2,:)*a2;
310     Ey_t = E3(end/2+1:end,:)*a2;
311     Hx_t = H3(1:end/2,:)*a2;
312     Hy_t = H3(end/2+1:end,:)*a2;
313 else
314     a2 = T12*a1;
315     b1 = R12*a1;
316     Ex_t = E2(1:end/2,:)*a2;
317     Ey_t = E2(end/2+1:end,:)*a2;
318     Hx_t = H2(1:end/2,:)*a2;
319     Hy_t = H2(end/2+1:end,:)*a2;
320 end
321
322 I_t = Lam^2*sum(real(Ex_t.*conj(Hy_t)-Ey_t.*conj(Hx_t)));
323 Ex_i = E1(1:end/2,:)*a1;
324 Ey_i = E1(end/2+1:end,:)*a1;
325 Hx_i = H1(1:end/2,:)*a1;
326 Hy_i = H1(end/2+1:end,:)*a1;
327 I_i = Lam^2*sum(real(Ex_i.*conj(Hy_i)-Ey_i.*conj(Hx_i)));
328 T = I_t/I_i;
329
330 Ex_r = E1(1:end/2,:)*b1;
331 Ey_r = E1(end/2+1:end,:)*b1;

```

```

332 Hx_r = H1(1:end/2,:) * b1;
333 Hy_r = H1(end/2+1:end,:) * b1;
334 I_r = Lam^2 * sum(real(Ex_r .* conj(Hy_r) - Ey_r .* conj(Hx_r)));
335 R = I_r / I_i;
336 gemT(i) = T;
337 gemR(i) = R;
338 end
339 toc
340
341 %%%%%%%%%%%%%%%%%%%%%%%%%%%%%%%%%%%%%%%%%%%%%%%%%%%%%%%%%%%%%%%%%%%%%%%%%
342
343 function [eps] = dielectric_constant_square_rod(xs,ys,P,a,eps1,eps2)
344     eps=eps1;
345     if xs>=P/2-a/2 && xs<=P/2+a/2,
346         if ys>=P/2-a/2 && ys<=P/2+a/2,
347             eps=eps2;
348         end
349     end
350 end
351
352 function [eps] = dielectric_constant_round_rod(xs,ys,P,a,eps1,eps2)
353     eps=eps1;
354     r=sqrt((xs-P/2)^2+(ys-P/2)^2);
355     if r<=a,
356         eps=eps2;
357     end
358 end

```

## E.2 2D FMM

### E.2.1 S-Polarization

```

1 %function [tv4] = fmm2igen(N)
2 % clear
3 % close all
4
5 %Dette er alt regnet i meter
6
7 N = 7;
8
9 h2 = 12.9*10^-6;
10 h3 = 92.1*10^-6;
11 Lam = 99.7*10^-6;
12 a = 42.5*10^-6;

```

```

13 G = 2*pi/Lam;
14
15 eps1 = 1;
16 eps3 = 3.4^2;
17
18 %w = linspace(0.9,2.4,1000)*10^12;
19 w = linspace(1.8,2,1000)*10^12;
20 c = physconst('lightspeed');
21 mu0 = 1.2566370621219*10^-6;
22 eps0 = c^2*mu0;
23 k0v = 2*pi*w./c;
24
25 rv1 = zeros(1,length(w));
26 rv3 = zeros(1,length(w));
27 tv1 = zeros(1,length(w));
28 tv3 = zeros(1,length(w));
29 tv4 = zeros(1,length(w));
30
31 for j=1:length(w)
32     E1 = eye(2*N+1); E3 = eye(2*N+1); E4 = eye(2*N+1);
33
34     n = -N:N;
35
36     H1 = diag(sqrt(k0v(j)^2*eps1-(n*G).^2));
37     H3 = diag(sqrt(k0v(j)^2*eps3-(n*G).^2));
38     H4 = H1;
39
40     K = diag(n*G);
41
42     m = 0:2*N;
43     eps2 = (eps3 - 1)/(2*pi)*2*sin(m.*G*a/2)./m; %(eps3-eps1)./(m.*2*pi).*2.*sin(w
(j)*m*2*pi/Lam/2);
44     eps2(1) = a/Lam*eps3 + (Lam - a)/Lam;
45     eps2 = toeplitz(eps2);
46
47     M = -K*K + (eye(2*N+1)*k0v(j))^2*eps2;
48
49     [E2,b2] = eig(M);
50
51     b2 = sqrt(b2);
52
53     for i = 1:2*N+1
54         if imag(b2(i,i))<0
55             b2(i,i) = b2(i,i)';
56         elseif imag(b2(i,i)) == 0
57             b2(i,i) = abs(b2(i,i));

```

```

58     end
59 end
60
61 H2 = E2*b2;
62
63 a1 = zeros(2*N+1,1);
64 a1(N+1) = 1;
65
66 R12 = (E2^(-1)*E1+H2^(-1)*H1)^(-1)*(H2^(-1)*H1-E2^(-1)*E1);
67 T12 = E2^(-1)*E1*(eye(2*N+1)+R12);
68
69
70 b1 = R12*a1;
71 a2 = T12*a1;
72
73 rv1(j) = abs(b1(N+1)/a1(N+1))^2;
74 tv1(j) = (abs(a2(N+1)))^2/(abs(a1(N+1)))^2;
75
76 %%%%%%%%%%
77
78 R21 = (E1^(-1)*E2+H1^(-1)*H2)^(-1)*(H1^(-1)*H2-E1^(-1)*E2);
79 R23 = (E3^(-1)*E2+H3^(-1)*H2)^(-1)*(H3^(-1)*H2-E3^(-1)*E2);
80 T21 = E1^(-1)*E2*(eye(2*N+1)+R21);
81 T23 = E3^(-1)*E2*(eye(2*N+1)+R23);
82
83 P2 = diag(exp(1i*diag(b2)*h2));
84
85 R13 = R12+T21*(eye(2*N+1)-P2*R23*P2*R21)^(-1)*P2*R23*P2*T12;
86 T13 = T23*(eye(2*N+1)-P2*R21*P2*R23)^(-1)*P2*T12;
87
88 b3 = R13*a1;
89 a3 = T13*a1;
90
91 rv3(j) = abs(b3(N+1)/a1(N+1))^2;
92 tv3(j) = (abs(a3(N+1)))^2/(abs(a1(N+1)))^2;
93
94 %%%%%%%%%%
95 P3 = diag(exp(1i*diag(H3)*h3));
96 R32 = (E2^(-1)*E3+H2^(-1)*H3)^(-1)*(H2^(-1)*H3-E2^(-1)*E3);
97 T32 = E2^(-1)*E3*(eye(2*N+1)+R32);
98 R31 = R32+T23*P2*(eye(2*N+1)-R21*P2*R23*P2)^(-1)*R21*P2*T32;
99 R34 = (E4^(-1)*E3+H4^(-1)*H3)^(-1)*(H4^(-1)*H3-E4^(-1)*E3);
100 T34 = E4^(-1)*E3*(eye(2*N+1)+R34);
101
102 T14 = T34*(eye(2*N+1)-P3*R31*P3*R34)^(-1)*P3*T13;
103

```

```

104     a4 = T14*a1;
105     tv4(j) = (abs(a4(N+1)))^2/(abs(a1(N+1)))^2;
106 end
107 %
108 % plot(w,rv1)
109 % axis([w(1) w(end) 0 0.3])
110 %
111 % figure
112 % plot(w,rv3)
113 % axis([w(1) w(end) 0 0.3])
114 %
115 % figure
116 % plot(w,tv4)
117
118
119 %Rand

```

## E.2.2 P-Polarization

```

1 %function [tv4] = Fmm2igenHpol(N)
2 %clear
3 %close all
4
5 %Dette er alt regnet i meter
6
7 N = 1;
8
9 h2 = 12.9*10^-6;
10 h3 = 92.1*10^-6;
11 Lam = 99.7*10^-6;
12 a = 32.5*10^-6;
13 G = 2*pi/Lam;
14
15 eps1 = 1;
16 eps3 = 3.4^2;
17
18 %w = linspace(0.9,2.4,1000)*10^12;
19 w = linspace(1.2,1.3,1000)*10^12;
20 c = physconst('lightspeed');
21 k0v = 2*pi*w./c;
22 mu0 = 1.2566370621219*10^-6;
23 eps0 = 1/(c^2*mu0);
24 test = 1/(a*eps0);%11.6; %0.0000000001/eps0;
25
26 rv1 = zeros(1,length(w));

```

```

27 rv3 = zeros(1,length(w));
28 tv1 = zeros(1,length(w));
29 tv3 = zeros(1,length(w));
30 tv4 = zeros(1,length(w));
31
32
33     n = -N:N;
34
35 for j=1:length(w)
36
37     test = 1;%11.55; %1/(w(j)*eps0);
38     H1 = eye(2*N+1); H3 = eye(2*N+1); H4 = eye(2*N+1);
39
40     E1 = diag(sqrt(k0v(j)^2*eps1-(n*G).^2)/eps1*test);
41     E3 = diag(sqrt(k0v(j)^2*eps3-(n*G).^2)/eps3*test);
42     E4 = E1;
43
44     K = diag(n*G);
45
46     m = 0:2*N;
47     eps2 = (eps3 - eps1)/(2*pi)*2*sin(m.*G*a/2)./m;
48     eps2(1) = a/Lam*eps3 + eps1*(Lam - a)/Lam;
49     eps2 = toeplitz(eps2);
50
51     eta2 = (1/eps3 - 1/eps1)/(2*pi)*2*sin(m.*G*a/2)./m;
52     eta2(1) = a/Lam*1./eps3 + 1/eps1*(Lam - a)/Lam;
53     eta2 = toeplitz(eta2);
54
55     %M = eta2^(-1)*(-K*eps2^(-1)*K+k0v(j)^2*eye(2*N+1));
56     M = eps2*(-K*eps2^(-1)*K+k0v(j)^2*eye(2*N+1));
57     [H2,b2] = eig(M);
58
59     b2 = sqrt(b2);
60
61     for i = 1:2*N+1
62         if imag(b2(i,i))<0
63             b2(i,i) = b2(i,i)';
64         elseif imag(b2(i,i)) == 0
65             b2(i,i) = abs(b2(i,i));
66         end
67     end
68
69     %E2 = eta2*H2*b2*test;
70     E2 = eps2^-1*H2*b2*test;
71
72     %%%%%%%%%%%

```

```

73
74 a1 = zeros(2*N+1,1);
75 a1(N+1) = 1;
76
77
78 R12 = (H2^(-1)*H1+E2^(-1)*E1)^(-1)*(E2^(-1)*E1-H2^(-1)*H1);
79 T12 = H2^(-1)*H1*(eye(2*N+1)+R12);
80
81 b1 = R12*a1;
82 a2 = T12*a1;
83
84 rv1(j) = abs(b1(N+1)/a1(N+1))^2;
85 tv1(j) = (abs(a2(N+1)))^2/(abs(a1(N+1)))^2;
86
87 %%%%%%%%%%
88
89 R21 = (H1^(-1)*H2+E1^(-1)*E2)^(-1)*(E1^(-1)*E2-H1^(-1)*H2);
90 R23 = (H3^(-1)*H2+E3^(-1)*E2)^(-1)*(E3^(-1)*E2-H3^(-1)*H2);
91 T21 = H1^(-1)*H2*(eye(2*N+1)+R21);
92 T23 = H3^(-1)*H2*(eye(2*N+1)+R23);
93
94 P2 = diag(exp(1i*diag(b2)*h2));
95
96 R13 = R12+T21*(eye(2*N+1)-P2*R23*P2*R21)^(-1)*P2*R23*P2*T12;
97 T13 = T23*P2*(eye(2*N+1)-R21*P2*R23*P2)^(-1)*T12;
98 b3 = R13*a1;
99 a3 = T13*a1;
100
101 rv3(j) = abs(b3(N+1)/a1(N+1))^2;
102 tv3(j) = (abs(a3(N+1)))^2/(abs(a1(N+1)))^2;
103
104 %%%%%%%%%%
105
106 P3 = diag(exp(1i*diag(E3*eps3)*h3));
107 R32 = (H2^(-1)*H3+E2^(-1)*E3)^(-1)*(E2^(-1)*E3-H2^(-1)*H3);
108 T32 = H2^(-1)*H3*(eye(2*N+1)+R32);
109 R31 = R32+T23*P2*(eye(2*N+1)-R21*P2*R23*P2)^(-1)*R21*P2*T32;
110 R34 = (H4^(-1)*H3+E4^(-1)*E3)^(-1)*(E4^(-1)*E3-H4^(-1)*H3);
111 T34 = H4^(-1)*H3*(eye(2*N+1)+R34);
112
113 T14 = T34*P3*(eye(2*N+1)-R31*P3*R34*P3)^(-1)*T13;
114
115 a4 = T14*a1;
116 tv4(j) = (abs(a4(N+1)))^2/(abs(a1(N+1)))^2;
117 end
118

```

```

119 % plot(w,rv1)
120 % axis([w(1) w(end) 0 0.3])
121 %
122 % figure
123 % plot(w,rv3)
124 % axis([w(1) w(end) 0 0.3])
125 %
126 % figure
127 % plot(w,tv4)
128
129 %Rand

```

## E.3 Guided Modes

### E.3.1 S-Polarization

```

1 clear
2 close all
3
4 %Dimensioner p struktur
5 d1 = 0; %12.9; %h jde
6 Lam = 100; %99.7; %Periode
7 a = 42.5; %Bredde
8
9 %d2 = 150-d1; % mono Si lag h jde
10 d2 = 92.1;
11
12 eps1 = 1;
13 eps3 = 3.4^2;
14 eps2 = (eps3*a^2+(Lam^2-a^2)*eps1)/Lam^2;
15 %eps2 = (eps3*a+(Lam-a)*eps1)/Lam; %eps2 med striber
16 eps4 = 1;
17
18 eps = [eps1 eps2 eps3 eps4];
19
20 %lambda = linspace(120,340,1000);
21 lambda = linspace(125,333,1000);
22 %nmv = zeros(1,length(lambda));
23
24 for ii = 1:length(lambda)
25 k0 = 2*pi./lambda(ii);
26 nm = 1:0.001:3.4;
27 f = zeros(length(nm),1);
28

```

```

29 for j = 1:length(nm)
30
31 %S polarisation
32 rs = cell(3,1);
33 ts = cell(3,1);
34 H = cell(3,1);
35
36 for i = 1:3
37     rs{i} = (sqrt(k0^2*eps(i)-k0^2*nm(j)^2)-sqrt(k0^2*eps(i+1)-k0^2*nm(j)^2)) ...
38           /((sqrt(k0^2*eps(i)-k0^2*nm(j)^2)+sqrt(k0^2*eps(i+1)-k0^2*nm(j)^2))
39           ;
40     ts{i} = rs{i} - 1;
41     H{i} = 1/ts{i}*[1 rs{i}; rs{i} 1];
42 end
43 L = zeros(2,1);
44 L1 = [exp(-1i*sqrt(k0^2*eps(2)-k0^2*nm(j)^2)*d1) 0; 0 exp(1i*sqrt(k0^2*eps(2)-
45 k0^2*nm(j)^2)*d1)];
46 L2 = [exp(-1i*sqrt(k0^2*eps(3)-k0^2*nm(j)^2)*d2) 0; 0 exp(1i*sqrt(k0^2*eps(3)-
47 k0^2*nm(j)^2)*d2)];
48 M = H{1}*L1*H{2}*L2*H{3};
49 f(j) = M(1,1);
50
51
52 end
53
54 n = 1;
55 for i = 1:length(f)-1
56     if real(f(i)) < 0 && real(f(i+1)) > 0 || real(f(i)) > 0 && real(f(i+1)) < 0
57         q(n) = (f(i)+f(i+1))/2;
58         nm0(n) = (nm(i)+nm(i+1))/2;
59         n = n + 1;
60     end
61 end
62 nm0 = nm0';
63 nmv(:,ii) = nm0;
64 t = lambda(ii)/lambda(end)
65
66 end
67 c = physconst('Lightspeed');
68 c = c*10^6;
69
70 % plot(c./lambda*10^-(12),nmv(:, :) *2*pi./lambda, '.', 'MarkerEdgeColor', 'k',
71       'markersize',0.05)

```

```

71 % axis([c./lambda(end)*10^(-12) c./lambda(1)*10^(-12) 0 0.22])
72 xlabel('\lambda_0')
73 ylabel('n_m')
74
75
76 plot(lambda,nmv(:, :)*2*pi./lambda, '.', 'MarkerEdgeColor','k','markersize',0.05)
77 axis([lambda(1) lambda(end) 0 0.22])
78
79 hold on
80 x = linspace(lambda(1),lambda(end),100);
81 for m = 1:3
82     y = m*2*pi/Lam*ones(1,length(x));
83     plot(x,y,'r--')
84 end
85 % For 100-300
86 % fano1 = [110.0000  122.0000  138.0000  158.0000  182.0000  213.0000  251.0000
87           291.0000;
88           0.0630   0.0630   0.0630   0.0630   0.0630   0.0630   0.0630
89           0.0630];
90 % fano2 = [101.0000  110.0000  120.0000  130.0000  141.0000  152.0000  161.0000
91           168.0000;
92           0.1260   0.1260   0.1260   0.1260   0.1260   0.1260   0.1260
93           0.1260];
94 % fano3 = [103.0000  107.0000  110.0000  112.0000;
95           0.1891   0.1891   0.1891   0.1891];
96
97 % fano1 = [138.8 168.6 209.5 262 314.9 316 328.8 331.3;
98           0.0630   0.0630   0.0630   0.0630 0.0630 0.0630   0.0630   0.0630
99           0.0630];
100 % fano2 = [139 154 165.35 165.7;
101           0.1260   0.1260   0.1260   0.1260];
102
103 % Hvis det er striber og ikke squares
104 % fano1 = [142.5 171.9 212.5 264.15 315.7 326.4 331.15;
105           0.0630   0.0630   0.0630 0.0630   0.0630   0.0630   0.0630   0.0630];
106 % fano2 = [139.8 154.4 165.39 165.6 166.7;
107           0.1260   0.1260   0.1260   0.1260   0.1260];
108
109 %squares med Lambda = 100
110 fano1 = [136.9 166.9 208.1 261.5 315.1 317.3 328.2 332.7;
111           0.0628   0.0628   0.0628   0.0628   0.0628   0.0628   0.0628   0.0628];
112 fano2 = [139 154.2 165.7 166.3;
113           0.1257   0.1257   0.1257   0.1257 ];
114
115 %squares med Lambda = 105
116 % fano1 = [138.4 169.4 212.7 269.8 328.7;

```

```

112 %           0.0598    0.0598    0.0598    0.0598    0.0598];
113 %   fano2 = [126.8  143.8  160.7  173.5   174.7;
114 %           0.1197    0.1197    0.1197    0.1197    0.1197];
115
116
117
118 %fano = [fano1 fano2 fano3];
119 fano = [fano1 fano2];
120
121 plot(fano(1,:),fano(2,:), 'bx')
122
123 Spol = 1;
124
125 %Modesort

```

### E.3.2 P-Polarization

```

1 clear
2 close all
3
4 %Dimensioner p struktur
5 d1 = 12.9; %h jde
6 Lam = 105; %99.7; %Periode
7 a = 42.5; %Bredde
8
9 %d2 = 150-d1; % mono Si lag h jde
10 d2 = 92.1;
11 eps1 = 1;
12 eps3 = 3.4^2;
13 eps2 = (eps3*a^2+(Lam^2-a^2)*eps1)/Lam^2;
14 %eps2 = (eps3*a+(Lam-a)*eps1)/Lam;
15 eps4 = 1;
16
17 eps = [eps1 eps2 eps3 eps4];
18
19 %lambda = linspace(120,340,1000);
20 lambda = linspace(125,333,1000);
21
22 for ii = 1:length(lambda)
23 k0 = 2*pi./lambda(ii);
24 nm = 1:0.001:3.4;
25 f = zeros(length(nm),1);
26
27 for j = 1:length(nm)
28

```

```

29 %P polarisation
30 rs = cell(3,1);
31 ts = cell(3,1);
32 H = cell(3,1);
33
34 for i = 1:3
35     rs{i} = (eps(i+1)*sqrt(k0^2*eps(i)-k0^2*nm(j)^2)-eps(i)*sqrt(k0^2*eps(i+1)-k0
36         ^2*nm(j)^2)) ...
37         /((eps(i+1)*sqrt(k0^2*eps(i)-k0^2*nm(j)^2)+eps(i)*sqrt(k0^2*eps(i
38         +1)-k0^2*nm(j)^2)));
39     ts{i} = rs{i} - 1;
40     H{i} = 1/ts{i}*[1 rs{i}; rs{i} 1];
41 end
42
43 L = zeros(2,1);
44 L1 = [exp(-1i*sqrt(k0^2*eps(2)-k0^2*nm(j)^2)*d1) 0; 0 exp(1i*sqrt(k0^2*eps(2)-
45     k0^2*nm(j)^2)*d1)];
46 L2 = [exp(-1i*sqrt(k0^2*eps(3)-k0^2*nm(j)^2)*d2) 0; 0 exp(1i*sqrt(k0^2*eps(3)-
47     k0^2*nm(j)^2)*d2)];
48
49 M = H{1}*L1*H{2}*L2*H{3};
50 f(j) = M(1,1);
51
52 end
53
54 n = 1;
55 for i = 1:length(f)-1
56     if real(f(i)) < 0 && real(f(i+1)) > 0 || real(f(i)) > 0 && real(f(i+1)) < 0
57         q(n) = (f(i)+f(i+1))/2;
58         nm0(n) = (nm(i)+nm(i+1))/2;
59         n = n + 1;
60     end
61 end
62 nm0 = nm0';
63 nmv(:, ii) = nm0;
64 t = lambda(ii)/lambda(end)
65
66 end
67
68 c = physconst('Lightspeed');
69 c = c*10^6;
70
71 % plot(c./lambda*10^-(12),nmv(:, :) *2*pi./lambda, '.', 'MarkerEdgeColor', 'k', '
72     markersize', 0.05)
73 % axis([c./lambda(end)*10^(-12) c./lambda(1)*10^(-12) 0 0.22])

```

```

70 xlabel('\lambda_0')
71 ylabel('n_m')
72
73
74 plot(lambda,nmv(:, :) * 2*pi./lambda, '.', 'MarkerEdgeColor', 'k', 'markersize', 0.05)
75 axis([lambda(1) lambda(end) 0 0.22])
76
77 hold on
78 x = linspace(lambda(1), lambda(end), 100);
79 for m = 1:3
80     y = m*2*pi/Lam*ones(1, length(x));
81     plot(x, y, 'r--')
82 end
83
84 % fano1 = [100 107 116 129 146 168 196 233 277;
85           0.0630 0.0630 0.0630 0.0630 0.0630 0.0630 0.0630 0.0630
86           0.0630 0.0630];
87 % fano2 = [106 116 126 138 149 159 167;
88           0.1260 0.1260 0.1260 0.1260 0.1260 0.1260 0.1260 0.1260];
89 % fano3 = [102 106 110 112;
90           0.1891 0.1891 0.1891 0.1891];
91 % fano = [fano1 fano2 fano3];
92
92 % fano1 = [127.1 150.7 185.9 237 301.5 320.4 328.8 332.3;
93           0.0630 0.0630 0.0630 0.0630 0.0630 0.0630 0.0630 0.0630 0.0630];
94 % fano2 = [133.2 150 149 164.2 166.2;
95           0.1260 0.1260 0.1260 0.1260 0.1260];
96 %
97 % %Striber
98 % fano1 = [131.3 155.4 190.35 240.8 303.58 321 328.7 332.3;
99           0.0630 0.0630 0.0630 0.0630 0.0630 0.0630 0.0630 0.0630 0.0630];
100 % fano2 = [134.6 150.9 164.2 164.4 166.1;
101           0.1260 0.1260 0.1260 0.1260 0.1260];
102
103 %square med Lambda = 100
104 % fano1 = [127.2 150.9 185.9 237.3 302.3 321.6 329.5;
105           0.0628 0.0628 0.0628 0.0628 0.0628 0.0628 0.0628];
106 % fano2 = [133.5 150.5 164.4 166.7 ;
107           0.1257 0.1257 0.1257 0.1257];
108
109 %square med Lambda = 105
110 % fano1 = [128.6 152.3 188.6 242.9 314.7;
111           0.0598 0.0598 0.0598 0.0598 0.0598];
112 % fano2 = [137.5 156.3 172.05 173 175 ;
113           0.1197 0.1197 0.1197 0.1197 0.1197];
114

```

```
115
116 fano = [fano1 fano2];
117
118 plot (fano(1,:), fano(2,:), 'bx')
```